UNIVERSIDAD DE EXTREMADURA

TESIS DOCTORAL

APLICACIÓN DE TÉCNICAS HIPERESPECTRALES PARA UNA MEJORA DE LA APARIENCIA VISUAL Y DE LA SENSACIÓN DE REALISMO EN DISPOSITIVOS DE REALIDAD VIRTUAL

FRANCISCO DÍAZ BARRANCAS

PROGRAMA DE DOCTORADO EN TECNOLOGÍAS INFORMÁTICAS

2022

UNIVERSIDAD DE EXTREMADURA

TESIS DOCTORAL

APLICACIÓN DE TÉCNICAS HIPERESPECTRALES PARA UNA MEJORA DE LA APARIENCIA VISUAL Y DE LA SENSACIÓN DE REALISMO EN DISPOSITIVOS DE REALIDAD VIRTUAL

FRANCISCO DÍAZ BARRANCAS

CONFORMIDAD DEL DIRECTOR:

*La conformidad del director de la tesis consta en el original en papel de esta Tesis Doctoral.

DR. PEDRO JOSÉ PARDO FERNÁNDEZ

PROGRAMA DE DOCTORADO EN TECNOLOGÍAS INFORMÁTICAS

2022

"No dejaremos de explorar y al final de nuestra búsqueda llegaremos a donde empezamos y conoceremos por primera vez el lugar."

Thomas Stearns Eliot

Agradecimientos

En primer lugar, me gustaría agradecer al Grupo de Investigación Orión, el cual ha hecho posible que hoy esta tesis pueda tener un final feliz. Gracias a todos sus integrantes por su apoyo, su cariño y su calidad humana. En especial, me gustaría agradecer a Halina, que fue mi profesora en el grado y que hoy se ha convertido en mi compañera de investigación más cercana, con la que la investigación se convierte en algo más llevadero. A mi director de tesis Pedro José Pardo, pilar fundamental para que todo el trabajo al final vea la luz. Gracias por no dejarme abandonar en ningún momento.

A la Universidad de Extremadura, y más específicamente al Centro Universitario de Mérida, que me han permitido formarme de una manera ejemplar desde que comencé el Grado en Ingeniería Informática en 2013 y ahora terminando mi doctorado 8 años después, pasando por su Máster de Investigación en Ingeniería y Arquitectura en 2018. A su excelente profesorado de una gran calidad docente y mejor calidad humana.

Al profesor Alessandro Rizzi, de la Universidad Dégli Studi di Milano, que me acogió de una manera excepcional durante mi estancia predoctoral en Milán. Gracias también al profesor João Manuel Maciel Linhares, de la Universidad de Minho de Braga, el cual ha colaborado en trabajos relacionados con dicha tesis.

A mi familia, en especial a mis hermanos y a mis padres, de los que aprendí todo de la vida. Gracias por darme la oportunidad de formarme académicamente, pero sobre todo, gracias por haberme forjado como la persona que soy hoy en día: todos los logros siempre serán vuestros.

Por último, y con un peso extraordinariamente importante, a los amigos que un día la carrera académica me brindó: Borja, Dani y África, sin los cuales acabar esta etapa de mi vida hubiera sido mucho más difícil. Nunca un Quijote tuvo semejantes Sanchos.

Y colorín colorado, aquí termina una dura etapa de mi vida, que resulta que era un sueño de un niño cabezón que al menos tenía que intentarlo y que ya hicimos realidad.

Gracias.

PALABRAS CLAVES

realidad virtual, experiencia inmersiva, fidelidad gráfica, colorimetría, gestión digital del color

RESUMEN

La Realidad Virtual es una de las numerosas tecnologías que se encuentran en continuo crecimiento en estos nuevos tiempos. Junto a otras grandes tecnologías como el 5G, el Big Data o la Inteligencia Artificial, lo que se busca es dar un paso más en la calidad de la experiencia ofrecida a las personas frente a la producción masiva y el abaratamiento de costes. Esta característica hace que cada vez tengamos que perfeccionar de forma más notable la tecnología para buscar nuevos retos y mejorar la experiencia de la vida humana. En este ámbito se ubica nuestro trabajo, cuyo objetivo principal es el de la mejora en el renderizado gráfico de escenas virtuales para conseguir una experiencia inmersiva completa. Este objetivo puede ser abordado desde diferentes puntos de vista de la computación gráfica, sin embargo, hemos decidido enfocar nuestra investigación utilizando un renderizado básico basado en las leyes de la física y, más específicamente, basado en el estudio de la interacción de la luz con la materia, la gestión del color y la iluminación. Estos dos últimos aspectos están muy relacionados con las propiedades del sistema visual humano y la complejidad de la percepción visual. Sin embargo, cuando hablamos de realidad virtual, la tecnología actual no permite que nuestro sistema visual humano responda de la misma manera que lo hace ante el mundo real. En este contexto, hemos utilizado técnicas de gestión del color y de computación gráfica, introduciendo texturas hiperespectrales para obtener un mejor resultado de visualización del mundo virtual basado en escenas del mundo real. Estas nuevas técnicas, unidas al gran abanico de posibilidades que nos ofrecen las diferentes plataformas de software para aplicar técnicas físicas que simulen el mundo real, hacen que la calidad gráfica en nuestra experiencia inmersiva sea notablemente mayor. Todo esto permite que estos dispositivos de realidad virtual puedan utilizarse en numerosos campos de gran relevancia como la medicina, la aviación, el ocio personal... En definitiva, podemos esperar que la Realidad Virtual desarrolle una prometedora carrera en su rápido crecimiento por ofrecer a las personas experiencias que en la vida real difícilmente podrían experimentar.

KEY WORDS

virtual reality, immersive experience, graphic fidelity, colorimetry, digital color management

ABSTRACT

Virtual Reality is one of the many technologies that are in continuous growth in these new times. Along with other great technologies such as 5G, Big Data or Artificial Intelligence, the aim is to take a step forward in the quality of the experience offered to people in the face of mass production and lower costs. This characteristic means that we have to increasingly perfect technology in order to seek new challenges and improve the experience of human life. This is the scope of our work, whose main objective is to improve the graphic rendering of virtual scenes in order to achieve a complete immersive experience. This objective can be approached from different points of view of computer graphics, however, we have decided to focus our research using a basic rendering based on the laws of physics and, more specifically, based on the study of the interaction of light with matter, colour management and lighting. These last two aspects are closely related to the properties of the human visual system and the complexity of visual perception. However, when it comes to virtual reality, current technology does not allow our human visual system to respond in the same way as it does to the real world. In this context, we have introduced colour management and computer graphics techniques, introducing hyperspectral textures to obtain a better visualisation result of the virtual world based on real world scenes. These new techniques, together with the wide range of possibilities offered by the different software platforms to apply physical techniques that simulate the real world, make the graphic quality of our immersive experience significantly higher. All of this means that these virtual reality devices can be used in numerous highly relevant fields such as medicine, aviation, personal entertainment... In short, we can expect Virtual Reality to develop a promising career in its rapid growth by offering people experiences that they could hardly experience in real life.

Lista de abreviaturas

BRDF Bidirectional Reflectance Distribution Function. 7

BSDF Bidirectional Scattering Distribution Function. 7

BTDF Bidirectional Transmittance Function. 7

CIE Comisión Internacional de la Iluminación. 15, 26

CMFs Color Matching Functions. 20

CMM Color Management Module. 15

CMS Color Management Systems. 15, 20

GPU Graphics Processing Unit. 3

HMD Head Mounted Display. 2, 22

ICC International Color Consortium. 15, 24

NDF Normal Distribution Function. 9

PBR Physically Based Rendering. 5

PBS Physically Based Shading. 5

PCS Profile Connection Space. 15, 20

VR Virtual Reality. 1, 2, 22

Lista de tablas

Índice de figuras

Índice general

Capítulo 1

Introducción

1.1. Realidad Virtual: Conceptos básicos y contextualización de la tecnología

La Realidad Virtual (en inglés *Virtual Reality* - VR) se define como un entorno real o simulado en el que un perceptor experimenta la telepresencia, siendo la telepresencia la experiencia de presencia en un entorno por medio de un medio de comunicación. Para conseguir esa sensación de presencia, nuestros sentidos juegan un papel crucial para hacer llegar al cerebro información correspondiente con una situación que no es real [1]. La sensación de presencia se consigue visualmente generando dos vistas diferentes de una misma escena, cada una con un punto de vista distinto que difieren en una distancia equivalente a la existente entre las pupilas de los ojos de los seres humanos. Con esto se consigue el efecto de visión estereoscópica o percepción tridimensional, que proporciona la sensación de profundidad a una escena [2].

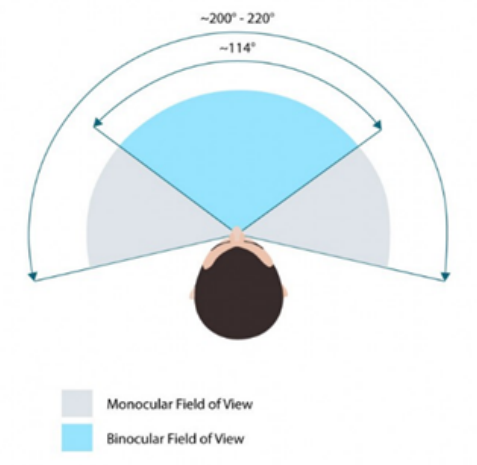

Figura 1.1: Campo visual humano monocular y binocular.

Para obtener una sensación de telepresencia de calidad no basta con generar una imagen estereoscópica, sino que es necesario que se den una serie de factores. Por ejemplo, es necesario tener un amplio campo visual, más allá de la información mostrada en una pantalla de cine o televisión. El ser humano tiene un campo visual de unos 200°, aunque con visión estereoscópica solo unos 110° (Fig. 1.1) [3].

Desde un punto de vista técnico, el gran campo visual se consigue situando la pantalla muy cerca de los ojos del sujeto, lo que obliga a introducir en todos los dispositivos de VR unas lentes que permitan acomodar el ojo sobre la pantalla a tan corta distancia [4]. Estas lentes a su vez pueden deformar el campo visual, debido a las aberraciones ópticas introducidas por ellas mismas, y también pueden hacer que se perciba el *dot-pitch* de la pantalla o el pixelado de la imagen. Además, para producir una buena sensación de telepresencia, el dispositivo VR debe ser capaz de detectar los movimientos de la cabeza y generar distintas vistas de la misma escena con la suficiente velocidad y muy poco retardo, lo que es más conocido como baja latencia.

El sistema de imágenes VR debe ser capaz de generar imágenes con una frecuencia suficiente para no percibir ningún parpadeo (entre 75 y 120 Hz) y, lo más difícil, cambiar la imagen generada en función de los movimientos que realiza la cabeza del observador lo más rápidamente posible [5]. Para conseguir esto, es necesario disponer de unos elementos de software y hardware que permitan hacer el seguimiento de los movimientos y el renderizado de las imágenes con la velocidad suficiente. Estos elementos hardware son: giróscopos, acelerómetros y cámaras de posicionamiento, que mediante cálculos sencillos, permiten conocer la posición exacta de la cabeza de la persona que usa el dispositivo de VR.

Los *Head Mounted Displays* (HMD) están experimentando un gran desarrollo durante los últimos años [6]. Este tipo de dispositivo permite realizar experiencias de inmersión visual en entornos virtuales y es de esperar que tenga muchas aplicaciones, tanto en el campo recreativo como en el profesional. Diversas empresas han sacado distintos dispositivos comerciales orientados a la realidad virtual: desde Google con su cardboard, que emplean como display la pantalla de cualquier teléfono móvil, hasta la famosa Oculus, propiedad de Facebook, con sus Oculus Rift pasando por Samsung, Sony, HTC, y un largo etcétera, muchos son los dispositivos de este tipo que inundan el mercado (Tabla 1.1). Todo este conjunto de dispositivos, han hecho resurgir el interés por el concepto de Realidad Virtual VR que no es tan nuevo como parece ya que fue utilizado por primera vez en 1989 por Jaron Lanier, *Chief Executive Officer* de VPL Research, Inc., un fabricante de guantes y HMD. Sin embargo, aunque se ha avanzado mucho en la mejora constante en el desarrollo de HMD y de técnicas de renderización que dotan a la Realidad Virtual de un mayor realismo [7], todavía quedan muchos aspectos por mejorar en el ámbito de la apariencia visual y la reproducción fiel de los colores bajo diferentes situaciones de iluminaciones. En este sentido, es necesario continuar esta introducción con una de las principales técnicas utilizadas que recoge las principales leyes de la física y las aúna para que puedan ser reproducidas en escenas 3D.

Modelo	Oculus Quest 2	Oculus Rift S	HTC Vive Pro	Varjo VR 3	HP Reverb G2
Año	2020	2019	2018	2020	2020
Requiere PC	No	Sí	Sí	Sí	Sí
Panel	LCD	Single Fast - Switch LCD	AMOLED	OLED y LCD	LCD
Resolución por ojo	1.920 x 1.832	1280 x 1440	1440 x 1600	2880 x 2720	2.160 x 2.160
Tasa de refresco	90 Hz	80 Hz	90 Hz	200 Hz	90 Hz
Campo de visión (grados)	90^o	110^o	110^o	115^o	114^o
Tracking	Inside-out 6DOF	Inside-out 6DOF	Steam VR Tracking	Steam VR 2.0	Inside-out 6DOF
Eye Tracking	No	No	No	Sí	Sí
IPD	Manual control deslizante	Mediante software	Manual control deslizante	Automático 59-71 mm	Manual control deslizante

Tabla 1.1: Tabla comparativa de los diferentes visores de realidad virtual de las marcas más relevantes

Desde un punto de vista óptico, ya se han mencionado los principales problemas de este tipo de dispositivos: aberraciones y percepción del píxel. Sin embargo, para producir una sensación de inmersión real, el dispositivo debe ser capaz de detectar los movimientos de la cabeza y generar distintas vistas de la misma escena con baja latencia [8, 9, 10, 11]. Para que este tipo de dispositivo genere las imágenes con la calidad y frecuencia necesaria, se necesitan tarjetas o chips gráficos de gran potencia [12]. Basta con hacer un pequeño cálculo teniendo en cuenta los píxeles del display de las gafas VR (2160x1200 píxeles para las HTC Vive mostradas en la figura 1.2) con la profundidad de color habitual de 24 bits/pixel y los 120 Hz para darse cuenta de que manejar 7.5 Gbps no es tarea trivial.

Además, hay que tener en cuenta que, si las imágenes que son mostradas en este tipo de dispositivos son imágenes renderizadas, es decir, generadas mediante cálculos de iluminación partiendo de una escena 3D, la complejidad de los cálculos necesarios elevan los requerimientos de hardware considerablemente [13].

La calidad de las imágenes renderizadas ha evolucionado mucho en los últimos años, como puede verse en la figura 1.3, pero siempre y cuando se disponga del tiempo suficiente para el procesado, que según el caso puede durar horas o días. Dado que en los dispositivos de realidad virtual no se dispone de ese tiempo, sino únicamente de unas 10 milésimas de segundo, esto hace inviable a primera vista el uso de este tipo de imágenes sintéticas de gran calidad, aunque esto supondría un considerable aumento de la calidad de la experiencia de inmersión virtual [14]. Actualmente, las Unidades de Procesamiento Grafico (GPU) han evolucionado también mucho en los últimos años, convirtiéndose en elementos electrónicos cuya potencia permite ser dedicada a la mejora sustancial de la calidad de los gráficos renderizados. En este sentido, se están utilizando distintas formas de procesado gráfico a la hora de manejar las condiciones de iluminación, como el *Deferred Rendering*, frente al más tradicional *Forward Rendering* [15].

Figura 1.2: Despiece de todos los componentes del HMD en su versión HTC Vive. https://eandt.theiet.org/content/articles/2018/05/teardown-htc-vive-pro-vr-headset/

Figura 1.3: Imagen renderizada mediante el software de trazado de rayos PovRay.

1.2. Phisically Based Rendering: El renderizado basado en la física aplicado a Realidad Virtual

Physically Based Rendering (PBR), o también llamado *Physically Based Shading* (PBS) en función del contexto, es una nueva forma de hacer renderizado de imágenes en los motores de renderizado en tiempo real (por ejemplo, en videojuegos) que mejoran muchísimo la calidad final de las escenas renderizadas gracias a que aplican leyes de la física real al mundo virtual. PBR proporciona una apariencia completamente realista al modelar el comportamiento de la incidencia de la luz sobre los diferentes objetos y materiales. Uno de los objetivos de la computación gráfica es generar imágenes que imiten la realidad con la mayor precisión posible. Esto tiene una amplia gama de aplicaciones, que incluyen entretenimiento, arquitectura o ingeniería. Sin embargo, renderizar imágenes fieles requiere simular los complejos fenómenos físicos de las interacciones de luz, resolviendo grandes integrales multidimensionales. La Representación Basada en la Física (PBR) es una combinación de trabajo artístico, propiedades físicas y sombreadores de materiales que trabajan juntos para brindar orden y consistencia a la representación gráfica. Utilizando los principios físicos subyacentes de cómo interactúan la luz y las superficies, podemos crear imágenes predecibles que funcionen en todas las condiciones de iluminación sin casos especiales. PBR es un concepto completamente innovador del renderizado en tiempo real. El término está muy expandido, lo que a menudo genera confusión en cuanto a lo que significa exactamente. Gran parte de lo que hace que un sistema de renderizado basado en la física sea diferente de sus predecesores es un razonamiento más detallado sobre el comportamiento de la luz y las superficies que intervienen en el mismo.

Para comprender cómo funciona PBR, necesitamos antes entender algunos conceptos físicos básicos de la interacción luz-materia y que se dan en el renderizado siguiendo modelos físicos. Para ello, se va a introducir brevemente el concepto de difusión de la luz para posteriormente citar los fenómenos físicos que lleva asociados, como son la reflexión especular y difusa por un lado y la translucidez y transparencia por otro.

1.2.1. La difusión de la luz

Desde el punto de vista de la óptica geométrica, se conoce como difusión de la luz al esparcimiento que se produce en los rayos de luz que componen un haz luminoso tras su reflexión sobre una superficie irregular o su transmisión a través de un medio traslúcido. El esparcimiento consiste en una desordenación de los rayos luminosos que componen el haz, asignando ángulos de reflexión o transmisión distintos a los de incidencia, de manera aleatoria en menor o mayor grado, produciendo así una distribución espacial aleatoria de los rayos de luz. Este fenómeno se puede producir al propagarse la luz dentro de un único medio (propagación) o al cambiar de medio material (reflexión y transmisión). A continuación, describiremos ambos fenómenos.

1.2.2. Reflexión de la luz: especular y difusa

Para una explicación sencilla, vamos a asumir el comportamiento corpuscular de la luz, sabiendo que hay otros fenómenos que no son cubiertos por este modelo, pero que no van a ser tratados en este trabajo. Cuando la luz incide sobre la superficie de un objeto, parte de ella se reflejará, es decir, rebotará sobre la superficie y se alejará del objeto en la dirección contraria a la de incidencia, pero con un ángulo igual al de incidencia. Este comportamiento es muy similar a una pelota lanzada contra el suelo o una pared. En una superficie perfectamente lisa, esto dará como resultado una apariencia de espejo, de ahí que se llame reflexión especular, y no se considera un caso de difusión. Si la superficie no es perfectamente lisa, sino que tiene rugosidades, esto dará lugar a que, aunque microscópicamente se siga cumpliendo la ley de la reflexión de la luz, macroscópicamente se produzca lo que se llama reflexión difusa y sea uno de los supuestos en los que se produce la difusión de la luz (figura 1.4). Ambos tipos de reflexiones superficiales, especular y difusa, son espectralmente neutras, por lo que el color de la luz reflejada es el mismo que la de la luz incidente.

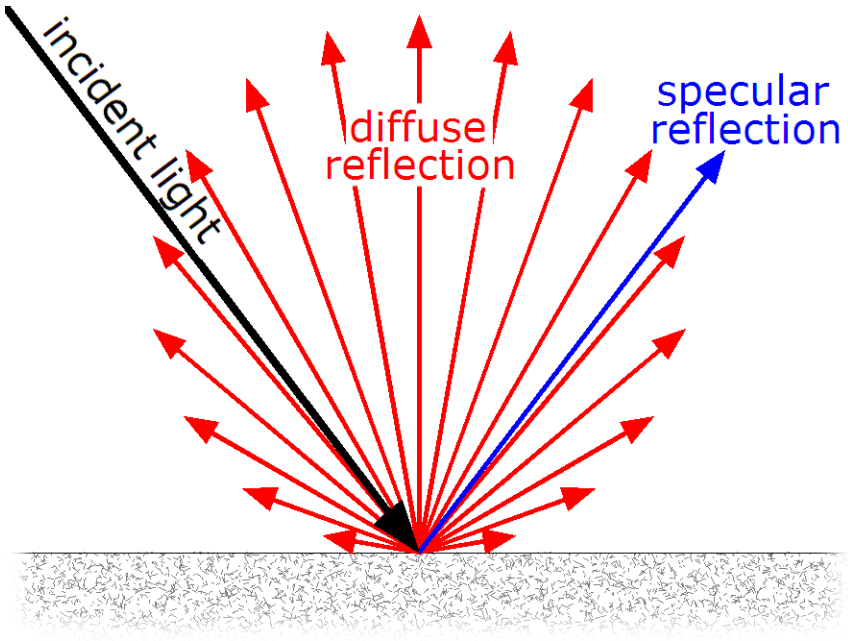

Figura 1.4: Explicación gráfica de la difusión y reflexión en la incidencia de la luz.

Sin embargo, no toda la luz se refleja desde la superficie del objeto. Por lo general, parte de la luz penetra en el interior del objeto iluminado interactuando con los pigmentos que forman el material del que está compuesto el objeto. Esta interacción puede darse en forma de absorción, re-emitiendose en otra zona del espectro como radiación infrarroja, o esparciendo la luz en todas direcciones en un fenómeno conocido como Esparcimiento (en inglés *scattering*). La conjunción de ambos fenómenos de absorción y esparcimiento constituyen lo que se conoce como color del material o color del objeto (*Object color* o *Material color* en inglés). Debido a que la absorción/esparcimiento de la energía luminosa

por parte de los pigmentos es selectiva en cuanto a las distintas longitudes de onda, este fenómeno es el responsable del color del objeto y suele comportarse desde un punto de vista macroscópico como una reflexión difusa, por lo tanto, también puede considerarse un ejemplo de difusión de la luz. Sin embargo, hay materiales que están constituidos con pigmentos especiales que tienen comportamientos distintos en función del ángulo de incidencia de la luz y del ángulo de observación. Este tipo de materiales son llamados genéricamente gonio-cromáticos y no serán analizados en este trabajo.

1.2.3. Transmisión de la Luz: translucidez y transparencia

En algunos casos, la difusión de la luz no se produce en la dirección contraria a la de incidencia en forma de reflexión difusa. Si el objeto es suficientemente delgado, la luz va a difundirse a través del objeto y salir por la parte posterior del mismo, y pasa a llamarse translúcido. Si el paso de la luz a través del medio material no provoca una desordenación de los rayos luminosos, manteniendo el mismo ángulo de salida para un mismo ángulo de entrada, el objeto pasará a denominarse transparente, como en el caso de los vidrios, y no se consideraría un caso de difusión de la luz.

1.2.4. Phisically Based Rendering: Modelos de material

Un modelo de material se describe matemáticamente mediante una BSDF (*Bidirectional Scattering Distribution Function*) que a su vez se compone de otras dos funciones: la BRDF (*Bidirectional Reflectance Distribution Function*) y la BTDF (*Bidirectional Transmittance Function*).

Dado que nuestro objetivo es modelar las superficies más comunes, nuestro modelo de material estándar se centrará en la BRDF e ignorará la BTDF, o la aproximará en gran medida. Por lo tanto, nuestro modelo estándar solo podrá imitar correctamente las superficies reflectantes, isotrópicas, dieléctricas o conductoras con longitudes de material cortas.

La BRDF describe la respuesta de la superficie de un material estándar como una función compuesta por dos términos:

- Una componente difusa, o f_d
- Una componente especular, o f_r

La relación entre una superficie, la normal de la superficie, la luz incidente y estos términos se muestra en la Fig. 1.5 (por ahora ignoramos la dispersión subsuperficial):

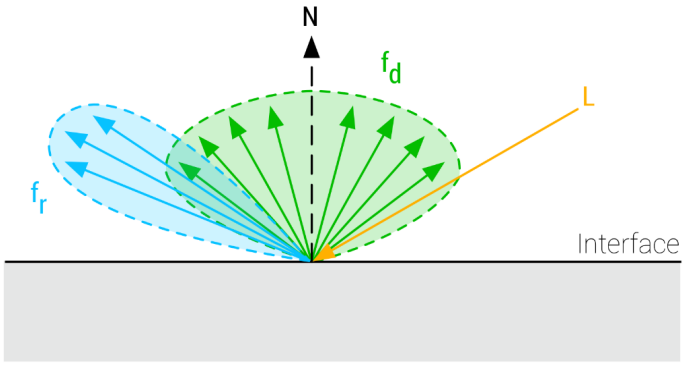

Figura 1.5: Relación entre una superficie, la normal de la superficie y la luz incidente

La ecuación de la superficie puede expresarse así:

$$f(v,l) = fd(v,l) + fr(v,l) \tag{1.1}$$

, donde v es el vector unitario y l es el vector unitario de la luz incidente.

Esta ecuación caracteriza la respuesta de la superficie para la luz incidente desde una sola dirección. La ecuación de representación completa requeriría integrar "l" en todo el hemisferio.

Las superficies más comunes no suelen estar formadas por una interfaz plana, por lo que necesitamos un modelo que pueda caracterizar la interacción de la luz con una interfaz irregular. Podemos modelar este tipo de superficies irregulares y rugosas como un conjunto de microsuperficies o microfacetas que sí son planas.

Una BRDF de microfacetas es una buena BRDF físicamente realista para este propósito. Dicha BRDF establece que las superficies no son lisas a nivel micro, sino que están formadas por un gran número de fragmentos de superficie plana alineados aleatoriamente, a los que se denomina microfacetas. La figura 1.6 muestra la diferencia entre una interfaz plana y una interfaz irregular a nivel micro:

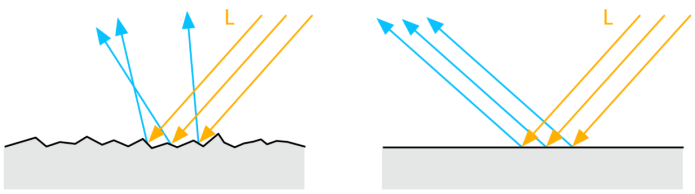

Figura 1.6: Superficies planas y con rugosidades o microfacetas

Solo las microfacetas cuya orientación esté a medio camino entre la dirección de la luz y la dirección de la mirada reflejarán la luz visible, como se muestra en la figura 1.7.

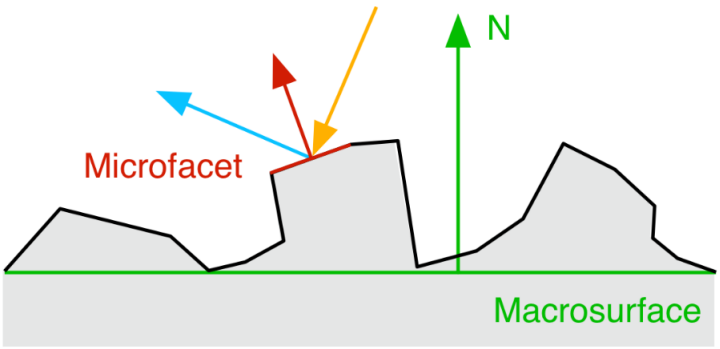

Figura 1.7: Superficie que refleja las microfacetas entre la dirección de la luz y la dirección de la mirada

Sin embargo, no todas las microfacetas con una normal correctamente orientada aportarán luz reflejada, ya que la BRDF tiene en cuenta el enmascaramiento y las sombras. Esto se ilustra en la figura 1.8.

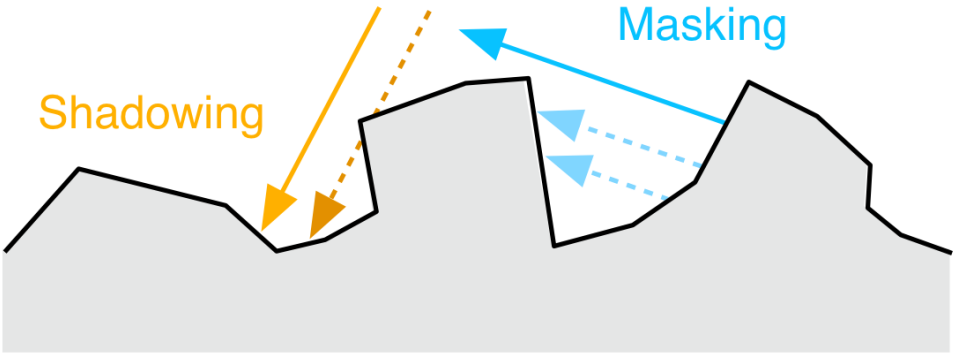

Figura 1.8: Ilustración del efecto de enmascaramiento y sombra

La BRDF de las microfacetas está fuertemente influenciada por un parámetro de rugosidad que describe lo suave (baja rugosidad) o lo áspera (alta rugosidad) que es una superficie a nivel micro. Cuanto más lisa es la superficie, más facetas están alineadas y más pronunciada es la luz reflejada. Cuanto más rugosa es la superficie, menos facetas están orientadas hacia la cámara y la luz entrante se dispersa lejos de la cámara después de la reflexión, dando un aspecto borroso a los reflejos especulares. Un modelo de microfacetas se describe mediante la siguiente ecuación (donde "x" representa la componente especular difusa):

El término "D" modela la distribución de las microfacetas (este término también se denomina NDF o *Normal Distribution Function*). Este término desempeña un papel primordial en la apariencia de las superficies, como se muestra en la figura 1.9. El término "G" modela la visibilidad (u oclusión o enmascaramiento de la sombra) de las microfacetas. Como esta ecuación es válida tanto para la componente especular como para la difusa,

la diferencia radica en la componente “fm” en la BRDF. Es importante señalar que esta ecuación se utiliza para integrarse sobre el hemisferio a nivel micro.

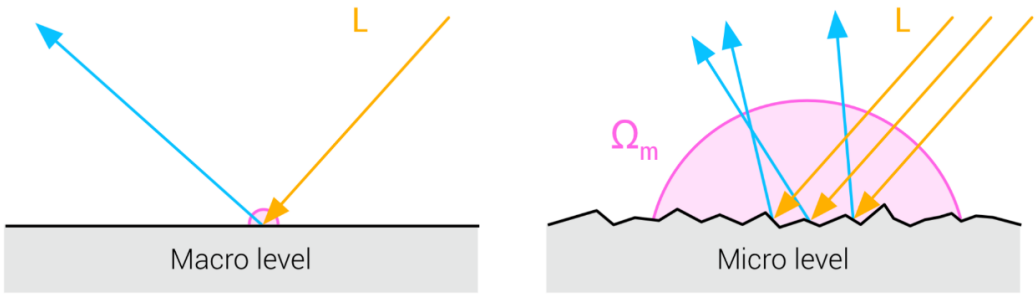

Figura 1.9: Diferencia entre hemisferio a nivel macro y micro

El diagrama anterior muestra que, a nivel macro, la superficie se considera plana. Esto ayuda a simplificar nuestras ecuaciones al suponer que un fragmento sombreado iluminado desde una única dirección corresponde a un único punto en la superficie. Sin embargo, a nivel micro, la superficie no es plana y ya no podemos suponer un único rayo de luz (sí podemos suponer que los rayos incidentes son paralelos). Dado que las microfacetas dispersarán la luz en diferentes direcciones, si se trata de un haz de rayos paralelos, debemos integrar la respuesta de la superficie en una semiesfera, que se indica como “m” en el diagrama anterior. Obviamente, no es práctico calcular la integración completa sobre el hemisferio de microfacetas para cada fragmento sombreado. Por lo tanto, nos basaremos en aproximaciones de la integración para las componentes especular y difusa.

Conductores y dieléctricos

Para comprender mejor algunas de las ecuaciones y comportamientos que se muestran a continuación, primero debemos entender claramente la diferencia entre superficies metálicas (conductoras) y no metálicas (dieléctricas). Como se ha comentado anteriormente, cuando la luz incide en una superficie, la luz se refleja como dos componentes separados: la reflectancia difusa y la reflectancia especular. La modelización de este comportamiento es sencilla, como se mostró en la figura 1.5.

Esta modelización es una simplificación de cómo la luz interactúa realmente con la superficie. En realidad, parte de la luz incidente penetrará en la superficie, se dispersará en su interior y saldrá de nuevo de la superficie como reflectancia difusa. Este fenómeno se ilustra en la figura 1.10.

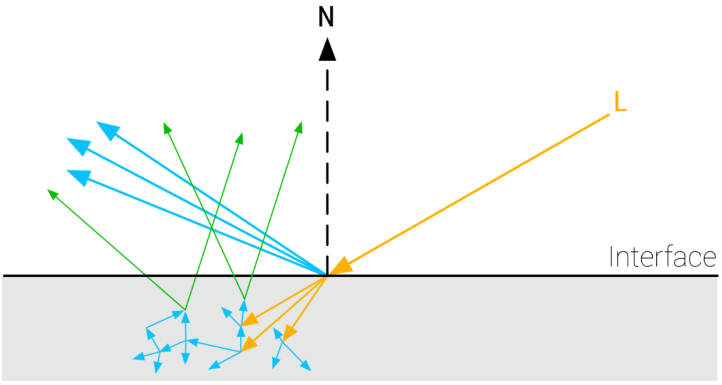

Figura 1.10: Ilustración de como parte de la luz incidente penetra en la superficie

Aquí radica la principal diferencia entre los conductores y los dieléctricos en cuanto a sus propiedades ópticas. En los materiales puramente metálicos no hay dispersión subsuperficial, lo que significa que no hay componente difusa (y más adelante se verá que esto influye en el color percibido de la componente especular). La dispersión se produce en los dieléctricos, lo que significa que tienen componentes especulares y difusas.

1.2.5. Conservación de la energía

La conservación de la energía es uno de los componentes clave de una buena BRDF para el renderizado basado en la física. Una BRDF que cumple el principio de conservación de la energía establece que la cantidad total de energía de reflectancia especular y difusa es menor que la cantidad total de energía incidente. Sin una BRDF que cumpla este principio, los artistas deben asegurarse manualmente de que la luz reflejada en una superficie nunca sea más intensa que la luz incidente.

Teniendo en cuenta las consideraciones anteriores, es posible afirmar que la difusión por reflexión y la difusión por transmisión son mutuamente excluyentes. Esto se conoce en el lenguaje de sombreado como un ejemplo de "conservación de energía", lo que significa que la luz que sale de una superficie nunca es más brillante que la que recae originalmente sobre ella. Esto es fácil de aplicar en un sistema de sombreado: uno simplemente resta la luz reflejada antes de permitir que ocurra el sombreado difuso. Esto significa que los objetos altamente reflectantes mostrarán poca o ninguna luz difusa, simplemente porque poca o ninguna luz penetra en la superficie, habiéndose reflejado de manera especular principalmente. Lo contrario también es cierto: si un objeto tiene una difusión importante, no puede ser especialmente reflexivo.

Ya se ha comentado que, cuando la luz incide sobre un material se divide fundamentalmente en dos componentes: una componente difusa y una componente especular. Existen otros fenómenos como la refracción, la luz absorbida en forma de calor y otros. Para explicar el concepto de conservación de la energía, la componente difusa y la especular son las realmente importantes. La componente difusa es aquella que se introduce en la superficie

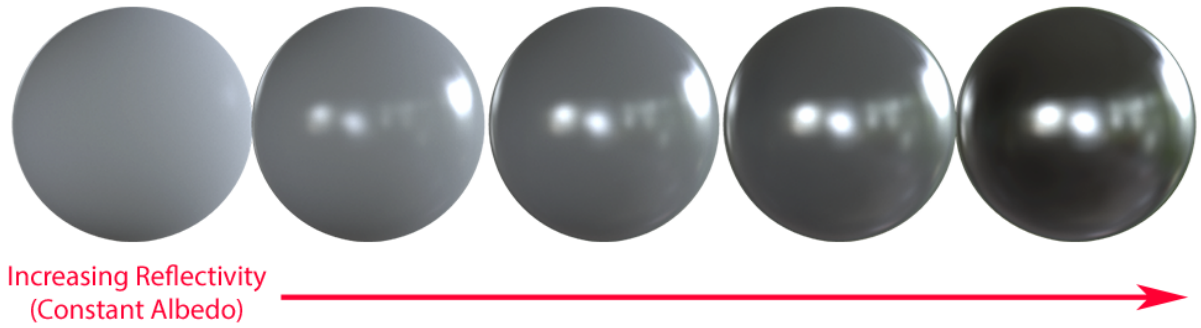

Figura 1.11: Fenómeno de conservación de la energía con el incremento de la reflexión. Fuente: https://programmerclick.com/article/35981204344/

y termina rebotando fuera del material. Esta componente de la luz es la responsable de dar el "color" principal de los materiales. El rojo de las manzanas o el amarillo de los plátanos.

La componente especular (o reflectiva) es aquella que rebota completamente sobre la superficie sin llegar a introducirse en el material. Al no introducirse en la superficie no se "contamina"del color del material. Esta componente especular es la causante de los reflejos. Estas dos componentes se dan simultáneamente y son las principales responsables de que los materiales se vean de la forma percibida en el mundo real.

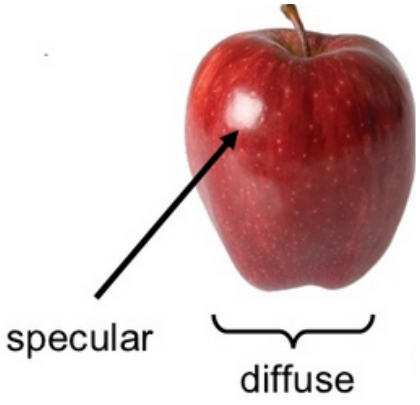

Figura 1.12: Componentes especular y difusa en una manzana

El principio de conservación de la energía indica que la luz que incide debe ser mayor o igual que la suma de sus componentes difusa y especular.

$$Li \geq Ld + Ls \tag{1.2}$$

Dónde Li es la luz que incide, Ld la componente difusa y Ls la componente especular. El principio de conservación de la energía nos revela un hecho muy importante: si el material tiene mucha componente difusa será a costa de la componente especular y viceversa.

1.2.6. Reflexión, Coeficientes de Fresnel y F_0

Hasta ahora se ha analizado la difusión de la luz fijando la existencia de componentes especular y difusa en la reflexión y fijando también la existencia de una transmisión difusa, que da lugar a los materiales translúcidos y una transmisión sin difusión que da lugar a los materiales transparentes. Sin embargo, que la luz se refleje o se transmita en mayor o menor medida depende del ángulo de incidencia sobre la superficie del objeto y de la interfaz de separación de dos medios. Esta dependencia ya fue estudiada por el insigne físico francés Agustine Fresnel y ha pasado a la literatura científica como los coeficientes de amplitud de Fresnel para la reflexión y transmisión que fijan la razón de los campos eléctricos reflejado e incidente r=E_r/E_i y transmitido e incidente t=E_t/E_i en función del ángulo de incidencia. Estos mismos valores, expresados sobre la potencia en lugar de sobre la amplitud de los campos se conocen como reflectancia y transmitancia en el caso de los materiales homogéneos.

Si hablamos de gráficos 3D por ordenador, la palabra Fresnel se refiere a la aplicación de los coeficientes anteriores en función de los ángulos de incidencia. Específicamente, la luz que incide sobre una superficie en un gran ángulo de incidencia será mucho más probable que se refleje que la que incide de manera normal sobre la superficie. Esto significa que los objetos renderizados con un efecto Fresnel adecuado obtendrán mucho más reflejos en los bordes que en la superficie central.

Los sombreadores PBR han hecho posible que se introduzcan las ecuaciones del Fresnel en el conjunto de transformaciones del modelo standard. La primera es que, para todos los materiales, la reflectividad se vuelve casi total para los ángulos de incidencia grandes: los "bordes" vistos en cualquier objeto liso deben actuar como espejos perfectos (sin color), sin importar el material. Cualquier sustancia puede actuar como un espejo perfecto si es suave y se ve en el ángulo correcto. La segunda anotación sobre las propiedades de Fresnel es que la curva o gradiente entre los ángulos no varía mucho de un material a otro. En la figura 1.13, podemos ver explicado el efecto Fresnel de una forma muy simple.

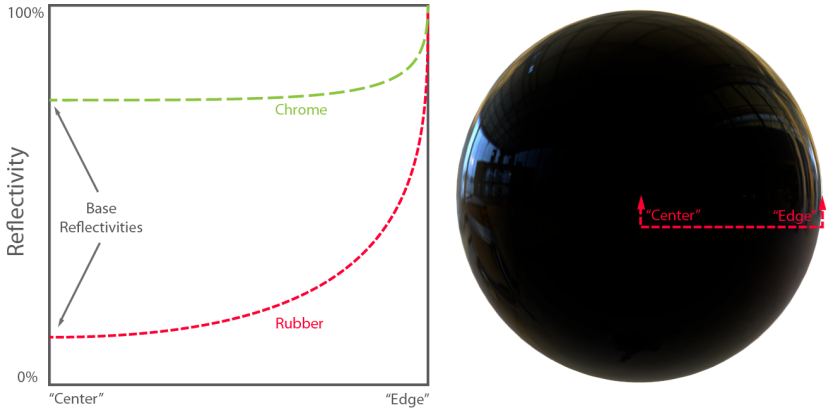

Figura 1.13: Explicación de cómo afecta la reflexión en las diferentes partes del objeto. Fuente: https://programmerclick.com/article/35981204344/

Hay una gran advertencia para el efecto Fresnel: rápidamente se vuelve menos evidente a medida que las superficies se vuelven menos lisas. La reflexión de la luz depende del ángulo de visión: En los bordes (el ángulo de visión es de 90º) se refleja casi con el 100 % de la luz (por tanto, hay 0 % de componente difusa) mientras que de frente (ángulo de visión de 0º) se refleja un porcentaje base llamado F0, a éste efecto se le llama Fresnel. En la figura 1.14 podemos ver una representación de un gráfico 3D con y sin el uso del Fresnel.

Figura 1.14: Comparación entre una figura con el uso de Fresnel y sin él.

1.3. Objetivos e hipótesis

Una forma de mejorar la calidad de la sensación de telepresencia en los dispositivos de realidad virtual es conseguir que la imagen reproducida en el HMD consiga tener la misma apariencia visual que la escena contemplada directamente. Es decir, que cuando un objeto presenta un color a los ojos de un observador fruto de la interacción de la luz, la materia y el sistema visual humano, la apariencia de ese mismo objeto reproducido a través de un dispositivo de realidad virtual sea la misma [16].

La consecución de un método de reproducción fidedigna del color es un tema tratado ampliamente en los últimos años debido al uso masivo de los distintos tipos de sistemas digitales que tienen la capacidad de producir color (agrupando bajo este epígrafe sistemas tan dispares como maquinaria de impresión offset, impresoras láser color, impresoras inyección de tinta, CRT, TFT, pantallas de plasma, LED, OLED, etc). Los primeros intentos de obtener una reproducción fidedigna del color se realizaban mediante ciclos cerrados de calibración realimentados, donde la entrada de una imagen patrón capturada en un dispositivo digital, como por ejemplo un escáner, era comparada con la salida en papel a través de la impresora. La desviación de la imagen impresa respecto a la imagen patrón original era calculada introduciéndola en el dispositivo de entrada y corregida en un nuevo ciclo. Este método permitía una reproducción más o menos buena del color para ese sistema productor de color en concreto, pero no podía extenderse a otros sistemas ya que entre ellos no existía conexión alguna. Posteriormente y respondiendo a las necesidades de la industria, se han realizado grandes avances en los últimos años en la reproducción

fidedigna de colores y la independencia del dispositivo en la especificación de un color.

Estos avances se han conseguido gracias a la utilización de sistemas informáticos tanto en la etapa de diseño como en la fase de producción de un producto y a la implementación en este soporte de Sistemas Administradores de Color (Color Management Ssystems- CMS) que mediante el uso de los perfiles colorimétricos de cada dispositivo, realizan la transición entre el color especificado en la fase de diseño hasta el color obtenido en la fase de producción, pasando por un espacio de conexión de color (Profile Conexion Space- PCS). La existencia de este espacio de conexión de color común para todos los dispositivos, permite la obtención de una reproducción fidedigna de color entre dispositivos pertenecientes a distintos sistemas.

La investigación y desarrollo de estos sistemas de gestión de color ha sido llevada a cabo tanto por Universidades e Institutos de investigación internacionales, como por empresas relacionadas con los dispositivos reproductores de color o los sistemas de Diseño Asistido por Ordenador- CAD (Microsoft, Adobe, Kodak, AGFA, Pantone, Apple, Sun, Silicon Graphics, etc.) que han constituido el Consorcio Internacional del Color (International Color Consortium- ICC). Fruto de esa asociación se ha propuesto el formato de perfil ICC para caracterizar a cada dispositivo y un método de gestión de color (CMM) que realiza la transformación de las coordenadas de color de un espacio de reproducción de un dispositivo, dependiente de ese dispositivo, a otro, utilizando para ello un espacio común de representación independiente del dispositivo que utilizarían tanto plataformas de ordenador, dispositivos y periféricos, como sistemas operativos y aplicaciones informáticas. Ejemplo de aplicaciones informáticas con estructura ICC son ColorSmart utilizado por Hewlett-Packard, KCMS de Kodak y ColorSync de Apple.

Sin embargo, el perfil ICC presenta problemas en la implementación debido, entre otros, al espacio de conexión de color que no satisface las complejas particularidades del sistema humano de visión del color. Para ello, la manera que se está estudiando para solucionar estos problemas es la introducción de modelos de apariencia del color del sistema visual humano como espacios de color de conexión. La investigación sobre modelos de visión cromática está avanzando en los últimos años debido a la propuesta de modelos vectoriales de visión del color, alguno de ellos muy elaborados [17, 18, 19], aunque todavía existen intentos de propuesta de modelos fisiológicos [20]. En todos los casos, los modelos se postulan para observadores normales, suponiendo como tales alguno de los observadores patrón propuestos por la Comisión Internacional de Iluminación (CIE). Estos observadores patrón fueron definidos mediante las funciones de mezcla obtenidas en las experiencias realizadas con una muestra de observadores más o menos grande a los que se les somete a sesiones de igualaciones cromáticas.

En cuanto a los nuevos medios disponibles para implementar matemáticamente las distintas transformaciones colorimétricas que se aplican al tratamiento digital de imágenes y a la reproducción fidedigna del color, cabe destacar la utilización de las redes neuronales artificiales que permiten realizar transformaciones que no serían posibles realizar de forma analítica o cuyo proceso no permitiese ser aplicadas en tiempo real por ser costosas en cuanto a tiempo de cálculo [21, 22, 23].

Para el caso de la realidad virtual, la cual para representar valores colorimétricos utiliza el espacio de color RGB, se presenta el problema añadido de tener que gestionar no solo el color final de un objeto sino todo el proceso de interacción de la luz y la materia. La interacción de una fuente luminosa sobre un objeto real no se puede reflejar de manera fidedigna únicamente desde los valores RGB de una imagen digital. El proyecto de tesis doctoral que se presenta tiene como fin último contribuir a mejorar la sensación de fidelidad en la reproducción de escenas 3D a través de dispositivos de realidad virtual. Para ello, se estudiará la forma de incluir un sistema de gestión de color en los dispositivos de realidad virtual, con la problemática añadida de tener que soportar una alta frecuencia de refresco en las imágenes y una baja latencia. Además, introduciremos el concepto de textura espectral asociada a objetos 3D en el renderizado de imágenes para realidad virtual, y por último, trabajaremos el concepto de apariencia visual en dispositivos de realidad virtual.

1.4. Contribuciones científicas realizadas

La presentación de esta tesis doctoral se ha realizado mediante el procedimiento de compendio de artículos, lo cual implica presentar varios artículos de gran impacto junto con dicho documento. Durante el desarrollo de este documento, se expondrán los diferentes artículos publicados como hilo principal de la tesis doctoral, en el orden que facilita la comprensión de la misma, no coincidiendo en algún caso en el orden de publicación debido a los avatares del proceso de revisión y envío de cada una de las revistas.

En primer lugar, se ha incluido el primer artículo publicado en la revista *Sensor*, cuya idea principal se basa en la calibración de un HMD mediante técnicas colorimétricas y de gestión de color. Para comprobar su correcto funcionamiento, hemos validado dicha calibración con un conocido test de deficiencias visuales como es el test de Ishihara [24]. Como paso posterior, se presenta el artículo publicado en la revista *Electronics* y cuya finalidad es la de conseguir aplicar texturas hiperespectrales en objetos previamente escaneados mediante un escaner 3D [25]. Esto ayuda a mejorar la fidelidad en la representación gráfica en cuanto a color se refiere. El tercer artículo presentado es un caso de uso de la aplicación de texturas hiperespectrales a un conocido test de detección de deficiencias visuales, como es el Farnsworth Munsell 100 Hue Test, con el principal objetivo de validar los dispositivos de realidad virtual para su uso profesional. Este artículo fue publicado en la revista *IEEE Access* [26]. Por último, el artículo publicado en la revista *Coloration Technology* presenta que, aunque las técnicas de calibración y gestión del color espectral funcionan de una forma excepcional, aún es necesario seguir desarrollando otras mejoras como pueden ser los modelos de apariencia para el tratamiento de escenarios virtuales [27]. En este último paso donde termina esta tesis es donde actualmente se encuentra la investigación de la que se espera seguir obteniendo nuevos resultados en investigaciones posteriores.

Además de los artículos utilizados para el desarrollo de la tesis también se han pre-

sentado numerosos congresos. Durante el desarrollo de la tesis, también se participó en varios proyectos de investigación. Todos los méritos relacionados con la tesis doctoral aquí expuesta se encuentran recogidos en el Anexo I.

Capítulo 2

Gestión del color

Un espacio de color es una representación matemática del conjunto de colores que permite la especificación de un color de manera estándar [28]. Todos los estímulos de color que la vista puede percibir constituyen un espacio estructurado. Los espacios de color ayudan a definir los colores a partir de números y fórmulas, ofreciendo así un criterio objetivo para clasificar los colores. La aparición de la medición del color en el año 1931 permitió describir con precisión la estructura de todos los colores perceptibles y definir los límites para su uso [29]. En las siguientes secciones se diferenciará entre los espacios de color independientes y los espacios dependientes del dispositivo. En el primer caso, se puede medir el color de forma absoluta, independientemente del dispositivo que se esté utilizando, y por tanto no estará ligado a un dispositivo concreto, pudiéndose descentralizar su representación. En el segundo caso, el color medido será propio del dispositivo representado, lo que quiere decir que, si cambiamos de dispositivo, el valor del color cambiará.

2.1. Espacios de color independientes del dispositivo

En esta sección haremos una introducción al espacio de color CIE XYZ 1931 y al espacio de color CIE L*a*b* 1976. Ambos espacios de color son independientes del dispositivo y serán utilizados durante todo el desarrollo de esta tesis doctoral como pieza fundamental en la búsqueda de conseguir una reproducción del color lo más fiel posible independientemente del dispositivo o visor de realidad virtual utilizado.

2.1.1. XYZ CIE 1931

El espacio CIE XYZ 1931 se basa en los trabajos llevados a cabo en el final de los años 20 del siglo XX para definir lo que se conoce como Observador Patrón Colorimétrico. Este observador patrón se definió mediante pruebas de igualación de color utilizando

tres primarios espectrales dando lugar así a las primeras funciones de igualación de color estandarizadas (Color Matching Functions – CMFs). Mediante la mezcla de estos primarios en las proporciones indicadas por estas CMFs se pueden obtener colores metámeros de todos los colores visibles por el ser humano. Estas funciones de mezcla, junto con las propiedades del sistema visual humano, permitieron definir el Espacio CIE XYZ Para visualizar el espacio CIE XYZ, hay que pensar en un sistema de coordenadas cartesianas tridimensional con ejes etiquetados como X, Y y Z. En el espacio de color XYZ, Y corresponde a la luminancia relativa; Y además contiene información de color relacionada con la respuesta de los conos "M"del ojo humano. Mientras X y Z contienen información adicional relacionada con la respuesta de los conos L y S respectivamente, aunque existen otros espacios de color más directamente relacionados con la respuesta de los conos.

El espacio CIE XYZ se utiliza normalmente como primer paso en la medida del color realizada por un colorímetro, un espectrofotómetro o un espectroradiómetro. Un colorímetro puede contener tan solo tres sensores, cada uno de ellos coincidente en respuesta con una de las funciones de mezcla CMFs que componen la terna XYZ, y suele utilizarse para calibrar y ajustar las pantallas, entre otros usos. Un espectroradiómetro, sin embargo, informará de la respuesta espectral completa a intervalos definidos a lo largo del espectro, por ejemplo, cada 10 nanómetros, y se utilizará normalmente para medir la distribución espectral de potencia de fuentes luminosas. Partiendo de esta distribución espectral de potencia y utilizando las CMFs, se puede definir el color de las fuentes luminosas en el espacio XYZ.

Otro uso del espacio XYZ es como espacio de conexión de perfiles PCS dentro de un sistema gestor de color (Color Management System – CMS), donde puede utilizarse en lugar de CIE Lab. Este espacio de color recoge todo el espectro visible humano, por eso se considera de gran fidelidad cromática [30].

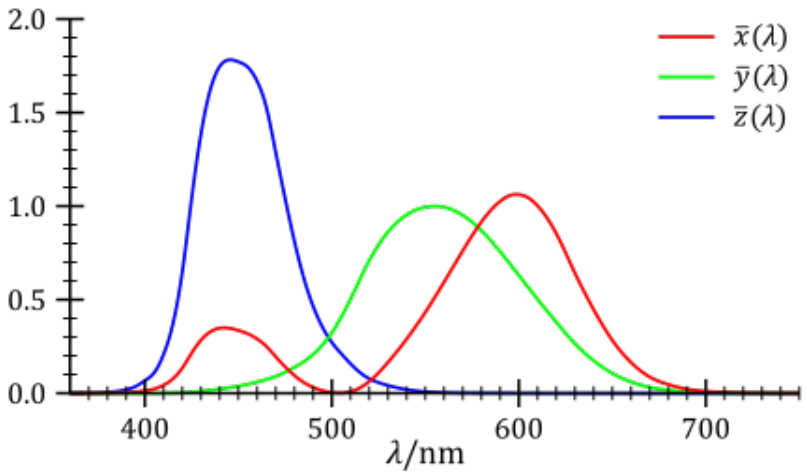

Figura 2.1: Funciones de igualación de color que definen el espacio de color CIE XYZ.

2.1.2. CIE L*a*b* 1976

El Espacio CIE L*a*b* o CIELAB, es uno de los sistemas de representación del color más usado en la industria. Las coordenadas cromáticas de este sistema son L* claridad y a* y b* que corresponden con los ejes de abscisas y coordenadas de un sistema de ejes perpendiculares que pueden tener valores positivos y negativos (Fig. 2.2). El eje a* positivo, se corresponde con el tono rojo y el valor a* negativo con el tono verde. El eje b* positivo se corresponde con el tono amarillo y el negativo con el tono azul-violáceo.

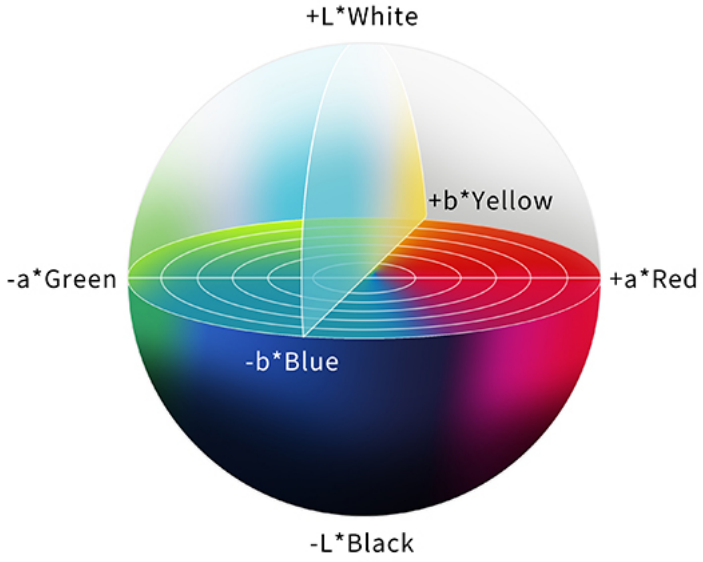

Figura 2.2: Diagrama de representación del espacio de color CIE L*a*b*.

El espacio de color CIE L*a*b* 1976 se deriva del espacio CIE XYZ 1931, ya que utiliza el mismo observador patrón definido en 1931 para campos visuales de 2^{o}, pero trata de recoger en una primera aproximación las no linealidades del sistema visual humano. Como principal diferencia, además de las no linealidades, cabría destacar que es un espacio cromático definido alrededor de un blanco de referencia, normalmente el correspondiente al iluminante D65.

$$\begin{aligned} L^* &= 116 f(\frac{Y}{Y_n}) - 16 \\ a^* &= 500(f(\frac{X}{X_n}) - f(\frac{Y}{Y_n})) \\ b^* &= 200(f(\frac{Y}{Y_n} - f(\frac{Z}{Z_n})) \end{aligned} \tag{2.1}$$

donde:

$$f(t) = \begin{cases} t^{\frac{1}{3}} & para \quad t>(\frac{6}{29})^3 \\ \frac{1}{3}(\frac{29}{6})^2 t + \frac{4}{29} & para \quad otro \quad valor \end{cases} \tag{2.2}$$

Durante el desarrollo de esta tesis, con el fin de poder comparar la diferencia entre el color real y el color reproducido en nuestro HMD, hemos utilizado este espacio de color y las fórmulas de diferencia de color que se basan en el mismo. En concreto, la fórmula de diferencia de color CIEDE2000 [31] nos ayuda a calcular la distancia perceptiva entre dos colores con representación en dicho espacio, de tal manera que nos hagamos una idea de cómo de fiel es nuestra representación con mejoras implementadas respecto a la representación del escenario clásico de VR.

2.2. Espacios de color dependientes del dispositivo

En esta sección se hará una introducción a los espacios de color dependientes del dispositivo. Dichos espacios limitan la representación fiel del color, ya que su espectro es mucho más acotado. Sin embargo, utilizar dicho espacio es indispensable en numerosas ocasiones. Nuestro caso es un caso en el que tenemos que trabajar con el espacio de color RGB, que es completamente dependiente del dispositivo utilizado, lo que nos obliga a realizar un complejo tratamiento y gestión para poder trabajar desde un punto de vista general como lo puede hacer XYZ y L*a*b* para finalmente transformarlo a RGB (Eq. 2.1).

2.2.1. Espacio de color RGB

El espacio de color RGB está formado por 3 dimensiones asociadas a 3 ejes ortogonales, el rojo, el verde y el azul. La representación espacial de estas 3 dimensiones se hace en forma de cubo, para así poder entender cómo se pueden conseguir el resto de colores del espacio cromático (Fig. 2.3). Una versión digital de este espacio de color es utilizado habitualmente por dispositivos tecnológicos, ya que hace fácil su representación. Un ejemplo de ello, es el uso en monitores o en todo tipo de pantallas. Este espacio de color ha sido criticado por los profesionales del campo editorial, debido a su limitado espectro de color, lo que significa que algunos colores que son visibles, incluso algunos que pueden ser reproducidos en CMYK, no pueden ser representados en el espacio sRGB (Fig. 2.4), espacio digital basado en RGB de amplio uso [32].

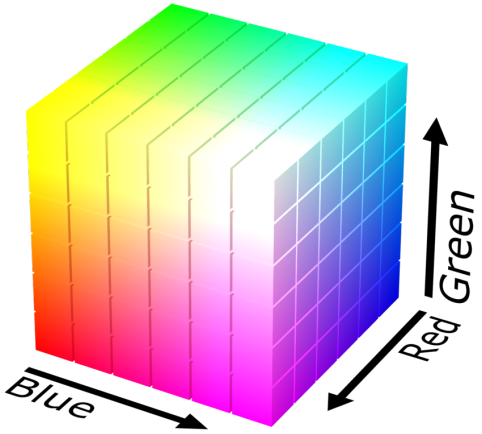

Figura 2.3: Modelo de espacio de color RGB representado en un cubo tridimensional.

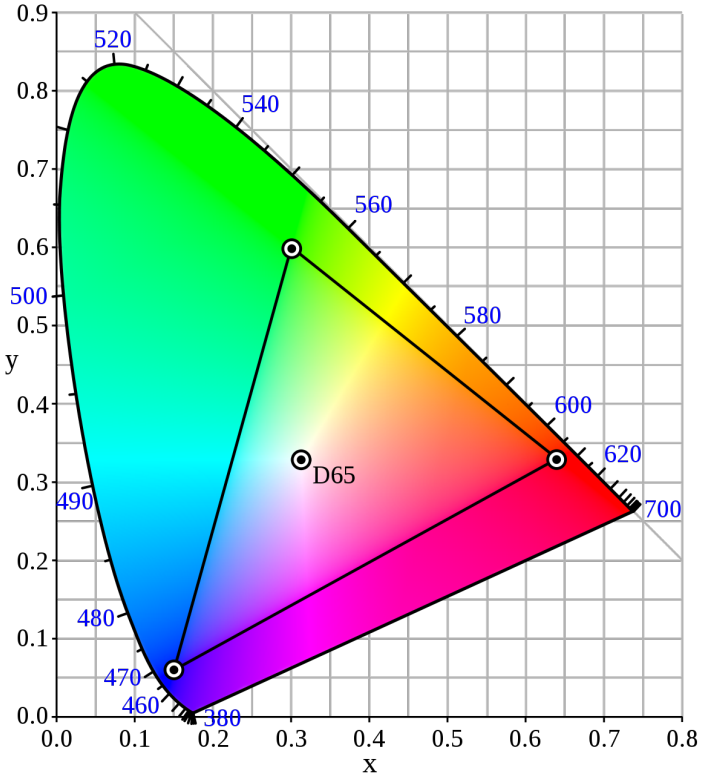

Figura 2.4: Gamut del espacio de color sRGB representado en un diagrama de cromaticidad x,y CIE 1931

2.3. Sistema de Gestión de Color

Un sistema de gestión del color establece una serie de transformaciones colorimétricas que permiten modificar las coordenadas de los espacios de color independientes del dispositivo (CIE XYZ, CIE Lab) en las de los espacios de color dependientes del dispositivo (RGB, CMYK) y viceversa. Todas estas transformaciones matemáticas requieren un tiempo de cálculo a menudo demasiado largo, ya que los valores de resolución y frecuencia de actualización del dispositivo son tales que la gestión del color se vuelve inviable desde el punto de vista técnico. Esto es debido a que es necesario vincular varias transformaciones colorimétricas. En la figura 2.5 podemos ver de una mejor forma el esquema de funcionamiento de un sistema de gestión del color.

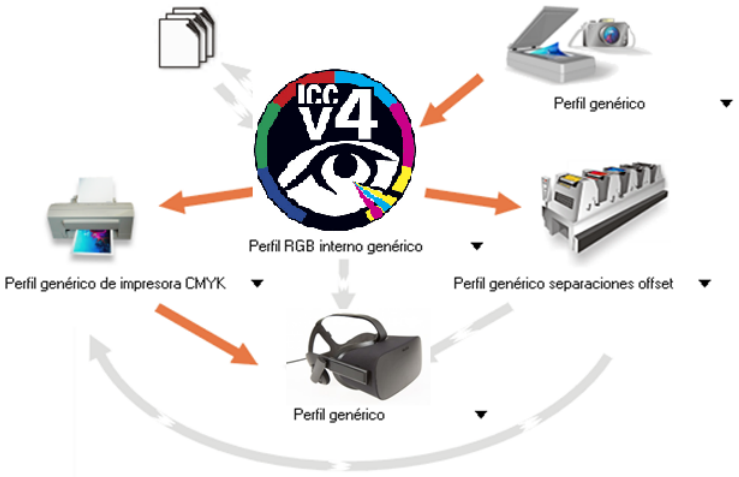

Figura 2.5: Flujo de trabajo de un perfil ICC.

El perfil ICC es un conjunto de datos que caracteriza a un dispositivo de entrada o salida de color según los estándares promulgados por el Consorcio Internacional del Color (ICC). Los perfiles de color establecen una correspondencia de color entre un espacio independiente del dispositivo y un espacio dependiente del dispositivo, el cual será CIELAB o CIEXYZ

Aunque pueda parecer la solución definitiva, el perfil ICC puede ocasionarnos una serie de problemas, ya que por defecto utiliza una fuente luminosa D50 para realizar sus cálculos y esto puede hacernos errar a la hora de realizar la transformación con cualquier otra fuente luminosa. Es por ello que, aunque nuestros primeros trabajos incluían un perfil ICC [33, 34] en el visor para realizar la gestión del color, finalmente se decidió prescindir de él y realizar los cálculos programando nosotros mismos la función en nuestro propio software con la matriz de transformación siguiente (Eqs. 2.3 y 2.4).

$$\begin{aligned} R' &= R^{\gamma_1} \\ G' &= G^{\gamma_2} \\ B' &= B^{\gamma_3} \end{aligned} \tag{2.3}$$

$$\begin{pmatrix} X \\ Y \\ Z \end{pmatrix} = \begin{pmatrix} X_{R'max} & X_{G'max} & X_{B'max} \\ Y_{R'max} & Y_{G'max} & Y_{B'max} \\ Z_{R'max} & Z_{G'max} & Z_{B'max} \end{pmatrix} * \begin{pmatrix} R' \\ G' \\ B' \end{pmatrix} \tag{2.4}$$

Durante el desarrollo de esta tesis, nuestro propósito ha sido el de conseguir valores finales RGB para que puedan ser reproducidos por cualquier visor de realidad virtual. Sin embargo, el cálculo matemático del color lo haremos con un espacio independiente y necesitaremos utilizar una función de transformación basada en matrices para que nuestro sistema digital entienda los valores cromáticos. La matriz de transformación que vamos a utilizar en todo momento durante el desarrollo de todos los trabajos es la que aparece a continuación (Eq. 2.4) y ha sido definida para el dispositivo de realidad virtual que se ha utilizado en esta tesis mediante un proceso de caracterización cromática. Además de dicha matriz, nuestro sistema necesita de una corrección gamma previa como la que representamos en la (Eq. 2.3).

2.4. Información hiperespectral para mejorar la representación del color

Cuando hablamos de texturas hiperespectrales tenemos que pensar que al tener información medida directamente del objeto como es la reflectancia podemos obtener un cálculo mucho más fiel del color, ya que estamos separando la dependencia que la fuente luminosa puede darle a la representación del color. Cuando medimos la reflectancia de un material estamos obteniendo el valor bruto de su componente espectral, lo cual nos da la gran posibilidad de calcular el color bajo cualquier fuente luminosa. Mientras que con un espacio de color como RGB tenemos que modelar cualquier color con 3 componentes principales, cuando tenemos la reflectancia espectral de un objeto tenemos mucha más información. Esto hace que podamos hacer un cálculo mucho más exacto y próximo a la realidad. En la siguiente imagen (Fig. 2.6) podemos ver la diferencia de representación entre un espacio blanco y negro, un espacio RGB, un espacio multiespectral y por último un espacio hiperespectral como el que en esta tesis se ha utilizado.

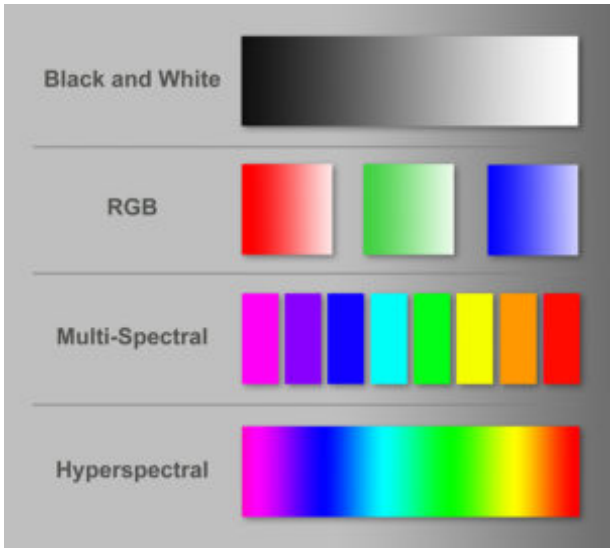

Figura 2.6: Comparativa de un espacio hiperespectral con otros espacios.

Además, es necesario saber que para calcular el color con una representación hiperespectral es necesario contar con tres componentes básicos: La reflectancia del material, el observador patrón y la fuente luminosa utilizada para representar el objeto. Hasta ahora hemos explicado el concepto de reflectancia y fuente luminosa, pero ¿Qué es el observador patrón u observador estándar? La gente percibe los colores de manera diferente. Para lograr la uniformidad de percepción, la CIE estipula funciones de ponderación espectral. Estas funciones describen cómo las personas perciben los colores. Se basan en curvas de sensibilidad determinadas experimentalmente del cono L de onda larga (X), el cono M de onda media (Y) y el cono S de onda corta (Z). Los receptores de color (conos) en la retina humana residen dentro de un arco de 2° de la fóvea en la llamada mácula. Una vez obtenidas los 3 elementos básicos de la componente del color, podemos empezar a dar una representación en el espacio CIE XYZ de la que más tarde pasaremos a RGB como anteriormente se ha explicado.

Capítulo 3

Revisión Sistemática de la literatura

Una revisión sistemática de la literatura (SLR) identifica, selecciona y evalúa críticamente la investigación para responder a una pregunta claramente formulada. La revisión sistemática debe seguir un protocolo o plan claramente definido en el que los criterios se establezcan claramente antes de realizar la revisión. Es una búsqueda completa y transparente realizada en múltiples bases de datos. Implica planificar una estrategia de búsqueda bien pensada que tenga un enfoque específico o responda a una pregunta definida. La revisión identifica el tipo de información buscada, criticada e informada dentro de los plazos conocidos.

3.1. Metodología seguida en el proceso de revisión

La metodología empleada durante la revisión de los artículos fue la de Kitchenham et al.[35], en la cual se planifica un objetivo de búsqueda con varias preguntas de investigación, se ejecuta el plan de búsqueda aplicando criterios de exclusión e inclusión y por último se valida el resultado. En la figura 3.1 se pueden observar las características de dicho modelo.

Dicha metodología es muy común entre las revisiones sistemáticas de la literatura en el campo de *Computer Science*. Para entender mejor como hemos aplicado dicha metodología a nuestro problema concreto, hemos elaborado el esquema 3.2.

3.2. Estrategia de búsqueda y criterios de selección

La localización de artículos se realizó el día 10 de Mayo de 2020, en SCOPUS y Web Of Science. Además, se añadieron otros artículos que se consideraron de gran relevancia para la revisión literaria. Las palabras clave utilizadas para la búsqueda en las 2 bases de

Figura 3.1: Metodología definida según Kitchenham

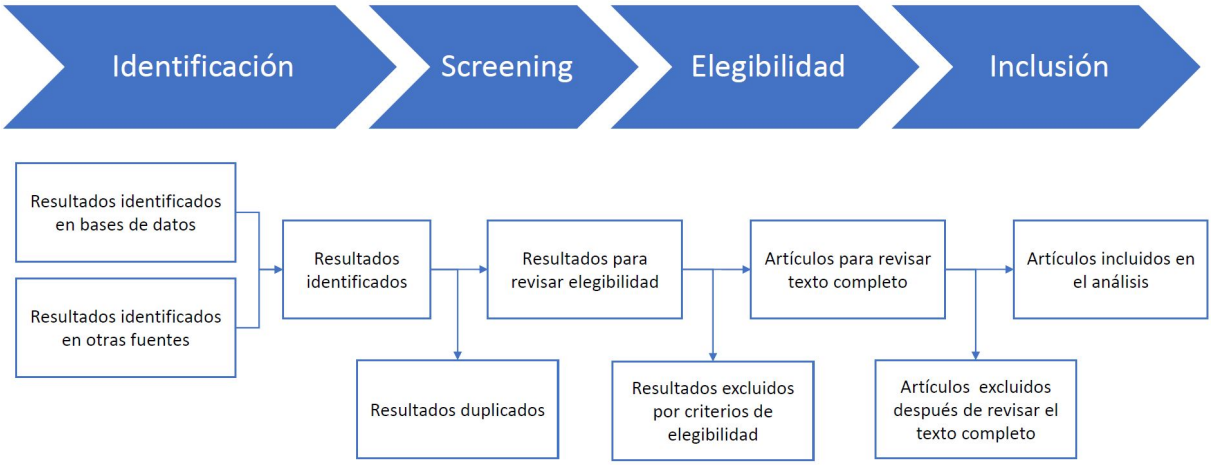

Figura 3.2: Metodología seguida para el proceso de revisión de artículos

datos, fueron: phisically based rendering y virtual reality. Los términos de búsqueda se utilizaron inicialmente en forma independiente, habiendo sido posteriormente agrupados empleando el término AND: phisically based rendering AND virtual reality. Respecto a los criterios de selección, se incluyeron artículos en inglés y en español que estuviesen publicados en revistas con indicios de calidad y revisión por pares, que mostrasen evidencias concluyentes, mediciones claras y resultados significativos. Los artículos seleccionados deberán de estar publicados con fechas posteriores a 1 de Enero de 2015.

Además se eligieron 3 preguntas de investigación en la cúales se basó la búsqueda. Todos los artículos seleccionados deben responder a dichas preguntas. Éstas preguntas de investigación son las siguientes:

- ¿Las técnicas propuestas son aplicables a entornos virtuales?
- ¿Mejora la técnica de renderizado basado en la física la calidad de la experiencia original?

- ¿Es importante el proceso de iluminación en la representación de realidad virtual?

Por último, bajo el criterio de resultados, se tuvieron en cuenta aquellos estudios y revisiones de la literatura que se consideraron oportunos y convenientes para el tema de la revisión literaria.

3.3. Extracción de datos y evaluación de calidad

La organización de los artículos incluidos se realizó mediante la web gestión de publicaciones y revisiones bibliográficas «Parsif.al». Se extrajeron datos de los estudios como los resultados obtenidos al aplicar esta técnica, nuevos desarrollos y mejoras en la realidad virtual conseguidas con el uso del nuevo renderizado. En cuanto a la evaluación de la calidad, se eligieron 3 parámetros en las que se podía valorar desde 0 a 5 según cumpliera el documento con ellos. Los parámetros de evaluación de calidad fueron los siguientes:

- Aplicación del PBR a realidad virtual
- Mejora de los resultados clásicos
- Claridad del documento

3.4. Proceso de selección de artículos y aspectos metodológicos

En la búsqueda realizada en Web Of Science se encontraron 72 artículos. Fue aplicada una limitación en el año 2015 de publicación resultando 28 artículos, seguidamente y tras limitar la búsqueda a texto completo resultaron los 28. Posteriormente, se filtró la búsqueda por idioma, seleccionando únicamente artículos en español e inglés resultaron 19 artículos, descartando cualquier otro idioma.

En la búsqueda realizada en Scopus se encontraron 16 artículos. Fue aplicada una limitación en el año 2015 de publicación resultando 10 artículos, seguidamente y tras limitar la búsqueda a texto completo resultaron los 10. Posteriormente, se filtró la búsqueda por idioma, seleccionando únicamente artículos en español e inglés resultaron 4 artículos, descartando cualquier otro idioma.

Todos estos artículos se encuentran en revistas de alto índice de impacto, no se contemplan conferencias. Además de las dos grandes bases de datos se añadieron otros artículos (4) considerados de gran relevancia para la revisión, que se extrajeron de fuentes como Schoolar. En la figura 3.3 se puede observar el esquema del proceso de selección de artículos.

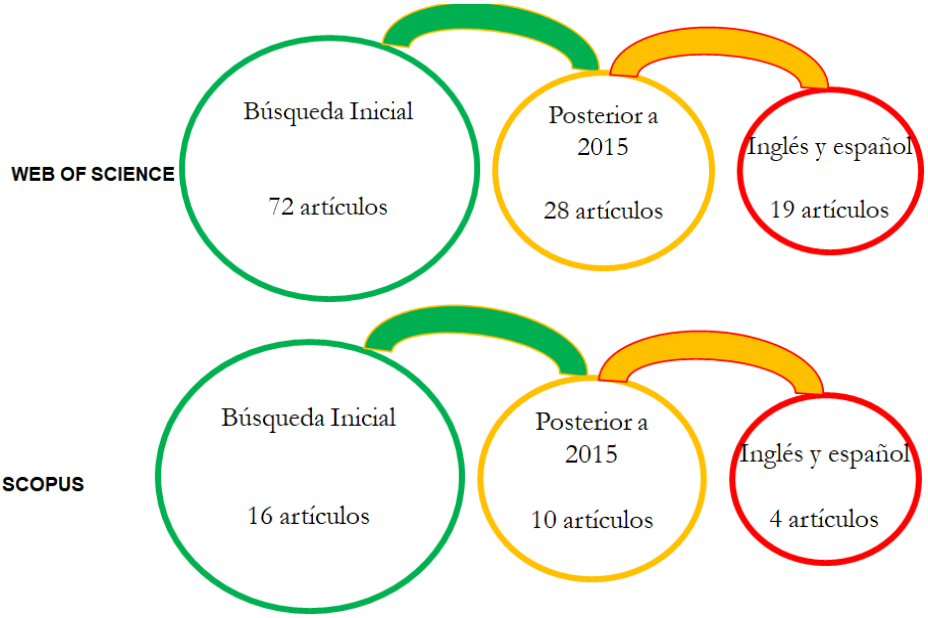

Figura 3.3: Proceso de selección de artículos en Web Of Science y Scopus

3.5. Análisis y resultados

En la siguiente tabla 3.1 se mostrarán los artículos que finalmente se seleccionaron indicando las puntuaciones obtenidas por los diferentes parámetros de evaluación de calidad. Hemos destacado aquellos artículos que su puntuación es mayor a 10 puntos sobre 15, para finalmente considerar estas contribuciones de carácter muy relevantes para el contenido de dicha tesis doctoral.

Finalmente, tras analizar en detalle los 5 artículos que consideramos de máxima relevancia, hemos sacado en conclusión los siguientes aspectos:

- Evidencias de que PBR mejora los resultados clásicos en renderizados 3D.
- El uso de PBR dificulta el renderizado en realidad virtual a tiempo real dado su alta coste computacional.
- El uso de técnicas como el Deep-learning pueden ayudar a mejorar la fidelidad en la representación.
- PBR se está imponiendo en escenas en la cuales se requieren una alta fidelidad de la realidad, videojuegos o en la industria del automóvil son algunos ejemplos.

Autores	Título	Base de datos	P1	P2	P3
Debattista, K. and Bashford-Rogers, T. and Harvey, C. and Waterfield, B. and Chalmers, A.	Subjective evaluation of high-fidelity virtual environments for driving simulations	SCOPUS	4	2	2
Park, J. and Park, H. and Yoon, S.-E. and Woo, W.	Physically-inspired Deep Light Estimation from a Homogeneous-Material Object for Mixed Reality Lighting	SCOPUS	3	3	3
Chamilothori, K. and Wienold, J. and Andersen, M.	Adequacy of Immersive Virtual Reality for the Perception of Daylit Spaces: Comparison of Real and Virtual Environments	SCOPUS	5	4	5
Nunes, A.L.P. and Maciel, A. and Cavazzola, L.T. and Walter, M.	A laparoscopy-based method for BRDF estimation from in vivo human liver	SCOPUS	2	4	2
Zibrek, Katja and Martin, Sean and Mcdonnell, Rachel	Is Photorealism Important for Perception of Expressive Virtual Humans in Virtual Reality?	WOS	4	2	2
Shen, Hongxue and Zhang, Zhifeng and Shang, Zhanlei	FAST GLOBAL RENDERING IN VIRTUAL REALITY VIA LINEAR INTEGRAL OPERATORS	WOS	5	5	5
Magoules, Frederic and Gbikpi-Benissan, Guillaume and Callet, Patrick	Ray-tracing domain decomposition methods for real-time simulation on multi-core and multi-processor systems	WOS	2	2	2
Wang, Q. H. and Huang, Z. D. and Ni, J. L. and Xiong, W. and Li, J. R.	A novel force rendering approach for virtual assembly of mechanical parts	WOS	3	3	3
He, Xue-Jian and Choi, Kup-Sze	Using analytical force model for efficient deformation simulation and haptic rendering of soft objects	WOS	4	1	2
Pulkki, Ville and Svensson, U. Peter	Machine-learning-based estimation and rendering of scattering in virtual reality	WOS	4	1	2
Sekhavat, Yoones A.	Privacy Preserving Cloth Try-On Using Mobile Augmented Reality	WOS	3	1	1
Nunes, A. L. P. and Maciel, A. and Cavazzola, L. T. and Walter, M.	A laparoscopy-based method for BRDF estimation from in vivo human liver	WOS	3	3	3
Aleotti, Jacopo and Micconi, Giorgio and Caselli, Stefano	Object interaction and task programming by demonstration in visuo-haptic augmented reality	WOS	2	1	2
Lincoln, Peter and Blate, Alex and Singh, Montek and Whitted,Turner and State, Andrei and Lastra, Anselmo and Fuchs, Henry	From Motion to Photons in 80 Microseconds: Towards Minimal Latency for Virtual and Augmented Reality	WOS	4	1	2
Liu, Shiguang and Yu, Zhuojun	Sounding fire for immersive virtual reality	WOS	4	1	1
Visell, Yon	Fast physically accurate rendering of multimodal signatures of distributed fracture in heterogeneous materials	WOS	2	4	3
Park, Jinwoo and Park, Hunmin and Yoon, Sung-eui and Woo, Woontack	Physically-inspired Deep Light Estimation from a Homogeneous-Material Object for Mixed Reality Lighting	WOS	4	2	3
Hassaballah, M. and Aly, Abdelraheem M. and Abdelnaim, A.	Interactive fluid flow simulation in computer graphics using incompressible smoothed particle hydrodynamics	WOS	2	2	2
Sabbadin, Manuele and Palma, Gianpaolo and Banterle, Francesco and Boubekeur, Tamy and Cignoni, Paolo	High Dynamic Range Point Clouds for Real-Time Relighting	WOS	4	4	3,5
Chamilothori, Kynthia and Wienold, Jan and Andersen, Marilyne	Adequacy of Immersive Virtual Reality for the Perception of Daylit Spaces: Comparison of Real and Virtual Environments	WOS	5	3	3,5
Lombardi, Stephen and Saragih, Jason and Simon, Tomas and Sheikh, Yaser	Deep Appearance Models for Face Rendering	WOS	4	4	3
Shen, Liang and Zhu, Dengming and Nadeem, Saad and Wang, Zhaoqi and Kaufman, Arie E.	Radiative Transport Based Flame Volume Reconstruction from Videos	WOS	1	2	2
Debattista, Kurt and Bashford-Rogers, Thomas and Harvey, Carlo and Waterfield, Brian and Chalmers, Alan	Subjective Evaluation of High-Fidelity Virtual Environments for Driving Simulations	WOS	2	3	2
Tuliniemi, Jere	Physically Based Rendering for Embedded Systems	SCHOOLAR	3	4	5
Pharr, Matt and Jakob, Wenzel and Humphreys, Greg	Physically based rendering: From theory to implementation	SCHOOLAR	2	4	4
Dmitry Afonkin and Dmitry Zhdanov	The problem of physically based rendering in the cloud computing system	SCHOOLAR	3	3	2
Haraké, Laura and Burkard, Eva	Towards Physically Based Material Appearance in the Thermal Infrared Spectrum: A Short Survey	SCHOOLAR	0	2	2

Tabla 3.1: Tabla comparativa de los estudios seleccionados en la SLR.

Capítulo 4

Article published in Sensors

sensors

IMPACT FACTOR 3.275

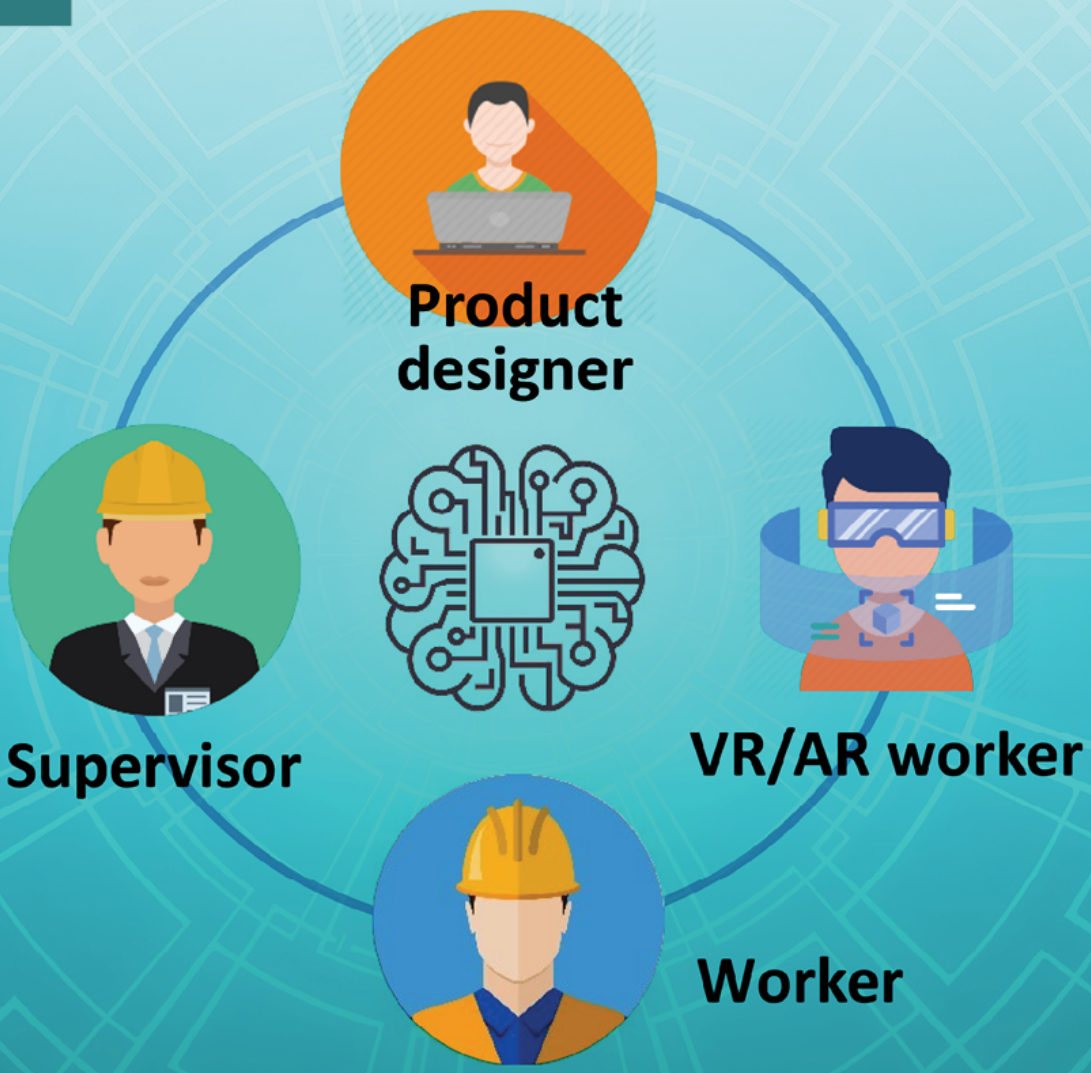

An Artificial Intelligence-Based Collaboration Approach in Industrial IoT Manufacturing: Key Concepts, Architectural Extensions and Potential Applications

Volume 20 · Issue 19 | October (I) 2020

MDPI

mdpi.com/journal/sensors
ISSN 1424-8220

sensors

MDPI

Article

Spectral Color Management in Virtual Reality Scenes

Francisco Díaz-Barrancas [1,*], Halina Cwierz [1], Pedro J. Pardo [1], Ángel Luis Pérez [2] and María Isabel Suero [2]

[1] Department of Computer and Network Systems Engineering, University of Extremadura, E06800 Mérida, Spain; hccwierz@unex.es (H.C.); pjpardo@unex.es (P.J.P.)
[2] Department of Physics, University of Extremadura, E06071 Badajoz, Spain; aluis@unex.es (Á.L.P.); suero@unex.es (M.I.S.)
* Correspondence: frdiaz@unex.es

Received: 21 July 2020; Accepted: 28 September 2020; Published: 3 October 2020

Abstract: Virtual reality has reached a great maturity in recent years. However, the quality of its visual appearance still leaves room for improvement. One of the most difficult features to represent in real-time 3D rendered virtual scenes is color fidelity, since there are many factors influencing the faithful reproduction of color. In this paper we introduce a method for improving color fidelity in virtual reality systems based in real-time 3D rendering systems. We developed a color management system for 3D rendered scenes divided into two levels. At the first level, color management is applied only to light sources defined inside the virtual scene. At the second level, we applied spectral techniques over the hyperspectral textures of 3D objects to obtain a higher degree of color fidelity. To illustrate the application of this color management method, we simulated a virtual version of the Ishihara test for color blindness deficiency detection.

Keywords: virtual reality; hyperspectral textures; Ishihara test; color fidelity

1. Introduction

Technology is constantly evolving, offering possibilities that were previously unthinkable. This is the case for image sensors that allow us to capture the three spatial dimensions and the temporal dimension of the real world and virtually represent that real world through digital images, digital videos, and, in recent years, virtual and augmented reality devices. In all cases, color is an essential part of the virtual representation of the world using digital media. This is because the recipient of that representation is a human being. For humans, color is a fundamental part of the external information they receive from their environment through their senses. The sense of sight provides more than 80% of the information received by the brain through the senses [1].

The color information captured by imaging devices often requires processing techniques to ensure correct color reproduction on various digital devices. First, it is necessary to carry out a correct chromatic characterization of both the capture device and the reproduction device. In this way, it is possible to establish a biunivocal correspondence between the device-dependent color coordinates (typically RGB or CMYK) and the device-independent color coordinates (CIE XYZ or CIE Lab). Over the last few years, a multitude of studies have been carried out on the color characterization of devices, from CRTS and TFT technology to Near-Eye Displays [2–5].

The differences in the calibration and colorimetric characterization of a color display device are always confusing [6]. Calibration of these devices consists of setting the device's state to a known value. This can be done by fixing the media's white point, the gain, and the offset of each channel for a cathode ray tube, for example. This process ensures that the device produces consistent results and that the calibration process can be completed without any information on the relationship between the device's

input coordinates and the colorimetric coordinates of the output. The colorimetric characterization of the device, however, requires this relationship to be known. From this characterization, the relationship between the device's input coordinates (typically RGB values in displays and other device-independent coordinates (i.e., the CIE 1931 XYZ tristimulus value)) are obtained. Presently, all display devices are digital, and the relation between digital and analog values is accomplished through a Digital to Analog Converter (DAC). Due to the large number of chromatic stimuli that can be shown by any digital device, the direct measurement of this relation is impossible; therefore, a mathematical model is applied, enabling one to reduce the number of runs.

In addition, it is necessary to implement color management systems that allow the exchange of chromatic information between different types of devices, such as displays and printers, thereby adapting the chromatic information based on different reproduction media, different white point values, and different gamut values. Based on this need, a wide field of study of gamut mapping has been developed and has had great relevance in recent years [7]. Recently, research has been done on the color appearance in optical see-through augmented reality devices [8].

All these developments were designed primarily for developing digital images from real scenes captured by photographic techniques. The generation of synthetic digital images from 3D models, which is commonly known as 3D rendering, has been left out of this type of color management technique since color, from beginning to end, has always been defined by native digital values such as RGB values. The only color correction currently carried out is the calibration of color player devices to a standard configuration that allows a similar appearance on all displays. However, 3D development environments used in virtual reality have great versatility and computing power thanks to the GPUs that are used to render at least 90 images per second for each eye [9,10].

There is a large difference between the digital images derived from photographic techniques and the digital images from 3D rendering scenes. In the first case, the image is captured by a sensor, typically CCD or CMOS, located in the image plane of the camera's optical system, where photons arrive from different parts of the scene. In the case of a digital image obtained by rendering a 3D scene (Figure 1), a process of ray tracing is carried out in the opposite direction to that of traditional optical systems, i.e., from the eye or the camera to the objects constituting the scene, passing through a matrix of points that correspond to the future pixels [11].

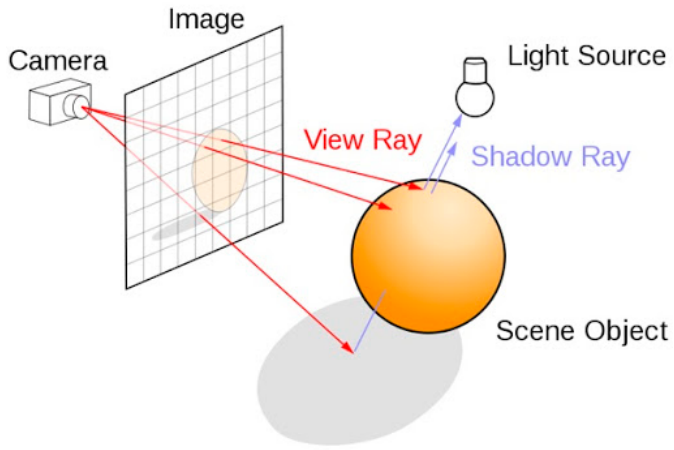

Figure 1. Simplified graphic representation of a lighting and shadowing method for rendering a 3D scene and how the final 2D image is generated [12].

From a visual point of view, Virtual Reality (VR) technology is based on the generation of two different images corresponding to two different views of the same three-dimensional scene. One of these images is shown to each eye, thereby covering a large field-of-view (FOV) and thus producing a stereoscopic image and a feeling of depth. The particularity of this stereoscopic view is that it is generated ("rendered", in the specific language of graphic computing) while considering the position

of the observer in real time, with a minimum delay and a high refresh rate of approximately 90 Hz. The position of the head and the body of the user of the VR device are continuously calculated through multiple sensors in such a way that the view of the scene corresponds exactly to the position of the observer. In this way, it is possible to create the visual sensation of immersion in a three-dimensional virtual world [13].

Large multinational companies are introducing virtual reality devices to the consumer market based on Head Mounted Displays (HMDs) with two different types of hardware: devices that do not have their own graphic hardware and need a personal computer for the task [14,15] and others that use a mobile phone or other specific graphic hardware without a personal computer [16,17]. There are significant differences in performance between both types of devices. In this work, we refer exclusively to the first type—devices associated with a personal computer with a dedicated graphics card.

The virtual world generated in VR devices is programmable and can be created in the image and likeness of the real world or not, as needed. Currently, there are two main software platforms for developing virtual reality content: Unreal Engine [18] and Unity Game Engine [19]. In both platforms, mathematical functions are used as basic rules of internal functioning that seek to reflect, to a greater or lesser extent, the real world through physical laws [20]. The geometry of the scene is supplied to the graphics card, and this hardware then projects the geometry and breaks it down into vertices (Figure 2). Then, the vertices are transformed and split into pixels, which obtain a final rendering treatment before they are passed to the screen through the Frame Buffer.

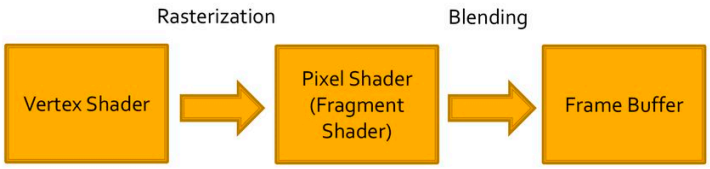

Figure 2. Sequence of transformations made in a Graphic Processing Unit (GPU) to generate the final 2D images for each display.

To handle the lighting and shading conditions, the graphic engine usually uses Physically-Based Rendering algorithms that apply a bidirectional reflectance distribution function model (BRDF) with four main components (diffuse, specular, normal, and smoothness). The diffuse component corresponds to the material color with a perfect diffuse illumination, the specular component corresponds to surface color, and the normal and smoothness components both correspond to surface texture. It is, therefore, possible to obtain rendered scenes with a high degree of visual fidelity when treating the light–matter interactions this way [21,22].

Physics-based representation (PBR) includes a combination of artwork, physical properties, and material shaders that work together to give consistency to graphic representation. Using the underlying physical principles of how light and surfaces interact, we can create images that work in all lighting conditions without special cases. The combination of the high computational power of current GPU-based virtual reality systems and the use of a physically-based rendering engine for lighting and shadowing a 3D virtual scene gives us the opportunity to determine if it is possible to obtain reliable color reproduction on these types of systems by comparing a real and virtual scene. The starting hypothesis of this work is that it is possible to introduce improvements in the color reproduction fidelity of real-time 3D rendered scenes in virtual reality systems. Therefore, we propose this goal as the main objective of this work. Notably, the key question of this objective is whether the improvement of color fidelity can be done in a real-time 3D rendered scene over lights and 3D objects and not over the final 2D images sent to an HMD. To do so, we will use two different levels of color fidelity: the first one based on the color management only of light sources defined in the 3D scene, retaining the color textures of the 3D virtual objects, and the second one using spectral rendering from hyperspectral textures associated with 3D objects. The secondary goal of this work is to determine if the first level of color management is sufficient to obtain a reliable reproduction or if it is necessary to implement both

levels. To illustrate the operation of this color management system applied to VR, we will create a virtual version of the famous *Ishihara Test for Colorblindness* that will help us assess the fidelity of the reproduction of a real test in a virtual scene.

2. Materials and Methods

The technical equipment used in this work is comprised of an *HTC Vive* HMD driven by a custom-made PC with an i7 processor (Intel, Santa Clara, CA, USA), 16 GB RAM memory, and a GeForce GTX 2060 super graphic card (Nvidia Corporation, Santa Clara, CA, USA) using the Windows 10 operating system (Microsoft, Redmond, WA, USA). The measurement instrument employed in this work was a CS-2000 tele-spectroradiometer (Konica-Minolta, Tokyo, Japan) with a spectral resolution of 1 nm between 380 and 780 nm, a <2% radiance measurement error, and CIE 1931 x = 0.0015; y = 0.0010 color error for illuminant A.

The methodology used in this work can be divided into two steps: (1) Colorimetric characterization of the VR display and (2) implementation of a color management system adapted to VR. Each step is explained in detail below.

2.1. Chromatic Characterization of a VR Device

The first step to use a virtual reality system in tasks related to color vision research is the chromatic characterization of the Head Mounted Display (HMD). Each device of this type has its own specific characteristics in terms of the chromaticity of its primary colors and its medium white point, as well as the relationship between the digital values of the analog-to-digital converter (DAC) and the associated tristimulus values of XYZ.

To chromatically characterize the VR device used in this study, spectroradiometric measurements were made with a tele-spectroradiometer aligned with the optical axis of the lenses with which the HMD is equipped. We measured over the display and lens assembly as a whole, leaving the measurement of the screen with and without lenses at different points of the screen for future studies. These lenses allow the user to correctly position their eyes on the displays and obtain an image from the displays with a large visual field. On the negative side, there is an increase in the image size of the pixels that makes those pixels perceptible to users. The values of chromaticity and the average relative luminance of both displays are shown in Table 1.

Table 1. The average and standard deviation of CIE 1931 chromaticity and the relative luminance of one point of each display of the HMD measured through the lens.

Channel	Chromaticity		Luminance	Gamma	
	x	y	Y (Relative)	Value	R^2
White	0.299 ± 0.002	0.315 ± 0.002	100.0		
Red	0.667 ± 0.004	0.332 ± 0.003	30.3 ± 1.1	2.43	0.999
Green	0.217 ± 0.007	0.710 ± 0.002	75.4 ± 2.4	2.38	0.999
Blue	0.139 ± 0.002	0.051 ± 0.002	7.8 ± 0.5	2.38	0.998
Black	0.311 ± 0.01	0.307 ± 0.004	0.4 ± 0.2		

The measured spectral power distribution of the RGB primaries is shown in Figure 3. The spectral radiance of each channel reveals the OLED nature of these displays with a narrow bandwidth for each channel's RGB.

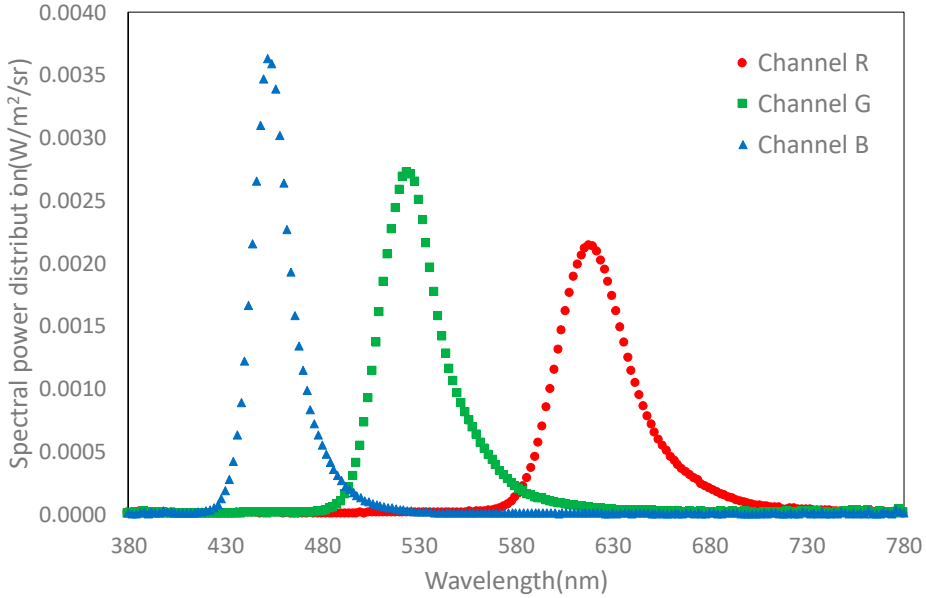

Figure 3. Spectral power distribution of the RGB channels measured at the maximum digital-to-analog converter (DAC) value.

The color gamut is a subset of colors that can be accurately represented in a given color space or by a certain output device like a display. In this work, we measured the color gamut of our HTC Vive device by comparing its color gamut with that of other devices, such as an Oculus Rift CV1 and classic CRT and TFT monitors (Figure 4).

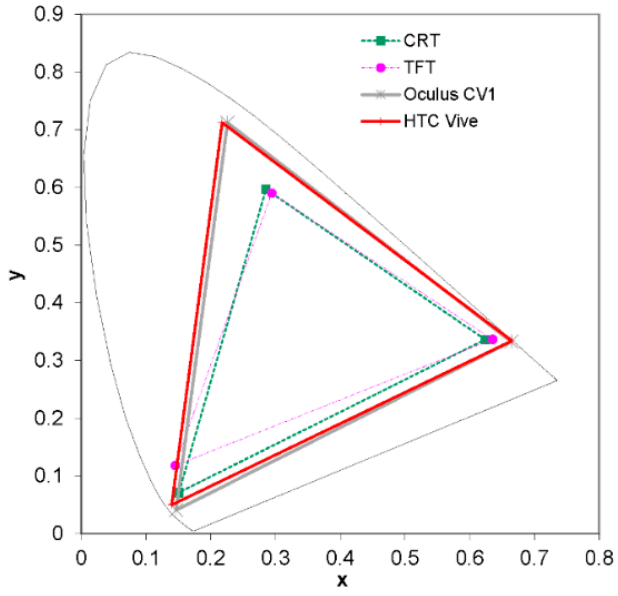

Figure 4. Color gamut of HTC Vive displays compared to the color gamut of different types of displays.

We analyzed the relationship between the values of the digital-to-analog converter (DAC) of each RGB channel and their corresponding values of luminance Y (Figure 5). The measurements were made using our tele-spectroradiometer for each of the R, G, and B chromatic channels independently, with a range of DAC values from 0 to 255 and a step of five units.

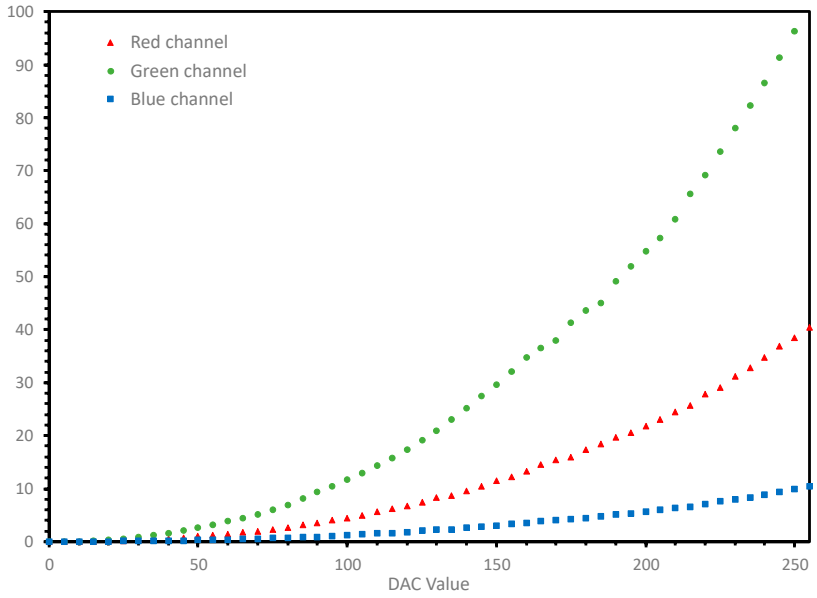

Figure 5. Relation between the DAC and luminance values for each RGB-independent channel.

As a result of this analysis and considering the computational time constraints of VR systems, a linear chromatic characterization model preceded by a gamma linearization stage was used. This simplified color characterization model is widely used in color management [23].

$$R' = R^{\gamma} G' = G^{\gamma} B' = B^{\gamma} \quad (1)$$

$$\begin{pmatrix} X \\ Y \\ Z \end{pmatrix} = \begin{pmatrix} X_{R'max} & X_{G'max} & X_{B'max} \\ Y_{R'max} & Y_{G'max} & Y_{B'max} \\ Z_{R'max} & Z_{B'max} & X_{B'max} \end{pmatrix} * \begin{pmatrix} R' \\ G' \\ B' \end{pmatrix} \quad (2)$$

This model uses a typical linear transformation between the RGB′ values and the normalized *XYZ* tristimulus values with a 3 × 3 matrix (Equation (2)). The RGB′ values were obtained after a gamma correction of the normalized RGB values that guaranteed the linearity of the system (Equation (1)). Table 1 shows the gamma value of each RGB channel and the statistical measurement of the R^2 fit index.

To confirm the goodness of the color characterization model, we measured 50 random RGB color samples. These values were compared to those predicted by the mathematical model, thereby obtaining an average color difference of $\Delta E^{00} = 1.8$. All measurement data together with the MATLAB script used to obtain the chromatic characterization model are available as Supplementary Material for this publication.

2.2. Implementation of a Color Management Procedure Adapted to VR Systems

After performing the spectral characterization of the HMD, the next necessary step to obtain a faithful reproduction of the color inside a Virtual Reality system is to introduce a color management procedure into the 3D graphics engine. The different combinations of lighting configurations in the 3D software used are practically unlimited; for example, it is possible to program different ways to perform the rendering using different shaders. The final appearance of the virtual reality scene will depend on the color of the light source used, the color of the material, the gloss, and the interaction of the different elements that form the virtual scene with shading, primary and secondary reflections, etc. For all these reasons, we assumed a series of simplifications that allow us to deal with the problem:

- We focus on the color matter, disregarding the participation of glossy objects and deactivating the secondary reflections.
- We limited the 3D software processing to real time processing, disabling the Baked and Global illumination options.
- We used Unity's standard shader and configured the player using its linear option with forward rendering activated.

By selecting these options, we aimed to establish a configuration to analyze and compare the results of the implemented color management system.

3D scene rendering engines do not use any default color management systems. The native format used to define both light sources and object textures in this type of software is sRGB digital color space with a bit depth of 8 bits per channel. This sRGB space is widely used in computer science and image processing and is characterized by a specific gamut, defined by the chromaticity of the primaries and by a non-linear transformation (gamma) of approximately 2.2. The media White Point of this color space is D65.

The color management procedure implemented in this work has two levels of accuracy. In the first level, a C# script was implemented, which allowed to calculate the RGB values of a simulated light source in the VR scene starting from the spectral power distribution of the source and the spectral characterization of the HMD used.

The second level of precision requires the introduction of the spectral texture of the virtual objects present in the virtual scene. For this part, we developed a C# script that performs all the computational processing of the virtual object texture, thereby generating a different RGB texture for each lighting change. Notably, although in virtual reality systems the rendering is performed with a minimum frequency of 90 Hz, this rendering is done with the same light sources and RGB textures, unless they are changed at run time.

Figure 6 shows a flux diagram for both levels of the color management procedure developed. The first level is only applied to the virtual light sources defined inside the virtual scene. The second level requires one to apply the first one and calculate the image texture of each 3D object starting from its hyperspectral image. The entire C# script for both procedures is attached as Supplementary Material for this paper.

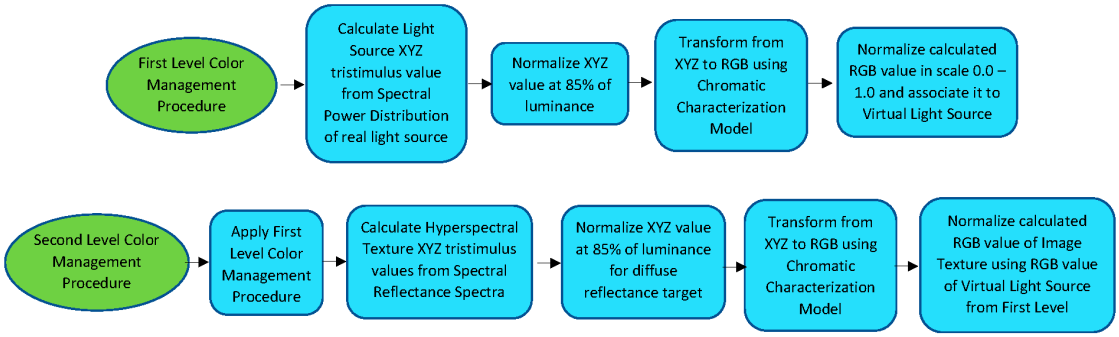

Figure 6. Flux diagram for both levels of the Color Management Procedure.

To analyze the results obtained by introducing both levels of color management, we used a sample of the ColorChecker color chart (X-rite, USA). This color chart is widely used in color management tasks in both scientific and professional fields. The manufacturer of this color chart provides the sRGB reference values that the color patches must present under D65 lighting. These values are presented in the first three columns of Table 2. The ColorChecker was scanned by a 3D color scanner, which provided the geometry of the object, as well as the color texture. The geometry is defined in an OBJ file as a dot-cloud. The color texture is defined by an 8-bit per channel BMP color file obtained under a D50 LED light source that the scanner is equipped with.

Table 2. Reference RGB values for the ColorChecker patches versus those calculated from the hyperspectral image.

ColorChecker	Reference			Measured		
Patch Number	**R**	**G**	**B**	**R**	**G**	**B**
1	115	82	68	115	82	67
2	194	150	130	195	149	129
3	98	122	157	93	123	157
4	87	108	67	90	108	65
5	133	128	177	130	129	176
6	103	189	170	99	191	171
7	214	126	44	219	123	45
8	80	91	166	72	92	168
9	193	90	99	194	85	98
−10	94	60	108	91	59	105
11	157	188	64	161	189	63
12	224	163	46	229	161	41
13	56	61	150	43	62	147
14	70	148	73	72	149	72
15	175	54	60	176	49	56
16	231	199	31	238	199	24
17	187	86	149	188	84	150
18	8	133	161	0	136	166
19	243	243	242	245	245	240
20	200	200	200	200	202	201
21	160	160	160	160	161	161
22	122	122	121	120	121	121
23	85	85	85	83	84	85
24	52	52	52	50	50	50

Average difference of $\Delta R = 3.4$, $\Delta G = 1.6$, $\Delta B = 1.9$.

Our main objective is to compare the efficiency of different color management methods in real-time 3D virtual environments, such as VR. The great challenge of this work is to perform the rendering in real time, thereby solving the computational complexities that exist. To carry out this comparative study, we require not only the geometry and color texture of the ColorChecker but also the hyperspectral texture—that is, the spectral reflectance of each point of the color chart defined in the color texture file. Since this object is flat, we obtained the hyperspectral texture via a hyperspectral camera, model UHD 285 (CubertGmbH, Ulm, Germany). In this way, we replaced the RGB color texture obtained from the 3D scanner with a hyperspectral texture defined between 400 and 1000 nm, using the 4 nm steps provided by the hyperspectral camera. Starting from this hyperspectral texture file, we calculated the average RGB values of each color patch of ColorChecker corresponding to the D65 illuminant and sRGB color space. We then compared these calculated RGB values with the theorical RGB values provided by the manufacturer. Table 2 shows the reference values specified by the manufacturer and the values obtained in our calculations.

To study the effects of these two levels of implemented color management, we used four different virtual light sources: a D65 illuminant, a D65 simulator obtained from a commercial lightbooth in our laboratory featuring 6-peak LED technology, and a theoretical LED source composed only of two spectral peaks chosen in such a way that the color of this source over a diffuse reflectance target coincides exactly with the color of the D65 illuminant. Figure 7 shows the spectral power distribution of all light sources employed in this work.

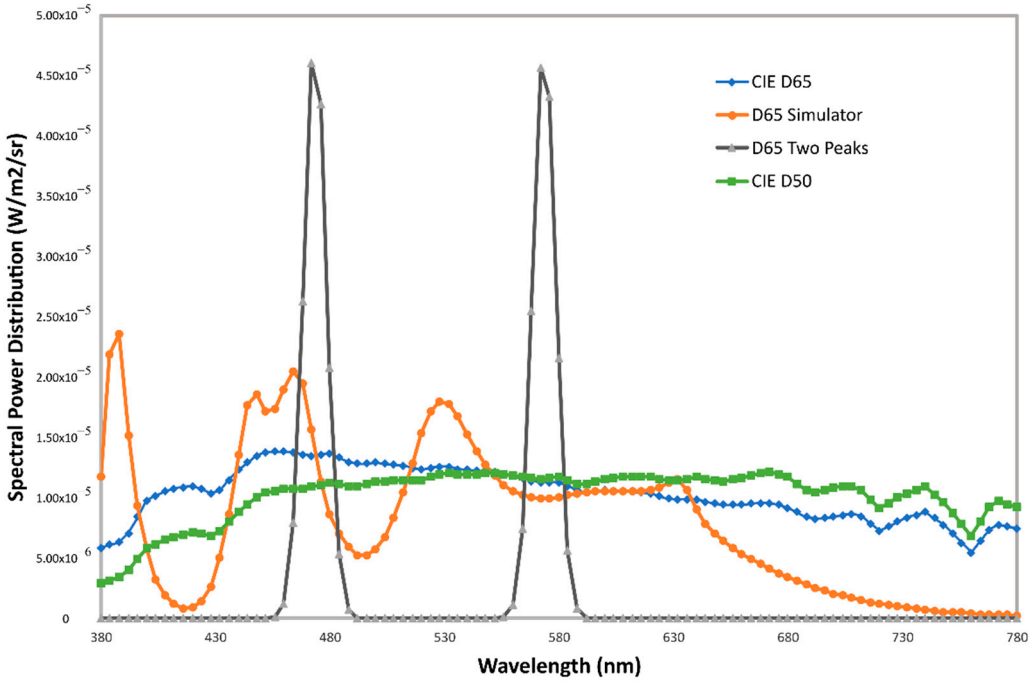

Figure 7. Spectral power distribution of the light sources employed in this work adjusted to a luminance value of 85 Cd/m^2.

Our 3D Graphics Engine uses sRGB as the native color space, and this space uses a medium-white-point, corresponding to the D65 illuminant. The CIE 1931 XYZ tristimulus values = (95.047 100.0 108.88) of this illuminant correspond to the digital 8-bit RGB values = (255, 255, 255). To prevent the incorrect definition of any light source whose X or Z values are above those corresponding to the illuminant D65, we chose to work with normalized sources whose relative luminance would be 85% that of the Illuminant D65. Therefore, we define the custom Illuminant D65 source as XYZ = (80.82, 85.00, 92.54), which corresponds to an RGB value = (237, 237, 237). Table 3 shows the XYZ and RGB values of the virtual light sources used, as well as their chromaticity values and Correlated Color Temperature (CCT).

Table 3. Numerical characterization of the light sources used in this work: CIE R_f, Color Fidelity Index; Correlated Color Temperature, CCT; CIE 1931 chromaticity coordinates and tristimulus values; and the RGB values corresponding to the sRGB standard.

Light Source	CIE Rf	CCT	CIE 1931 x,y	CIE 1931 XYZ	RGB
CIE D65	100	6503	0.3127, 0.3289	80.81, 85.00, 92.57	237, 237, 237
D65 Simulator	88.2	6568	0.3107, 0.3344	79.00, 85.00, 90.31	232, 239, 234
D65 Two Peaks	3.2	6501	0.3127, 0.3291	80.74, 85.00, 92. 53	237, 237, 237
CIE D50	100	5000	0.3458, 0.3585	81.98, 85.00, 70.11	255, 235, 205

The color of the objects present in a scene depends on the objects themselves but also on the light source illuminating them. The quality of a light source in terms of the fidelity of the colors it generates in a scene compared to those obtained by illuminating the scene with a reference light source can be calculated using the Color Fidelity Index R_f, defined by the International Lighting Commission (CIE) [24]. This value is included in Table 3, which describes the characteristics of the light sources used.

To assess the efficiency of the implemented color management system, a scene was designed in our 3D graphics engine, where only the virtual ColorChecker is illuminated by a single directional light source. The RGB values shown in Table 2 for different virtual light sources were assigned to this directional source to simulate this aspect of the ColorChecker under different light sources. In this

way, the effectiveness of the first level of color management implemented (first row of Figure 8) was tested. Subsequently, the second level of color management was enabled, in which the chromatic textures of the 3D objects were recalculated according to the light source used, in addition to the actions performed at the first level (second row of Figure 8).

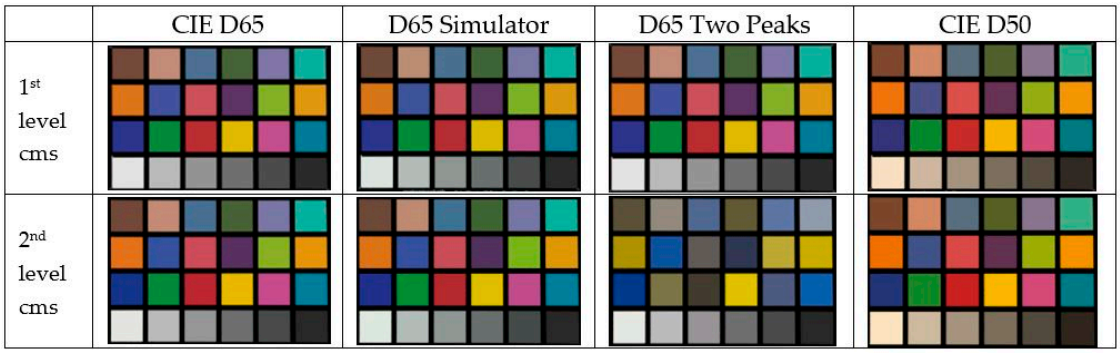

Figure 8. Screen capture of ColorChecker shown in the VR graphics engine with two levels of color management applied to four light sources: (first row) only applying changes in the color of the light sources and (second row) applying changes in the color of the light sources and recalculating the texture color of the VR object.

Figure 8 shows the results obtained when applying the two levels of color management within the 3D scene equipped with a virtual ColorChecker. At first glance, it is difficult to see the difference between the two levels of color management, except in the case of the two-peak source. In this case, the color difference is evident and results from the low Color Fidelity Index of that source, which is composed of only two spectral peaks, one blue and one yellow, making it impossible for this light source to reproduce any reddish or greenish tone. To more accurately evaluate the efficiency of both levels of color management, Table 4 shows the average color differences for each RGB channel. The RGB values measured from the screenshots are compared to those theoretically calculated from the spectral reflectance of each color patch of the ColorChecker using the different light sources. These color differences were calculated on each digital RGB channel since RGB is the native value of the implemented color management system.

Table 4. Average and standard deviation of the color differences between the calculated and measured RGB colors for the four light sources employed.

Light Source	1st Level CMS			2nd Level CMS		
	R	G	B	R	G	B
CIE D65	3.1 ± 3	1.4 ± 1	2.0 ± 2	0.2 ± 0.4	0.5 ± 0.5	0.2 ± 0.4
Simulator D65	2.6 ± 2	1.7 ± 1	3.3 ± 5	0.5 ± 0.5	0.2 ± 0.4	0.4 ± 0.6
D65 Two Peaks	30 ± 29	9.0 ± 8	6.5 ± 7	0.5 ± 0.5	0.4 ± 0.5	0.5 ± 0.5
CIE D50	3.1 ± 3	1.7 ± 2	4.6 ± 7	0.1 ± 0.3	0.4 ± 0.5	1.2 ± 0.9

In all cases, an improvement in color fidelity can be observed by applying the second level of color management. However, this difference is small, except for the case of the light source composed of two spectral peaks. There is no absolute criterion that allows knowing when it is enough to apply the first level of color management and when it is necessary to apply the two levels of color management, since it will depend on the spectral power distribution of the light source used and its interaction with the spectral reflectance of the materials of the objects used in the VR scene. In this work, it is pointed out that the Color Fidelity Index can be an indicator of when a light source may require the use of the second level of color management but setting a CFI reference value requires further research.

3. Results

Color reproduction can be handled at different levels of exigency depending on the need for accurate color reproduction. One of the most critical cases for color accuracy is testing for detecting color vision deficiencies. To illustrate the results obtained in this work, a reduced version of the well-known Ishihara Test for color-blindness detection [25] was virtually implemented. First, a virtual lightbooth was designed using VR-compatible 3D rendering software and then hyperspectral captures of the original test were used to introduce the captures into the virtual lightbooth. We measured the color of the virtual version of the test and compared it to the color measured in the real test. Finally, the behavior of the virtual version of the Ishihara Test was validated on real users.

3.1. Design of the Virtual Lightbooth and Reflectance Diffuse Reference Pattern

To analyze the results obtained in this work, a virtual scene was created by simulating a real lightbooth model, *LED Color Viewing* (Just NormLicht GmbH, Weilheim an der Teck, Germany). For this purpose, the real scale of the lightbooth and the size and position of the LED light bulbs were simulated. We performed the necessary adjustments in the 3D design software to obtain the right illuminating angle of the LED spotlights, as well as the lighting range and intensity parameters. We also created a virtual diffuse reflectance standard to perform the system calibration. Since the whole color management system is based on relative colorimetry, we need an element that allows us to determine where to locate the maximum luminance value. For this virtual lightbooth, we defined the same four virtual light sources employed in the previous step using ColorChecker.

In this way, the final simulation scene was created and prepared to introduce the hyperspectral textures of the Ishihara plates. Figure 9 shows the final virtual scenario with the test plate of the Ishihara test. In this test plate, all observers must recognize the number 12.

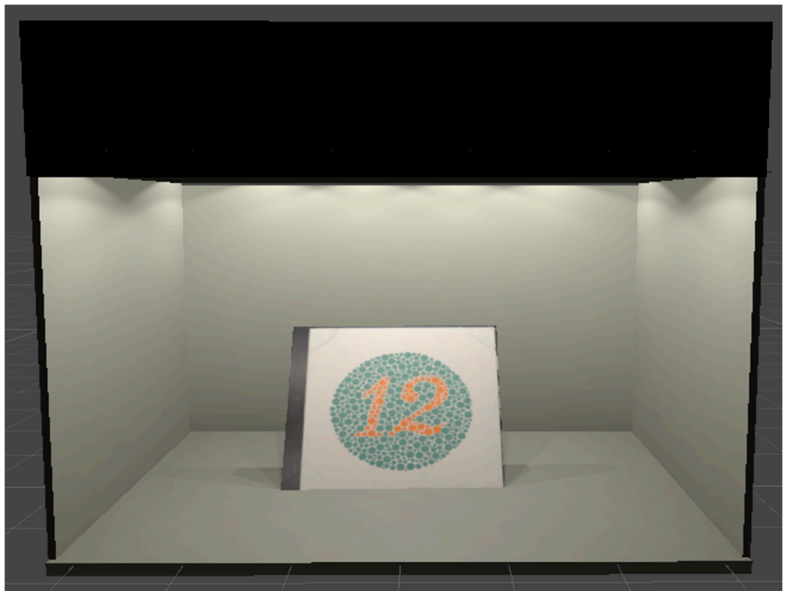

Figure 9. Visual appearance of the virtual lightbooth with the Ishihara test plate.

3.2. Hyperspectral Textures

One of the most innovative aspects of this work is the introduction of hyperspectral textures associated with virtual 3D objects in a Virtual Reality graphics engine [26–28]. To illustrate this point, we created a virtual version of the Ishihara test for detecting colorblindness. In this way, we employed the database provided by the *Color Imaging Lab* of the *University of Granada* [29]. This database contains, among other elements, hyperspectral images of each plate of the Ishihara Test. The researchers of this lab also provided us a MATLAB code to process the original hyperspectral cubes corresponding to

each Ishihara plate. Although the spectral range of the hyperspectral cubes is wider, the spectral range used to create the hyperspectral textures was 380–780 nm using 4 nm steps.

The virtual version of the Ishihara test consists of a reduced number of Ishihara plates because the only purpose of this test is to show the capabilities of this new color management system for managing hyperspectral images inside a Virtual Reality Scene with faithful color reproduction (see Figure 10). The Ishihara Test uses a reduced number of differently colored points on each slide, making it possible to easily identify the points that will be confusing to different types of defective observers based on the lines of confusion in the CIE 1931 diagram [30]. For example, to check whether correct color management was achieved in our virtual reality system and, therefore, obtain a virtual version of the original Ishihara test, we measured the 10 different colors that make up slide 3 of the virtual Ishihara test and the 10 colors that should be present, according to the colorimetric calculation from the hyperspectral images.

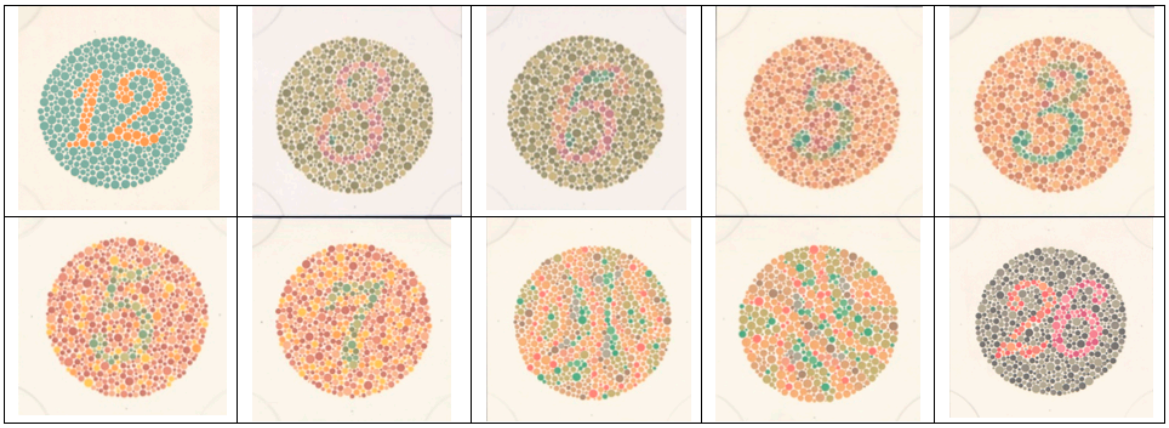

Figure 10. Set of 10 Ishihara plates selected to develop a quick virtual version test for colorblindness detection.

Table 5 shows the calculated chromaticity of 10 different color dots of plate number 3 starting from the hyperspectral image of this plate using CIE D65 as a light source. These 10 dots belong to 10 different colors labelled from P1 to P10, as shown in Figure 11. In the same way, the measured chromaticity of the virtual reality scene for these 10 color dots is shown on the right side of Table 5. The average color difference between the calculated and measured chromaticity of these 10 samples was below 1.0 units using the CIEDE2000 color difference formula. By checking each individual difference, it can be seen that the main difference is due to luminance rather than chromaticity.

Table 5. Chromatic coordinates calculated from the hyperspectral image and measured from the virtual reality scene for 10 different color dots of Ishihara Test plate number 3.

Color Dot	Calculated Color			Measured Color			ΔE
	x	y	Y	x	y	Y	DE2000
P1 Green Dark	0.3560	0.3854	24.6	0.3557	0.3850	25.4	1.00
P2 Green Medium	0.3602	0.3906	29.1	0.3601	0.3903	30.0	1.05
P3 Green Light	0.3734	0.3986	38.4	0.3731	0.3984	41.0	0.82
P4 Ochre Dark	0.3901	0.3656	27.1	0.3895	0.3655	28.1	0.70
P5 Ochre Medium	0.4022	0.3746	33.1	0.4014	0.3743	34.3	0.76
P6 Ochre Light	0.3945	0.3834	41.5	0.3941	0.3834	42.8	1.28
P7 Purple Dark	0.3713	0.3282	24.2	0.3709	0.3282	25.6	1.14
P8 Purple Light	0.3884	0.3576	36.1	0.3878	0.3573	38.0	0.72
P9 Bluish-Green Dark	0.3158	0.3759	23.7	0.3159	0.3763	22.7	0.64
P10 Bluish-Green Light	0.3182	0.3881	33.3	0.3182	0.3887	31.7	1.47

Average $\Delta E^{00} = 0.96$.

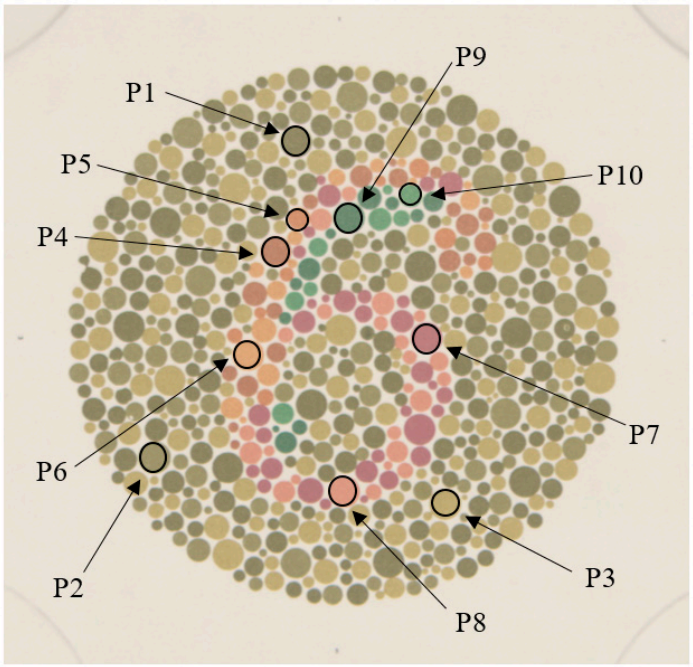

Figure 11. Screenshot Ishihara Plate number 3 selected to check the effectivity of color management.

3.3. Validation of the Procedure of Color Management in VR

Finally, a validation of the virtual version of the rapid test for detecting color vision deficiencies based on a reduced version of the *Ishihara Test* was conducted. This test was carried out on 10 observers previously assessed in our laboratory for their color perception abilities. Of these 10 observers, six had previously been classified as normal observers using the Farnsworth–Munsell 100 Hue test and another four as defective observers (1 deutan and 3 protan). Table 6 shows the detailed responses for each plate of the virtual test, as well as the reference responses following the Ishihara Test instructions. The results obtained by the virtual test match those obtained by the real test and the previous cataloguing of the results. The purpose of this test was to validate the color management procedure carried out in the virtual reality environment via a psychophysical test, rather than to validate the test itself, which would require a greater number of tests and observers.

Table 6. Numerical responses of the 10 real observers to the 10 plate virtual version of the Ishihara Test.

Observer	Qualification	P1	P2	P3	P4	P5	P6	P7	P8	P9	P10
Ref1	Normal	12	8	6	5	3	7	3	-	-	26
Ref2	Protan	12	3	5	2	5	-	-	5	8	6
Ref3	Deutan	12	3	5	2	5	-	-	5	8	2
Ob1	Normal	12	8	6	5	3	5	7	-	8	26
Ob2	Normal	12	8	6	5	3	5	7	-	-	26
Ob3	Normal	12	8	6	5	3	5	7	-	-	26
Ob4	Normal	12	8	6	5	3	5	7	-	-	26
Ob5	Normal	12	8	6	5	3	5	7	-	-	26
Ob6	Normal	12	8	6	5	3	5	7	-	-	26
Ob7	Protan	12	3	5	2	-	-	-	5	2	6
Ob8	Protan	12	3	5	2	5	-	-	5	8	6
Ob9	Deutan	12	3	5	2	-	-	-	5	8	2
Ob10	Protan	12	3	5	2	5	-	-	5	8	6

4. Conclusions

The results of this work can be measured in terms of the color reproduction fidelity obtained through the two levels of color management implemented. From this point of view, the results indicate that the application of the first level of color management, which only affects the lights and employs 3D scanned textures, may be sufficient in cases where high accuracy color reproduction is not required, provided that the spectrum of the simulated light source does not differ much from the spectrum of the reference illuminant. Under these assumptions, color differences of about 2 RGB digital units are achieved. This is not the case if the simulated light source has a low R_f color rendering index. In this case, it will be necessary to apply both levels of color management using the hyperspectral textures of the objects represented in the virtual reality scene. Applying these two levels of color management in VR will result in a very high color fidelity, with an average color difference below one RGB digital unit on each channel. In this case, then, the only significant color difference will be that coming from the chromatic characterization of the HMD, which will depend on the characteristics of each display used in the HMD.

The first level of color management implemented can be applied to any 3D object captured using a 3D scanner or other 3D capture technology. However, the second level requires the use of a hyperspectral camera to capture the information related to the spectral reflectance of the materials that conform the object. In the case of objects with flat geometry, such as the Ishihara test plates used in this work, their use in virtual reality environments is immediate. In the case of objects with other less simple geometry, it is necessary to use photogrammetric technics, like Multi-View 3D Reconstruction to capture a virtual 3D object from a real 3D object. This technique belongs to the category of *Structure From Motion* (SFM) technics, in which three-dimensional structures are estimated from two-dimensional image sequences. Traditionally, all these technics are based on RGB images captured by one or several digital RGB cameras. Our approach to solve this limit consists in substituting the RGB camera by a hyperspectral camera with different spectral channels. In this way we could obtain the 3D point cloud that defines the geometry of the 3D object and also, we could obtain the associated hyperspectral texture. This is a line of research we are currently working on.

Considering the above, we can conclude that the implemented color management methods can be applied in virtual reality scenes to facilitate the correct simulation of scenes where light and color fidelity are important factors. Obviously, these results can be applied to other non-VR 3D rendering systems, but the challenge was to define a color manage procedure for VR systems because of the high refresh rates of such systems.

Supplementary Materials: The following are available online at http://www.mdpi.com/1424-8220/20/19/5658/s1, Source Code S1: Calibration Script. Source Code S2: Color Management Script.

Author Contributions: Conceptualization, F.D.-B., H.C., and P.J.P.; methodology, Á.L.P. and M.I.S.; software, F.D.-B., H.C., and P.J.P.; validation, Á.L.P., M.I.S., and H.C.; formal analysis, P.J.P. and F.D.-B.; investigation, F.D.-B., H.C., and P.J.P.; writing—original draft preparation, F.D.-B., H.C., and P.J.P.; writing—review and editing, F.D.-B., H.C., Á.L.P., M.I.S., and P.J.P.; supervision, P.J.P. and M.I.S.; All authors have read and agreed to the published version of the manuscript.

Funding: This work was supported by the grants GR18131 and IB16004 of the Regional Government of the Junta de Extremadura and partially financed by the European Regional Development Fund.

Acknowledgments: We would like to thank the Color Imaging Lab at the University of Granada who provided us with their Ishihara hyperspectral database, which we used to develop the virtual test.

Conflicts of Interest: The authors declare no conflict of interest.

References

1. LeGrand, Y.; ElHage, S.G. *Physiological Optics*; Springer: Berlin/Heidelberg, Germany, 2013.
2. Berns, R.S. Methods for characterizing CRT displays. *Displays* **1996**, *16*, 173–182. [CrossRef]
3. Pardo, P.J.; Pérez, A.L.; Suero, M.I. Validity of TFT-LCD displays for color vision deficiency research and diagnosis. *Displays* **2004**, *25*, 159–163. [CrossRef]

4. Penczek, J.; Boynton, P.A.; Meyer, F.M.; Heft, E.L.; Austin, R.L.; Lianza, T.A.; Leibfried, L.V.; Gacy, L.W. 65-1: Distinguished Paper: Photometric and Colorimetric Measurements of Near-Eye Displays. *SID Symp. Dig. Tech. Pap.* **2017**, *48*, 950–953. [CrossRef]
5. Penczek, J.; Boynton, P.A.; Meyer, F.M.; Heft, E.L.; Austin, R.L.; Lianza, T.A.; Leibfried, L.V.; Gacy, L.W. Absolute radiometric and photometric measurements of near-eye displays. *J. Soc. Inf. Disp.* **2017**, *25*, 215–221. [CrossRef]
6. Suero, M.I.; Pardo, P.J.; Pérez, A.L. Color characterization of handheld game console displays. *Displays* **2010**, *31*, 205–209. [CrossRef]
7. Morovič, J. *Color Gamut Mapping*; Wiley: Hoboken, NJ, USA, 2008; Volume 10.
8. Hassani, N.; Murdoch, M.J. Investigating color appearance in optical see-through augmented reality. *Color Res. Appl.* **2019**, *44*, 492–507. [CrossRef]
9. ElBamby, M.S.; Perfecto, C.; Bennis, M.; Doppler, K. Toward Low-Latency and Ultra-Reliable Virtual Reality. *IEEE Netw.* **2018**, *32*, 78–84. [CrossRef]
10. Shao, X.; Xu, W.; Lin, L.; Zhang, F. A multi-GPU accelerated virtual-reality interaction simulation framework. *PLoS ONE* **2019**, *14*, e0214852. [CrossRef] [PubMed]
11. Ray Tracing on Programmable Graphics Hardware. Available online: https://dl.acm.org/doi/10.1145/566654.566640 (accessed on 29 September 2020).
12. Ray Trace diagram.svg. Available online: https://en.wikipedia.org/wiki/Ray_tracing_(graphics)#/media/File:Ray_trace_diagram.svg (accessed on 17 September 2020).
13. Schnack, A.; Wright, M.; Holdershaw, J.L. Immersive virtual reality technology in a three-dimensional virtual simulated store: Investigating telepresence and usability. *Food Res. Int.* **2019**, *117*, 40–49. [CrossRef] [PubMed]
14. Oculus Rifts. Available online: https://www.oculus.com/rift-s/?locale=es_ES (accessed on 16 July 2020).
15. HTC Vive. Available online: https://www.vive.com/mx/product/ (accessed on 16 July 2020).
16. Daydream. Available online: https://arvr.google.com/daydream/ (accessed on 16 July 2020).
17. Manual de las Gafas VR ONE Plus. Available online: https://www.zeiss.com/content/dam/virtual-reality/english/downloads/pdf/manual/20170505_zeiss_vr-one-plus_manual_and_safety_upd_digital_es.pdf (accessed on 16 July 2020).
18. Unreal Engine. Available online: https://www.unrealengine.com/en-US/ (accessed on 16 July 2020).
19. Unity. Available online: https://unity.com/es (accessed on 16 July 2020).
20. Pardo, P.J.; Suero, M.I.; Pérez, Á.L. Correlation between perception of color, shadows, and surface textures and the realism of a scene in virtual reality. *J. Opt. Soc. Am. A* **2018**, *35*, B130–B135. [CrossRef] [PubMed]
21. Shen, H.; Zhang, Z.; Shang, Z. Fast global rendering in virtual reality via linear integral operators. *Int. J. Innov. Comput. Inf. Control* **2019**, *15*, 67–77.
22. Tuliniemi, J. Physically Based Rendering for Embedded Systems. Master's Thesis, University of Oulu, Oulu, Finland, 2018.
23. Díaz-Barranca, F.; Pardo, P.J.; Suero, M.I.; Pérez, A.L. Is it possible to apply colour management technics in Virtual Reality devices? In Proceedings of the XIV Conferenza del Colore, Firenze, Italy, 11–12 September 2018.
24. CIE 2017 Colour Fidelity Index for Accurate Scientific Use. Available online: http://cie.co.at/publications/cie-2017-colour-fidelity-index-accurate-scientific-use (accessed on 29 September 2020).
25. Anstis, S.; Cavanagh, P.; Maurer, D.; Lewis, T.; MacLeod, D.A.I.; Mather, G. Computer-generated screening test for colorblindness. *Color Res. Appl.* **1986**, *11*, S63–S66.
26. Diaz-Barrancas, F.; Cwierz, H.C.; Pardo, P.J.; Perez, A.L.; Suero, M.I. Visual fidelity improvement in virtual reality through spectral textures applied to lighting simulations. *Electron. Imaging* **2020**, *259*, 1–4. [CrossRef]
27. Díaz-Barrancas, F.; Cwierz, H.; Pardo, P.J.; Suero, M.I.; Perez, A.L. Hyperspectral textures for a better colour reproduction in virtual reality. In Proceedings of the XV Conferenza del Colore, Macerata, Italy, 5–7 September 2019.
28. Diaz-Barrancas, F.; Cwierz, H.C.; Pardo, P.J.; Perez, A.L.; Suero, M.I. Improvement of Realism Sensation in Virtual Reality Scenes Applying Spectral and Colour Management Techniques. In Proceedings of the 12th International Conference on Computer Vision Systems (ICVS 2019), Riga, Latvia, 5–9 July 2019.

29. Martínez-Domingo, M.Á.; Gómez-Robledo, L.; Valero, E.M.; Huertas, R.; Hernández-Andrés, J.; Ezpeleta, S.; Hita, E. Assessment of VINO filters for correcting red-green Color Vision Deficiency. *Opt. Express* **2019**, *27*, 17954–17967. [CrossRef] [PubMed]
30. Wyszecki, G.; Stiles, W.S. *Color Science*; Wiley: New York, NY, USA, 1982.

Capítulo 5

Article published in Electronics

electronics

IMPACT FACTOR 2.397

CITESCORE 2.7 SCOPUS

An Improved Deep Convolutional Neural Network-Based Autonomous Road Inspection Scheme Using Unmanned Aerial Vehicles

Volume 10 · Issue 22 | November (II) 2021

MDPI

mdpi.com/journal/electronics
ISSN 2079-9292

electronics

MDPI

Article

Real-Time Application of Computer Graphics Improvement Techniques Using Hyperspectral Textures in a Virtual Reality System

Francisco Díaz-Barrancas *,†, Halina Cwierz † and Pedro J. Pardo †

Department of Computer and Network Systems Engineering, University of Extremadura, Centro Universitario de Mérida, C/Santa Teresa de Jornet 38, E06800 Mérida, Spain; hccwierz@unex.es (H.C.); pjpardo@unex.es (P.J.P.)

* Correspondence: frdiaz@unex.es

† These authors contributed equally to this work.

Abstract: In virtual reality technology, it is necessary to develop improvements and apply new techniques that allow rapid progress and innovative development. Nowadays, virtual reality devices have not yet demonstrated the great potential they could develop in the future. One main reason for this is the lack of precision to represent three-dimensional scenarios with a similar solvency to what our visual system obtains from the real world. One of the main problems is the representation of images using the RGB color system. This digital colorimetry system has many limitations when it comes to representing faithful images. In this work we propose to develop a virtual reality environment incorporating hyperspectral textures into a virtual reality system. Based on these hyperspectral textures, the aim of our scientific contribution is to improve the fidelity of the chromatic representation, especially when the lighting conditions of the scenes and its precision are relevant. Therefore, we will present the steps followed to render three-dimensional objects with hyperspectral textures within a virtual reality scenario. Additionally, we will check the results obtained by applying such hyperspectral textures by calculating the chromaticity coordinates of known samples.

Keywords: virtual reality; color rendering; computer graphics; hyperspectral textures

Citation: Díaz-Barrancas, F.; Cwierz, H.; Pardo, P.J. Real-Time Application of Computer Graphics Improvement Techniques Using Hyperspectral Textures in a Virtual Reality System. *Electronics* **2021**, *10*, 2852. https://doi.org/10.3390/electronics10222852

Academic Editors: Hai Huang and Ye Duan

Received: 20 October 2021
Accepted: 17 November 2021
Published: 19 November 2021

1. Introduction

The digital revolution, has continued inexorably since the invention of the transistor in the 1950s, the beginning of the information age [1]. This progress can be seen in many aspects of our everyday life, such as our communication or our computing skills, and even in recreational aspects such as television, cinema, video games, etc. [2]. One of the latest twists and turns of this technological advance has been the generalization of the use of the 3D world in digital environments. Not only thinking about the visualization of 3D contents, but also about the design of all kinds of products in 3D environments, from furniture or vehicles to videogames or films. This form of native 3D design has been complemented by the existence of new devices that allow capturing and digitization of the real world in 3D, such as 3D scanners. These devices are also constantly evolving and have advanced a lot, from the first laser scanners that obtained the black and white point cloud, to the current, much simpler ones, which use image-based techniques and structured lighting to determine the point cloud with an associated RGB color texture [3]. Recently, a new technique has emerged that allows real 3D objects to be digitized by capturing multiple images of the same object from different angles. This type of technique, based on photogrammetric calculations, also generates the point cloud of the 3D object and an RGB color texture and can be used for all types of small or large objects [4,5]. In the above cases, the generated spatial coordinates XYZ that form the 3D point cloud are complemented with additional color information in the form of an RGB color texture in the best case. The RGB color space is used as native digital space to represent the color of 3D objects; however, this

option is not the most appropriate if maximum fidelity is sought in the color reproduction of the object in the digital world compared with the visual appearance of the object in the real world [6]. When the color appears in this type of real-world digital capture, there exists also the need to make those captures with the greatest possible color fidelity, as is done with other types of 2D digital captures, such as digital cameras and flatbed scanners [7]. More pressing is this need with the emergence of new 3D visualization devices such as virtual reality devices.

Virtual Reality (VR) has experienced great development in recent years. The quality improvement of head-mounted displays (HMD) allows immersive visual experiences in virtual environments and is expected to have many applications, in both recreational and professional fields [8–10]. The quality of these immersive experiences is a key factor and depends on the capability to generate the feeling of presence over a distance. From this perspective, virtual reality is achieved by creating an immersive experience, in which the senses receive different information from that of the real world. This immersive experience is based on deceiving our senses, bringing the corresponding information to the brain with a situation that is not real. Over the years, there have been several attempts to achieve this goal of deceiving our senses causing minimal visual fatigue [11,12]. Based on the need to improve the ability to reproduce more faithful images within a virtual reality system, the main aim of our work is to apply hyperspectral textures to objects scanned with a 3D scanner. This task has the complexity of introducing spectral files into a virtual reality system and working with them, considering the changes of light sources.

2. Related Work

From an immersive image quality point of view in a virtual reality scenario, we have seen how numerous works have made great efforts in applying computer graphics techniques to improve the final rendering. Examples are ray tracing [13,14], eye tracking [15] or zone-based rendering [16,17]. All these improvements make virtual reality systems more realistic [18] but none of them are focused on color fidelity using different light sources. However, just as in the physical world the light source plays a determining role in the human visual system and in the way we perceive the color of objects, it also does so in virtual reality. Therefore, it is necessary to use advanced techniques such as the use of spectral information in the color texture assigned to a 3D object to create a feeling of similarity to reality [19,20].

The rendering of real 3D objects in virtual reality systems is done by scanning physical objects and then inserting them into a three-dimensional scene [21], in which depth plays an important role, since we are not talking about 2D images. Currently, the RGB color space is used to specify the color of such objects, as the use of the RGB color space is widespread across all digital devices. However, this color space is not the most appropriate if we want to ensure maximum color fidelity because this color space is device-dependent [22,23]. Moreover, if we want to reproduce how the light interact with objects in the real world inside a virtual reality scene, it will be necessary to use a more adequate color space such as CIE 1931 XYZ [24]. This device-independent color space allows us to compute the color of the real objects using the spectral reflectance of the surface of the objects and the spectral power distribution of the light source [25]. Of course we still have a need to use the RGB color space because this is the native color space of all HMDs. It is necessary to remark that we are still working in the framework of metameric matching of real-world colors using the light stimuli generated at the displays located inside the HMDs [26]. In this paradigm we have only three primary lights mixed in proper amounts to match the desired color. There is no spectral matching of the color generated at the display and the real-world color used as a reference. Like all tri-primary color systems, we are only matching the color using the phenomenon of metamerism. This is the reason why it is important to include spectral information of the light source and the objects at virtual reality systems, because metamerism does not support changes in light sources.

The aim of the work has been to develop a system capable of introducing spectral information on previously scanned objects. For this purpose, we simulated an LED light booth (Just Normlicht) with 12 LED spotlights [27]. Inside that light booth we included several fruits, 3D geometrical figures and a Color-Checker (X-rite) chart. The colors of these 3D objects were chosen to have well-known basic hues (red, orange, yellow, green and blue). The reason for not including any blue fruit or food was the difficulty of obtaining it. To complete the chromatic rainbow we included 3D geometrical figures (one blue) and a 3D capture of an original ColorChecker chart that provide us several important colors at daily-live like (brown, pink, purple and mid-tones). In the light booth simulation, we can switch between different light sources (TL84 and simulators of A, D50 and D65 illuminants).This means that the color of the objects shown at the virtual light booth will be calculated and represented in relation to the chosen light source. In our hypothesis, this allows the user to obtain a more faithful image of the displayed scenario and its components. The representation of 3D objetcs with hyperspectral textures, previously presented as preliminary work [28], will improve the graphical representation of the virtual scenario. Figure 1 shows the initial representation of the project created in the virtual reality system.It shows a ColorChecker, a caps with an absolute white diffuser (Labsphere, North Sutton, NH, USA), four fruits and four geometrical figures.

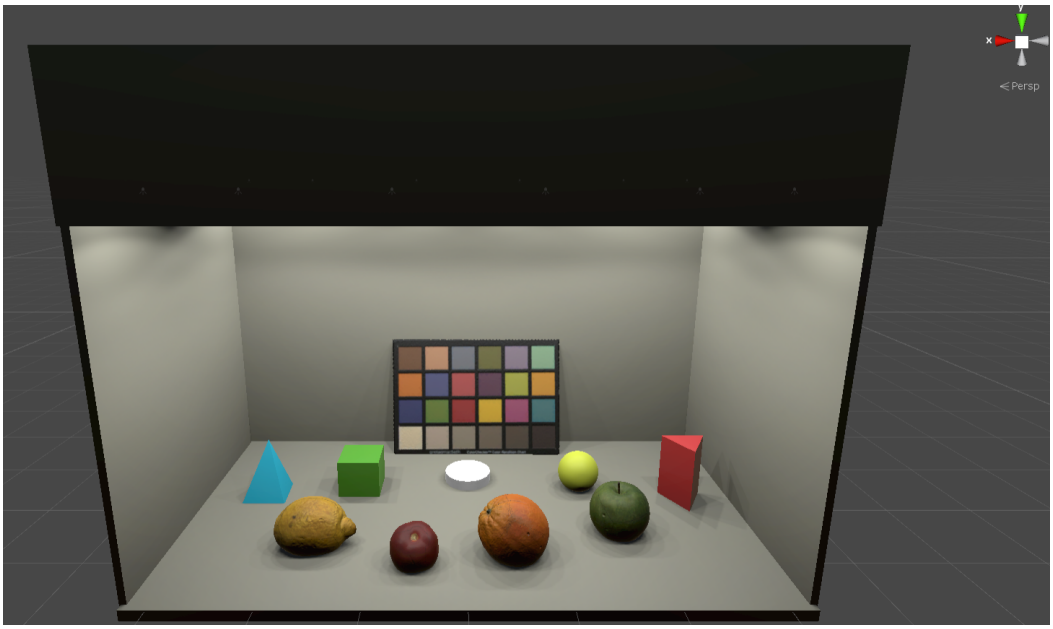

Figure 1. Proposed virtual reality scenario for the introduction of hyperspectral information.

3. Materials and Methods

3.1. Color Characterization of Head Mounted Display

One of the main problems regarding the color management in virtual reality devices is the high refresh frequency of images, between 90 and 120 Hz, due to the low latency in the interaction of the user with the environment. This high frequency reduces the time available for colorimetric calculations. For this reason, we chose a display characterization model that does not require complex calculations, but only seeks to relate, as simply and accurately as possible, the values of the Digital-to-Analog-Converter (DAC) with the chromatic values of the stimulus in any reference color space. In a recent work, the authors detailed a simple color characterization model for this type of VR device [29]. This model follows the typical structure of a linear transformation between XYZ and $R'G'B'$ color spaces using a 3×3 matrix (Equation (2)) where the $R'G'B'$ vector is a linearized value using a gamma correction (Equation (1)) of the original RGB coordinates.

$$\begin{aligned} R' &= R^{\gamma_1} \\ G' &= G^{\gamma_2} \\ B' &= B^{\gamma_3} \end{aligned} \tag{1}$$

$$\begin{pmatrix} X \\ Y \\ Z \end{pmatrix} = \begin{pmatrix} X_{R'max} & X_{G'max} & X_{B'max} \\ Y_{R'max} & Y_{G'max} & Y_{B'max} \\ Z_{R'max} & Z_{G'max} & Z_{B'max} \end{pmatrix} * \begin{pmatrix} R' \\ G' \\ B' \end{pmatrix} \tag{2}$$

Based on this chromatic characterization model, we carried out the necessary measurements to characterize chromatically the display of a HTC Vive Headset for Virtual Reality. The measurement instrument employed in this work was a Konica-Minolta CS-2000 tele-spectroradiometer with a spectral resolution of 1 nm between 380 and 780 nm, a <2% radiance measurement error and CIE 1931 x = 0.0015; y = 0.0010 color error for an illuminant A. The measurements were performed through the lens of the HMD following the recommendations about color measurements in Near-eye displays (NEDs) [30–32]. To perform the measurements, we set up the virtual light booth showing only one color capsule at a central point on the booth floor. The color of this capsule was fixed directly in RGB coordinates without any relation to the light or the texture because, at this stage of the chromatic characterization, we only want to record the relation between the digital RGB values and their color coordinates in a space independent of the device. First, we measure the XYZ tristimulus values for each independent R, G, and B channel on the display, in steps of 5 DAC values from 0 to 255 (8-bit depth) per channel. Next, we determined the relationship between the device-dependent and the device-independent color space coordinates (RGB vs. XYZ). This allowed us to obtain a gamma value, with which we linearize the color transformation, and generate the final matrix necessary for the color management. This matrix is the one we will finally use in our Algorithm 1 in Section 4 to apply the color space change. This chromatic characterization is applicable to any scene or scenario since the color relation is established between the RGB DAC values and the XYZ color space, without any other constrain. It should be noted that, strictly speaking, this 3 × 3 matrix and the 3 gamma values are only valid for our system, composed of an HTC Vive HMD, a PC with Windows 10 and Unity as the graphics engine, since any adjustment made in hardware or in software set-up will influence the values of that matrix and constants. However, previous works have indicated that the variations from one individual system to another of the same manufacturer, always taking the default values, are usually small [33]. Another option is to work with the gamma and matrix of the sRGB standard, since all display manufacturers tend to use this standard, although the appropriate checks would have to be made. Figure 2 shows the measurement procedure in the HMD.

3.2. 3D Reconstruction with a Scanner

In order to achieve the structure of the real objects, we used a 3D scanner. We scanned them with a Go!Scan 20 3D scanner (Creaform, Levis, QC, Canada) and processed the 3D object model with VXscan and VXelements 4 software (Creaform, Levis, QC, Canada). This scanner has a resolution of 0.5 mm and an accuracy of 0.100 mm. With this device we can capture the geometry of an object with good representation; however, the color representation is not good enough. Together with the point cloud that defines the geometry of the object, this scanner provides an image file with the RGB color texture associated with the 3D object. To obtain that texture, this device employs an RGB CCD camera and an internal dual peak LED light source with a color temperature of 5000 K. In order to add the spectral information to the RGB texture provided by the 3D scanner, we developed a MATLAB script that calculates the color RGB of the measured points of the object using the spectral reflectance of these points. In order to do this we employed the spectral power distribution of the internal light source of the 3D scanner and the custom ICC color profile of this device. By computing the color difference between the RGB colors from the 3D

Scanner and the RGB color from the MATLAB script, we associated a spectral reflectance to each pixel of the RGB texture following the criteria of minimizing the color difference. Figure 3 shows the scanner used to obtain the geometry of the objects used in the virtual representation. In addition, Figure 3 shows the spectral power curve of the internal LED light source employed by the 3D scanner. This LED is specific to the scanner and its power distribution was measured with our Konica-Minolta CS-2000 tele-spectroradiometer.

Figure 2. Experimental setup used for the chromatic characterization of the HTC Vive Device.

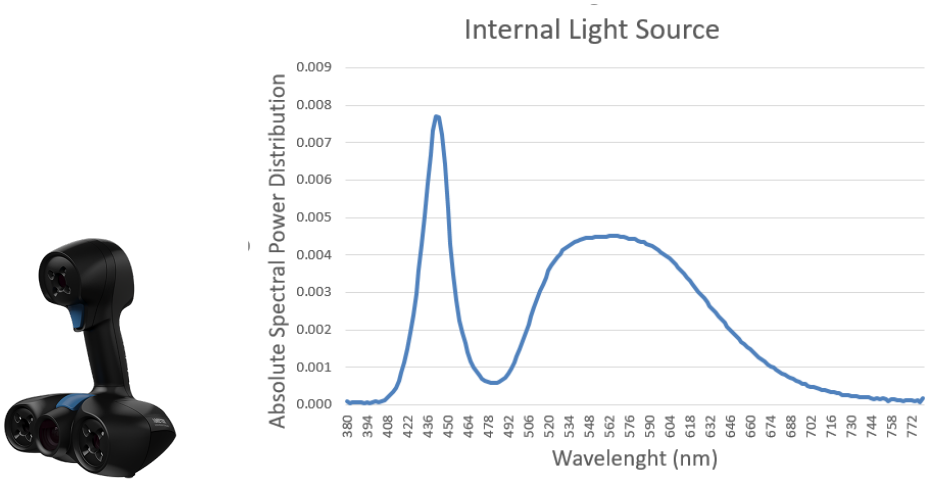

Figure 3. Scanner used for the object simulation process (**left**) and spectral power distribution of the scanner (**right**).

3.3. Hyperspectral Texture Datasets

Firstly, we defined the 3D objects by means of .obj files and their corresponding color texture file with RGB values. Then, we used the database of a published work that analyzed the spectral reflectance of several fruits and vegetables [34]. By means of a script developed in MATLAB, we replace the texture generated by the scanner in RGB values by another texture file using the spectral reflectance values of the published datasets. This hyperspectral texture was originally generated using several .bmp files, defining for each file the spectral reflectance of a different wavelength, in 4 nm steps from 380 to 780 nm. After this, the hyperspectral texture files were converted to a binary file in order to be read by graphics engine software (Unity) as a binary array of bytes. In this manner, it is possible to make the necessary spectral calculations inside Unity software, including the effect of different light sources over the 3D objects. As a result from these calculations we will

obtain the colorimetric information expressed in tristimulus values XYZ to be represented in the virtual reality system.

3.4. Light Sources Measurements

In order to represent and simulate different light sources in a virtual reality system, the first step is to obtain the spectral power distribution (SPD) of these light sources. For this purpose, we measured the SPD of the light sources of a real light booth in our laboratory.The measurements were performed employing our tele-spectroradiometer with a measurement geometry of 0°/45° over a Spectralon (Labsphere, USA), a diffuse reflectance standard with a Lambertian spectral reflectance of 99.9% in the visible range. Figure 4 shows the set up scenario used to obtain these spectral curves.

Figure 4. Set up of measurement of spectral power curves of real light sources.

Once the measurement was completed, we obtained the SPD of the simulator for TL84, D50, A and D65 light sources. Figure 5 shows the spectral curves of these LED light sources.

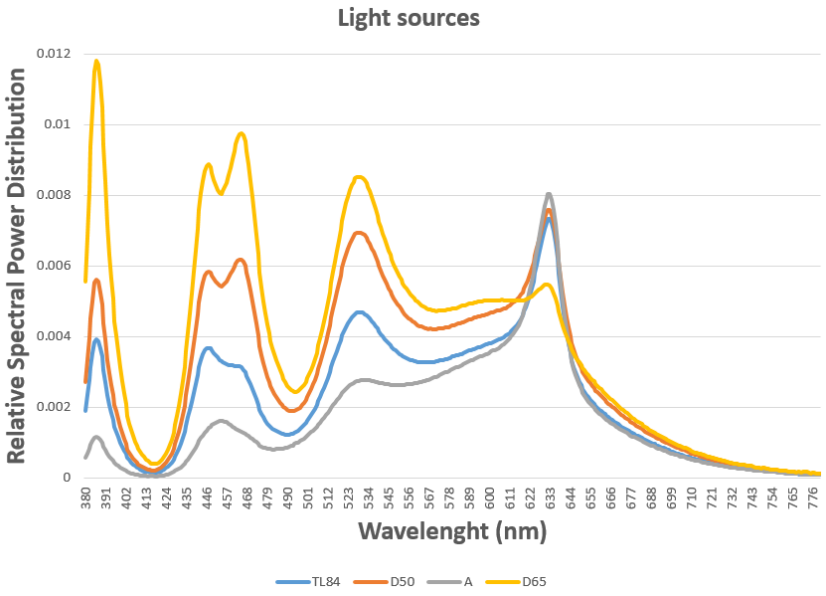

Figure 5. Absolute Spectral Power Distribution of different light sources.

4. System Development

4.1. Light Representations in a Virtual Reality System

The first step of our system was to simulate different light sources in a virtual reality system using its spectral power distribution curves, defined in separates .csv files. The Unity Game Engine permit allows us to read those .csv files and incorporate the different SPDs to a script that calculates the tristimulus value for each light source using a CIE 1931 colorimetric standard observer. Using the chromatic characterization model defined before, we can obtain the RGB value necessary to simulate each light source in a virtual reality system. Figure 6 shows the different simulations of light sources that we made to compare objects with hyperspectral textures. These scenes represent an LED light booth (Just Normlicht) with 12 LED spotlights.

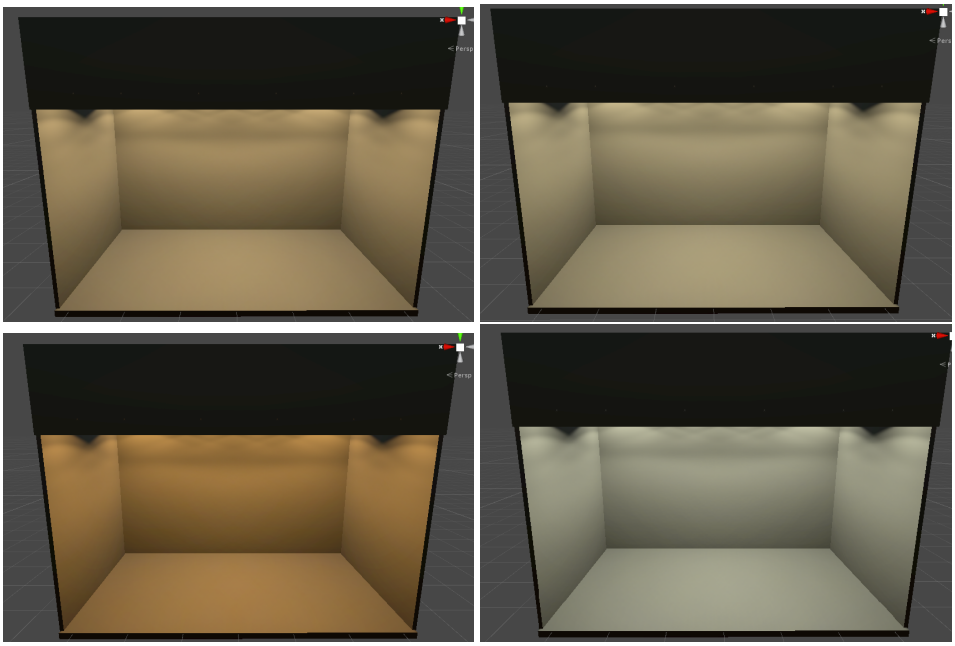

Figure 6. Different light sources represented in our virtual reality scene. TL84 (**top left**), D50 (**top right**), A (**bottom left**) and D65 (**bottom right**).

4.2. Graphics and Lighting Settings

In order to obtain the best visual appearance and the most realistic graphic rendering possible [35], we chose the high quality options in the set up of the Unity Software. In addition, options such as reflections were activated to give a more natural look to the virtual scenario. Furthermore, we need to know that The High Definition Render Pipeline (HDRP) allows us to render Lit Materials using either Forward or Deferred rendering. Unity allows us to configure our Unity Project to only use one of these modes, or allow it to use both and switch at runtime on a per-Camera basis. When we use a Forward HDRP, Unity calculates the lighting in a single pass when rendering each individual Material. However, if we use Deferred HDRP, Unity processes the lighting for every GameObject in the Scene. With this definition, based on giving the best possible image of the virtual scenario, we considered using a Deferred render pipeline.

As for the illumination settings, a spot light type was used. Like a point light, a spot light has a specified location and range over which the light falls off. However, the spot light is constrained to an angle, resulting in a cone-shaped region of illumination. The center of the cone points in the forward (Z) direction of the light object. The light also diminishes at the edges of the spot light's cone. By widening the angle the width of the cone is increased and this increases the size of this fade, known as the 'penumbra'. To simulate the scenario most realistically, the illumination range and the angle of each spotlight of the

physical light booth was measured. Figure 7 shows the operation of a Spot light and the screenshot of the settings used in Unity.

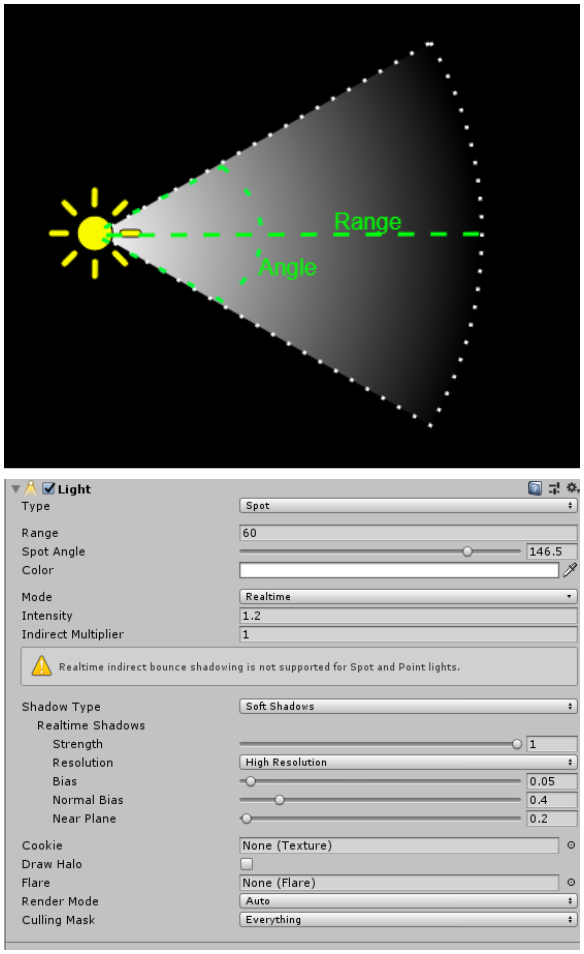

Figure 7. An image of the operation of a spot light (**top**) and a screenshot of the options chosen in our virtual reality system for the simulation of lights (**bottom**).

4.3. Algorithms for Hyperspectral Rendering

Once our hyperspectral textures have been read, we have to calculate the RGB values corresponding to the result of the obtained XYZ tristimulus values. For this, we used the 3×3 transformation matrix. The procedure to obtain this matrix is detailed in Section 3.1. In Algorithm 1, we can see the code we developed for this function in our virtual reality system. The calibration matrix is independent of the virtual stage, and will be able to generate all the RGB colors corresponding to the X, Y and Z values passed by the parameters. We have to say that this matrix will be different for each virtual reality device, but it will be valid on the same device for any scenario and color. To calculate the color of each object, we will have to pass by parameter the X, Y and Z values and the model used will convert it to RGB.

In addition, to obtain the final RGB values, it is necessary to apply the non-linear transform using the three gamma values, one for each RGB channel. Algorithm 2 shows the code corresponding to this function.

Algorithm 1: Algorithm transformation from XYZ values to RGB.

```
// Funtion to transform colors from XYZ to RGB values (0-255)
void XYZ2RGB(double X, double Y, double Z, ref double[] RGB)
{
    RGB = new double[3];
    double r, g, b;

 // XYZ to RGB matrix from Chromatic Characterization of Display HTC
    r = 2.19 * X - 0.69 * Y - 0.32 * Z;
    g = (-0.87) * X + 1.80 * Y + 0.02 * Z;
    b = 0.04 * X - 0.086 * Y + 0.88 * Z;
    // Apply gamma transform
    (RGB[0]) = (gamma(r, 1) * 255.0);
    (RGB[1]) = (gamma(g, 2) * 255.0);
    (RGB[2]) = (gamma(b, 3) * 255.0);
}
```

Algorithm 2: Gamma function example.

```
// Funtion to apply gamma transform
private double gamma(double r, int opcion)
{
    double result;
    result=0;
    switch(opcion)
    {
        case 1:
            result = Math.Pow(r, (1.0 / 2.34));
            break;
        case 2:
            result = Math.Pow(r, (1.0 / 2.30));
            break;
        case 3:
            result = Math.Pow(r, (1.0 / 2.26));
            break;
    }
    return result;
}
```

5. Results

After performing all the above tasks, we obtained a virtual reality system in which we introduced a spectral color management system and we applied it to hyperspectral textures associated to 3D objects. Figure 8 shows the result of the scenario presented in Section 2 under the four light sources studied in this work and its application of hyperspectral textures on the objects.

Figure 8 shows that it is possible to simulate real objects in a virtual reality scenario by changing their color appearance when the spectral properties of light change. However, it is necessary to carry out quantitative checks that allow us to confirm or not our hypothesis that with this new procedure we can obtain a more faithful color representation than that used by the classical system up to now. This verification will be done in the following sections in two ways. First of all, it is necessary to check whether in our system a simple surface color measured in a real light booth can be faithfully reproduced in a virtual reality scene. Secondly, it is necessary to verify that, by applying hyperspectral textures, we can obtain greater fidelity in the reproduction of the color when we apply spectral changes to the light sources.

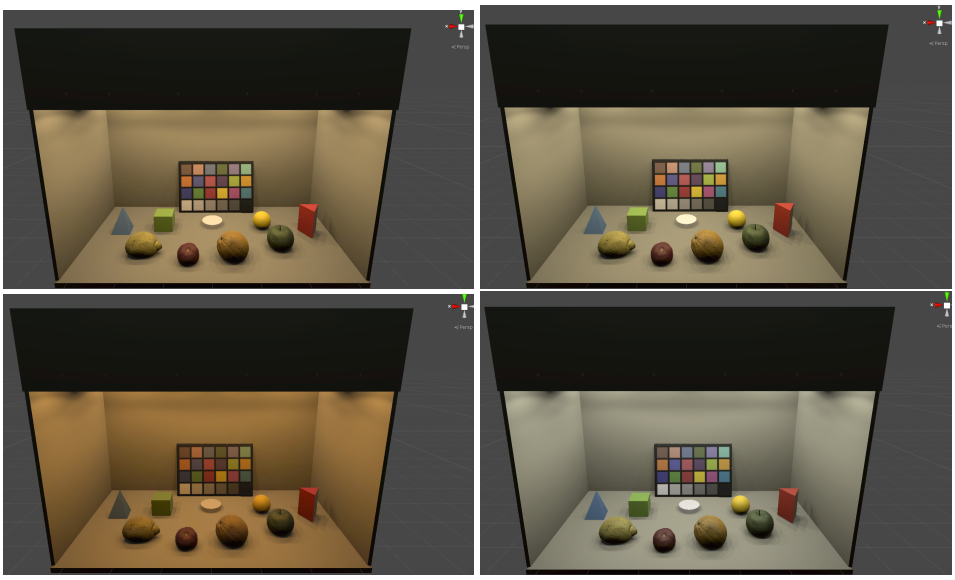

Figure 8. Screenshots of the final virtual scenarios using hyperspectral information and different light sources. TL84 (**top left**), D50 (**top right**), A (**bottom left**) and D65 (**bottom right**).

5.1. Checking Correspondence between Reality and Virtual World

In order to check if we have developed a system with a high degree of fidelity in color reproduction or not, we used 10 samples from the NCS (Natural Color System) atlas book. NCS was developed after 15 years of scientific research with the aim of creating a standard in color specification in the Swedish industry. However, it has already spread worldwide as an universal color language, and is a national standard in countries as diverse as Sweden, Mexico, South Africa, and Spain. Today it is a widely used system both at industrial and professional or private level, from the process of product design in large companies or branding, to the choice of color for projects by individuals, designers, architects, interior designers, etc. It is also supported by color tools of the best quality and repeatability year after year, with which to choose the color through a physical sample [36,37].

For the purpose of reproducing these color samples in our virtual reality system, we measured the color of these samples with the tele-spectroradiometer. We obtained the CIE 1931 x,y chromaticity coordinates when the samples are illuminated by any of the four light sources studied in this work. Figure 9 shows the set up used to perform these measurements as well as the 10 chosen samples.

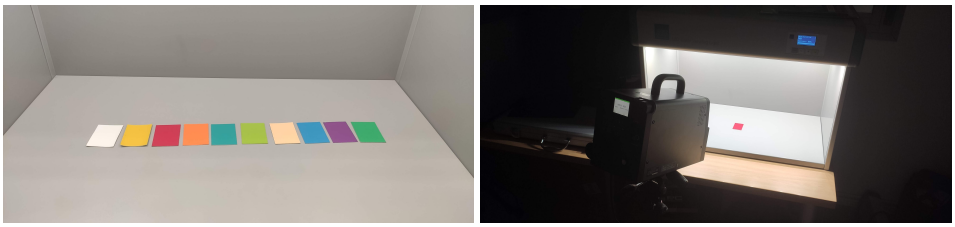

Figure 9. NCS samples used to check results (**left**) and the chromaticity measurement procedure (**right**).

Once the physical measurements of the 10 randomly chosen NCS samples were taken, we entered the spectral reflectances provided by the manufacturer into our virtual reality system. Again, we repeated the same measurement procedure but this time directly on the HMD. This procedure is similar to the one used in the chromatic characterization measurements in Section 3.1 but, in this case, the RGB color assigned to the circular capsule came from the spectral color management system. With these new measurements, we have the CIE 1931 x,y chromaticities for the physical values and for the values measured in

our virtual reality system. Figure 10 shows the comparison between physical and virtual samples under the four light sources studied.

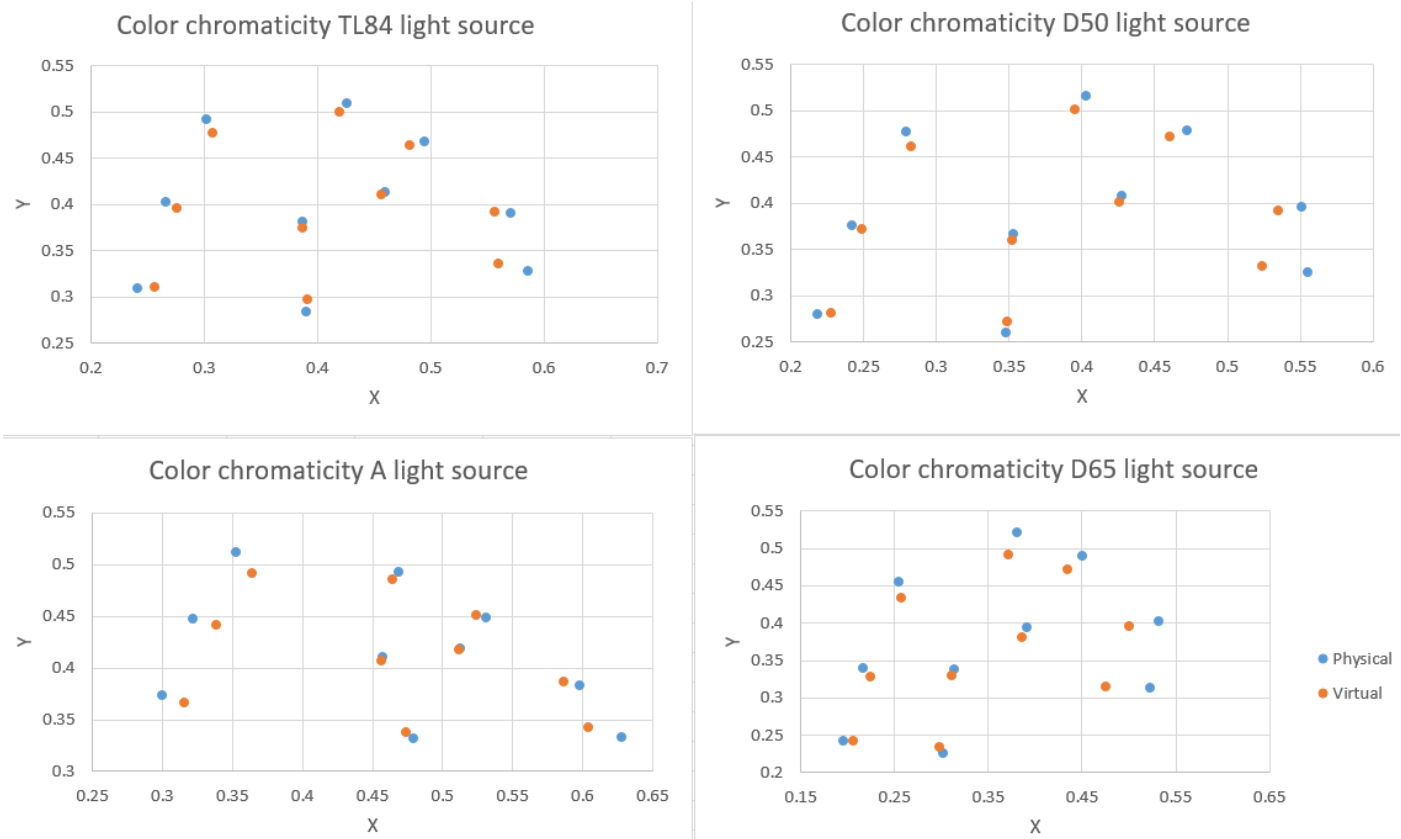

Figure 10. Different x,y chromaticity coordinates of NCS samples for different light sources. TL84 (**top left**), D50 (**top right**), A (**bottom left**) and D65 (**bottom right**).

In order to establish an error level between the two measurements, we have applied the CIEDE2000 formula that allows us to know the color difference between two samples, one real and the other virtual. In Table 1 we can see the different errors obtained for each light source in each of the NCS samples chosen.

Table 1. Color difference between real and virtual NCS samples under different light sources.

NCS Samples	ΔE^* 00 TL84 Light Source	ΔE^* 00 D50 Light Source	ΔE^* 00 A Light Source	ΔE^* 00 D65 Light Source
S 0300-N	1.46	2.52	2.09	1.75
S 1080-Y	4.16	2.75	3.26	2.84
S 1565-G	3.45	3.56	2.94	3.26
S 1080-R	5.25	6.05	4.70	6.20
S 1565-B	2.74	3.74	3.64	3.07
S 2060-B50G	2.88	3.98	3.39	3.48
S 1075-G50Y	3.20	3.38	3.36	2.96
S 0585-Y50R	3.33	3.18	2.62	3.33
S 3055-R50B	5.23	4.92	4.18	4.32
S 0530-Y30R	2.41	1.85	1.73	2.90
Mean Error (Std)	3.41 (1.19)	3.60 (1.21)	3.19 (0.90)	3.41 (1.17)

5.2. Color Differences Found Using Both Color Management Procedures

As a second point of checking, it is necessary to verify that, by applying hyperspectral textures to 3D objects, we can obtain a greater fidelity in the reproduction of the color when we apply spectral changes to the light sources. In order to perform this check, we measured the color of the 3D objects shown at the virtual reality scenario under the four light sources used in this work. We made this measurement in two ways, applying the hyperspectral texture and the spectral computation of color and only applying the RGB texture provided by the 3D scanner. Table 2 shows the color difference between both color representation system and the color reference calculated theoretically from the spectral reflectance obtained from the published dataset and the measured SPDs of the four light sources. We used CIEDE2000 again as the color difference formula.

Table 2. Color difference in all objects in the scene under different light sources with and without hyperspectral textures.

Objects	**ΔE^* 00 Without Hyperspectral Textures**				**ΔE^* 00 Using Hyperspectral Textures**			
	A	**D50**	**D65**	**TL84**	**A**	**D50**	**D65**	**TL84**
ColorChecker sample 1	6.28	4.98	5.06	4.76	3.35	2.83	1.37	2.89
ColorChecker sample 2	4.94	6.79	6.18	5.55	7.08	6.24	3.01	6.93
ColorChecker sample 3	5.46	4.39	2.72	4.65	4.95	2.52	0.74	3.56
ColorChecker sample 4	8.32	5.08	4.63	6.50	3.63	1.13	0.81	1.13
ColorChecker sample 5	9.61	6.19	4.30	7.85	6.84	2.94	1.62	3.24
ColorChecker sample 6	12.50	7.61	6.29	9.06	6.33	4.35	1.72	5.36
ColorChecker sample 7	7.06	7.72	7.81	7.83	2.61	4.98	1.40	5.08
ColorChecker sample 8	17.49	15.11	11.12	15.85	13.04	3.78	0.79	8.72
ColorChecker sample 9	3.21	2.96	3.90	2.73	3.74	3.88	1.38	4.60
ColorChecker sample 10	4.50	1.38	0.71	1.91	5.68	1.38	1.47	1.77
ColorChecker sample 11	9.14	5.74	4.51	6.56	4.24	2.07	1.24	2.49
ColorChecker sample 12	10.86	8.39	7.27	9.15	4.66	3.82	0.86	4.74
ColorChecker sample 13	21.12	16.18	12.69	19.41	16.84	8.94	2.34	13.22
ColorChecker sample 14	6.01	5.17	4.06	5.79	2.93	1.22	1.20	0.24
ColorChecker sample 15	6.07	3.87	4.33	1.28	7.11	2.76	1.28	2.86
ColorChecker sample 16	12.78	9.88	8.08	10.63	7.19	3.56	1.61	4.90
ColorChecker sample 17	3.39	1.71	1.73	1.07	4.54	2.13	0.48	2.16
ColorChecker sample 18	8.36	5.80	4.32	6.95	5.31	3.68	0.57	4.95
ColorChecker sample 19	2.04	2.04	2.04	2.04	2.04	2.04	2.04	2.04
ColorChecker sample 20	6.58	7.03	7.41	7.62	2.50	3.14	0.89	2.67
ColorChecker sample 21	7.70	5.21	4.28	5.03	1.15	2.97	1.01	2.65
ColorChecker sample 22	1.89	1.25	3.13	2.91	2.89	1.40	1.35	0.98
ColorChecker sample 23	2.82	4.86	4.58	5.15	2.88	0.65	1.26	1.65
ColorChecker sample 24	3.96	2.84	7.18	2.93	8.36	4.10	2.77	5.61
Average ColorChecker samples	**7.59**	**5.93**	**5.35**	**6.38**	**5.41**	**3.19**	**1.38**	**3.94**
Lemon	6.34	7.39	8.64	7.00	1.22	0.46	0.73	0.55

Table 2. *Cont.*

Objects	ΔE^* 00 Without Hyperspectral Textures				ΔE^* 00 Using Hyperspectral Textures			
	A	**D50**	**D65**	**TL84**	**A**	**D50**	**D65**	**TL84**
Tomate	4.88	10.43	13.07	8.25	2.81	5.18	2.39	4.48
Green apple	6.00	7.96	5.86	5.44	3.24	1.99	1.67	2.56
Orange	11.18	13.23	14.34	8.03	1.46	3.20	3.33	3.32
Average fruits	**7.10**	**9.75**	**10.48**	**7.18**	**2.18**	**2.71**	**2.03**	**2.73**
Green Cube	3.51	1.85	2.98	3.42	1.66	1.85	1.88	1.91
Yellow Sphere	3.27	3.79	3.76	3.62	2.47	3.01	2.90	2.86
Red Prism	4.14	5.16	5.40	4.81	3.75	4.89	4.91	4.64
Blue Pyramid	3.24	3.81	4.13	4.67	2.08	3.68	4.09	3.22
Average figures	**3.54**	**3.65**	**4.07**	**4.13**	**2.49**	**3.36**	**3.44**	**3.16**

6. Conclusions

In view of the results obtained, we can extract several conclusions related to the introduction of hyperspectral information into a virtual reality system. The first conclusion is that we were able to control the colorimetric values of virtual objects related to real objects shown in a real light booth when the lighting conditions are changed. In order to check whether the results obtained guarantee a good color representation and to estimate the average error, we analyzed 10 physical samples of known NCS values. The average color differences obtained for each light source when we compare the real and the virtual samples are in the range from 3.19 to 3.60 units at the ΔE^* 00 color difference formula. If we take into account that the chromatic characterization error committed in Section 3.1 was 1.8 (calibration error) and this error is one of the contributions to the color reproduction error, we can conclude that the obtained average color reproduction error associated to our method has little relevance to the human visual system. On the other hand, we checked whether our new method of representing 3D objects in virtual reality systems using hyperspectral textures is better or not than the usual method based on RGB textures. The average color difference obtained when comparing the color of the 3D objects displayed in virtual reality with the theoretical color of these objects is always less when we use hyperspectral textures than when we do not use them. Therefore, this provides an obvious improvement in the color rendering of three-dimensional objects in a virtual reality system. We can emphasize that the registered color differences are better using this procedure than those recorded using a color management system with RGB textures. This gives us a breakthrough within the virtual reality paradigm. At the same time, it opens up a wide range of possibilities for future work.

Author Contributions: Conceptualization, F.D.-B., H.C., and P.J.P.; methodology, F.D.-B. and P.J.P; software, F.D.-B., H.C. and P.J.P.; validation, F.D.-B., P.J.P. and H.C.; formal analysis, P.J.P.; investigation, F.D.-B., H.C. and P.J.P.; writing—original draft preparation, F.D.-B., H.C. and P.J.P.; writing—review and editing, F.D.-B., H.C. and P.J.P.; supervision, P.J.P.; All authors have read and agreed to the published version of the manuscript.

Funding: This works was supported by the grants GR18131, IB16004 and IB20094 of the Regional Government of the Junta de Extremadura, and partially financed by the European Regional Development Fund.

Acknowledgments: We would like to thank Ángel M. Felicísimo and María-Eugenia Polo for their collaboration in this work, with great knowledge in photogrammetry and 3D modeling, who have provided us with their scanner to be able to reconstruct 3D objects.

Conflicts of Interest: The authors declare no conflict of interest.

References

1. Greenwood, J. *The Third Industrial Revolution: Technology, Productivity, and Income Inequality*; Number 435; American Enterprise Institute: Washington, DC, USA, 1997.
2. Javidi, B.; Okano, F. *Three-Dimensional Television, Video, and Display Technologies*; Springer Science & Business Media: Berlin/Heidelberg, Germany, 2002.
3. Polo, M.E.; Felicísimo, Á.M. Analysis of uncertainty and repeatability of a low-cost 3D laser scanner. *Sensors* **2012**, *12*, 9046–9054. [CrossRef]
4. Aicardi, I.; Chiabrando, F.; Lingua, A.M.; Noardo, F. Recent trends in cultural heritage 3D survey: The photogrammetric computer vision approach. *J. Cult. Herit.* **2018**, *32*, 257–266. [CrossRef]
5. Barba, S.; Barbarella, M.; Di Benedetto, A.; Fiani, M.; Gujski, L.; Limongiello, M. Accuracy assessment of 3D photogrammetric models from an unmanned aerial vehicle. *Drones* **2019**, *3*, 79. [CrossRef]
6. Choi, I.; Kim, M.; Gutierrez, D.; Jeon, D.; Nam, G. *High-Quality Hyperspectral Reconstruction Using a Spectral Prior*; Technical Report; ACM: New York, NY, USA, 2017.
7. Durán-Dominguez, G.; Felicisimo, A.; Polo, M. 3D study of cultural heritage for conservation: Reliability of the portable 3D laser scanners. In Proceedings of the International Congress on Science and Technology for the Conservation of Cultural Heritage, Seville, Spain, 24–27 June 2014; pp. 357–362.
8. Wang, Y.; Liu, W.; Meng, X.; Fu, H.; Zhang, D.; Kang, Y.; Feng, R.; Wei, Z.; Zhu, X.; Jiang, G. Development of an immersive virtual reality head-mounted display with high performance. *Appl. Opt.* **2016**, *55*, 6969–6977. [CrossRef] [PubMed]
9. Xu, M.; Hua, H. High dynamic range head mounted display based on dual-layer spatial modulation. *Opt. Express* **2017**, *25*, 23320–23333. [CrossRef]
10. Cwierz, H.; Díaz-Barrancas, F.; Llinás, J.G.; Pardo, P.J. On the Validity of Virtual Reality Applications for Professional Use: A Case Study on Color Vision Research and Diagnosis. *IEEE Access* **2021**, *9*, 138215–138224. [CrossRef]
11. Kongsilp, S.; Dailey, M.N. Motion parallax from head movement enhances stereoscopic displays by improving presence and decreasing visual fatigue. *Displays* **2017**, *49*, 72–79. [CrossRef]
12. Lambooij, M.; Fortuin, M.; Heynderickx, I.; IJsselsteijn, W. Visual discomfort and visual fatigue of stereoscopic displays: A review. *J. Imaging Sci. Technol.* **2009**, *53*, 30201. [CrossRef]
13. Wald, I.; Dietrich, A.; Benthin, C.; Efremov, A.; Dahmen, T.; Gunther, J.; Havran, V.; Seidel, H.P.; Slusallek, P. Applying ray tracing for virtual reality and industrial design. In Proceedings of the IEEE Symposium on Interactive Ray Tracing, Salt Lake City, UT, USA, 18–20 September 2006; IEEE: Piscataway, NJ, USA, 2006, pp. 177–185.
14. Fujita, M.; Harada, T. Foveated real-time ray tracing for virtual reality headset. In Proceedings of the SIGGRAPH Asia, Shenzhen, China, 3–6 December 2014.
15. Clay, V.; König, P.; Koenig, S. Eye tracking in virtual reality. *J. Eye Mov. Res.* **2019**, *12*. [CrossRef]
16. Seay, A.F.; Krum, D.M.; Hodges, L.; Ribarsky, W. Simulator sickness and presence in a high FOV virtual environment. In Proceedings of the IEEE Virtual Reality, Yokohama, Japan, 13–17 March 2001.
17. Hilton, P. *Ultra-Wide FOV Retinal Display*; Physics Applications Ltd.: Dayton, OH, USA, 2008; Volume 56.
18. Hvass, J.; Larsen, O.; Vendelbo, K.; Nilsson, N.; Nordahl, R.; Serafin, S. Visual realism and presence in a virtual reality game. In Proceedings of the 3DTV Conference: The True Vision-Capture, Transmission and Display of 3D Video (3DTV-CON), Piscataway, NJ, USA, 7–9 June 2017; pp. 1–4.
19. Kim, M.H. 3D Graphics Techniques for Capturing and Inspecting Hyperspectral Appearance. In Proceedings of the International Symposium on Ubiquitous Virtual Reality, Daejeon, Korea, 10–13 July 2013; IEEE: Piscataway, NJ, USA, 2013; pp. 15–18.
20. Guimarães, T.T.; Mariani, D.H.D.; Kupssinskü, L.S.; Rossa, P.; Horota, R.K.; De Freitas, R.; Roupinha, L.; Weppo, B.E.; Weschenfelder, A.; Spigolon, A.L.D.; et al. Mosis Lab Hyperspectral-Visualization and Correlation of Hyperspectral Data on Immersive Virtual Reality. In Proceedings of the IEEE International Geoscience and Remote Sensing Symposium IGARSS, Brussels, Belgium, 11–16 July 2021; IEEE: Piscataway, NJ, USA, 2021; pp. 5747–5750.
21. Bruno, F.; Bruno, S.; De Sensi, G.; Luchi, M.L.; Mancuso, S.; Muzzupappa, M. From 3D reconstruction to virtual reality: A complete methodology for digital archaeological exhibition. *J. Cult. Herit.* **2010**, *11*, 42–49. [CrossRef]
22. Hill, B.; Roger, T.; Vorhagen, F.W. Comparative analysis of the quantization of color spaces on the basis of the CIELAB color-difference formula. *Acm Trans. Graph. (TOG)* **1997**, *16*, 109–154. [CrossRef]
23. Ibraheem, N.A.; Hasan, M.M.; Khan, R.Z.; Mishra, P.K. Understanding color models: a review. *ARPN J. Sci. Technol.* **2012**, *2*, 265–275.
24. Diaz-Barrancas, F.; Cwierz, H.; Pardo, P.; Perez, A.; Suero, M. Improvement of realism sensation in virtual reality scenes applying spectral and colour management techniques. In Proceedings of the 25th Symposium of the International Colour Vision Society (ICVS 2019), Riga, Latvia , 5–9 July 2019; p. 79.
25. Rhyne, T.M. Applying color theory to digital media and visualization. In Proceedings of the 2017 CHI Conference Extended Abstracts on Human Factors in Computing Systems, Denver, CO, USA, 6–11 May 2017; pp. 1264–1267.
26. Akbarinia, A.; Gegenfurtner, K.R. Color metamerism and the structure of illuminant space. *JOSAA* **2018**, *35*, B231–B238. [CrossRef]
27. Cwierz, H.C.; Diaz-Barrancas, F.; Pardo, P.J.; Perez, A.L.; Suero, M.I. Colour Management in Virtual Reality applied to Lighting Simulations. *AIC Lisbon* **2018**. [CrossRef]

28. Diaz-Barrancas, F.; Cwierz, H.C.; Pardo, P.J.; Perez, A.L.; Suero, M.I. Visual fidelity improvement in virtual reality through spectral textures applied to lighting simulations. *Electron. Imaging* **2020**, *2020*, 259-1–259-4. [CrossRef]
29. Díaz-Barrancas, F.; Cwierz, H.; Pardo, P.J.; Pérez, Á.L.; Suero, M.I. Spectral Color Management in Virtual Reality Scenes. *Sensors* **2020**, *20*, 5658. [CrossRef]
30. Penczek, J.; Austin, R.L.; Obheroi, S.; Hasan, M.; Cook, G.J.; Boynton, P.A. 54-5: Measuring Direct Retinal Projection Displays. In *SID Symposium Digest of Technical Papers*; Wiley Online Library: Hoboken, NJ, USA, 2020; Volume 51, pp. 807–810.
31. Hong, H. A measurement method of the focal distance of the virtual image in an augmented reality or virtual reality device. *J. Soc. Inf. Disp.* **2021**, *29*, 230–236. [CrossRef]
32. Varshneya, R.; Draper, R.S.; Penczek, J.; Pixton, B.M.; Nicholas, T.F.; Boynton, P.A. 50-4: Standardizing Fundamental Criteria for Near Eye Display Optical Measurements: Determining the Eye-box. In *SID Symposium Digest of Technical Papers*; Wiley Online Library: Hoboken, NJ, USA, 2020; Volume 51, pp. 742–745.
33. Pardo, P.J.; Martínez-Borreguero, G.; Pérez, Á.L.; Suero, M.I. Worldwide Uniformity of Color Reproduction in Handheld Video-Game Consoles and Applications. *J. Disp. Technol.* **2012**, *8*, 233–240. [CrossRef]
34. Ennis, R.; Schiller, F.; Toscani, M.; Gegenfurtner, K.R. Hyperspectral database of fruits and vegetables. *JOSAA* **2018**, *35*, B256–B266. [CrossRef] [PubMed]
35. Díaz-Barrancas, F.; Cwierz, H.C.; Pardo, P.J.; Perez, A.L.; Suero, M.I. Colour appearance in immersive three-dimensional virtual environments. *Color. Technol.* **2021**, *137*, 38–43. [CrossRef]
36. Hård, A.; Sivik, L.; Tonnquist, G. NCS, natural color system—From concept to research and applications. Part I. *Color Res. Appl.* **1996**, *21*, 180–205. [CrossRef]
37. Smith, N.; Whitfield, T.; Wiltshire, T. Accuracy of the NCS atlas samples. *Color Res. Appl.* **1991**, *16*, 108–113. [CrossRef]

Capítulo 6

Article published in IEEE Access

IEEE Access

Multidisciplinary ⋮ Rapid Review ⋮ Open Access Journal

AN IEEE JOURNAL

Volume 9
2021

A multidisciplinary, applications-oriented, all-electronic archival journal continuously presenting the results of original research or development across all of IEEE's fields of interest. Supported by author publication fees, its hallmarks are a rapid peer review and publication process with open access to all readers.

(IAECCG)
(ISSN 2169-3536)

IEEE

IEEE Access
Multidisciplinary ⋮ Rapid Review ⋮ Open Access Journal

Received September 20, 2021, accepted October 2, 2021, date of publication October 6, 2021, date of current version October 14, 2021.

Digital Object Identifier 10.1109/ACCESS.2021.3118438

On the Validity of Virtual Reality Applications for Professional Use: A Case Study on Color Vision Research and Diagnosis

HALINA CWIERZ, FRANCISCO DÍAZ-BARRANCAS, JULIA GIL LLINÁS, AND PEDRO J. PARDO

Centro Universitario de Mérida, Department of Computer and Network Systems Engineering, University of Extremadura, 06800 Mérida, Spain

Corresponding author: Francisco Díaz-Barrancas (frdiaz@unex.es)

This work was supported in part by the Regional Government of the Junta de Extremadura under Grant GR18131, Grant IB16004, and Grant IB20094; and in part by the European Regional Development Fund.

This work involved human subjects or animals in its research. The authors confirm that all human/animal subject research procedures and protocols are exempt from review board approval.

ABSTRACT In recent years, there have been very important advances in graphic computing and technology related to the capture and representation of real objects in both 2 and 3 dimensions. One of these technologies is virtual reality, which can be incorporated into common tasks in research laboratories, especially in laboratories related to color vision and lighting research. To incorporate virtual reality devices into research tasks, newly developed applications must be validated with existing and known tests or techniques. The objective of this work was to study the validity of a commercial VR system for research and diagnosis in color vision. We carried out a comparative study on the behavior of these immersive systems for viewing 3D scenes in real time using a color vision test. In particular, we implemented a virtual version of the Farnsworth-Munsell 100 Hue test and compared the results obtained by 17 normal and 3 defective observers in both the physical and virtual tests. The results show that the functionality of both tests is very similar and that the diagnosis of both methods is equivalent. Detailed analysis of the results of both tests indicates that there is a slight difference in scale between the two tests. This difference in scale indicates a greater difficulty in the case of the virtual test but does not affect the final diagnosis. This could be due to the greater difficulty in using a head-mounted display (HMD).

INDEX TERMS Virtual reality, 3D scenes, computer vision, color research, color reproduction, color deficiency.

I. INTRODUCTION

Technology is continuously evolving and offering new devices and/or techniques that professionals, researchers or end users try to incorporate into their daily lives, whether for professional, research or personal reasons, to obtain the possible benefits of the new technology. This integration process can be part of a long process in which the industry develops a new professional and specific device or service, and after several years of the refinement process, it finally reaches the end-user market. Another integration process is directly targeting new devices or techniques to the final end-user market, pursuing a generalization of their use, and after this generalization, several professional or specific applications can be developed by third-party researchers. The last case corresponds to the current state of evolution and development of virtual reality (VR) devices or services. The fact that virtual reality system have been developed with the consumer market in mind does not invalidate their use for research or professional applications. It is only necessary to check the validity of this new technology against a well-known traditional tool or application.

In relation to the specific fields of color vision and lighting research, the introduction of virtual reality systems is not the first time that new commercial devices have been introduced in research laboratories to replace specific scientific devices such as visual colorimeters or anomaloscopes: image devices based on cathode ray tubes were first applied [1], [2], with LCD [3], [4] and OLED screens being launched later [5]. In all these previous cases, the chromatic

The associate editor coordinating the review of this manuscript and approving it for publication was Charith Abhayaratne.

characterization of these new types of devices has been a key point [6]–[11].

From a visual point of view, VR technology creates the visual sensation of immersion in a three-dimensional world. This 3D visual sensation is created using specific hardware and software components. The hardware component is always based on head-mounted displays (HMDs). There are two different types of hardware: devices that do not have their own graphic hardware and need a personal computer for this task and devices that use a mobile phone or other specific graphic hardware without a personal computer. There are significant differences in performance between the two types of devices. In this work, we will refer exclusively to the first type: those devices that are associated with a personal computer with a dedicated graphics card.

In terms of the software component of a VR system, there are two main commercial software platforms for developing virtual reality content: Unreal Engine and Unity Game Engine. In both platforms, mathematical functions are used as basic rules of internal functioning that try to reflect to a greater or lesser extent the real world through physical laws [12].

It is possible to obtain rendered scenes with a high degree of visual appearance fidelity when treating the light–matter interaction simulating the physical laws governing this phenomenon. To handle the lighting and shading conditions, the graphic engine uses a physical bidirectional reflectance distribution function model (BRDF) with four main components: diffuse, specular, normal, and smoothness. The diffuse component corresponds to material color, the specular component corresponds to surface color, and the normal and smoothness components correspond to surface texture.

In this study we research whether it is possible to use virtual reality technology for research tasks related to color vision and lighting. There are other examples of the utility of this new technology in other research fields [13]–[15]. We can approach this topic from different perspectives. On the one hand, we have the paradigm of classical colorimetry which characterizes the image device through spectroradiometric measurements, from which we can distinguish between absolute colorimetry or relative colorimetry. In both cases, the only relationship with human visual perception is through the standard observer CIE XYZ 1931 defined by the International Commission on Illumination (CIE) [16]. On the other hand, we have the paradigm of psychometry, where we would measure the effect of a scene shown on a VR device on the perception of the observer without having to be linked to any physical property [17]. Finally, the paradigm of psychophysics tries to relate the physical world with the perceptual world but this case has an intermediate processing layer dedicated to the simulation of a physical world in a virtual world, in such a way that we could call it virtual psychophysics [18], [19].

The objective of this work is to check the validity of a commercial virtual reality system to be used in research and diagnosis tasks in color vision and lighting laboratories. This validity arises from the point of view of what we have previously called virtual psychophysics, since it uses the simulation of the physical laws related to light-matter interaction. However, we have also studied the effect of this physical simulation on visual perception to check both aspects of psychophysics. Determining the validity of a specific use of this type of virtual reality system does not validate these systems for all uses in research tasks related to color vision research. However, if the result is positive, it opens the door to a wider future use in different fields provided each of its applications has been previously validated.

Specifically, in this study, a virtual version of the Farnsworth-Munsell 100 Hue test (FM 100) for color vision assessment has been implemented in a virtual reality environment. To verify its validity as a research and diagnosis tool, first, a relative colorimetric reproduction of the FM 100 test is necessary, and second, the results obtained with this virtual test are compared to those obtained with a real version of the mentioned test. This comparison is based on the analysis of the results obtained by both versions on the same population sample. These tasks try to answer the research questions posed previously: Is it possible to use virtual reality technology for research tasks related to color vision and illumination? What would be the validity of a commercial test implemented in a virtual reality environment?

In Section II of this paper, we review the state-of-the-art color vision testing methods and explain in detail how the FM 100 test works. In Section III, we describe the methodology used in this work, including the chromatic characterization of the VR system, the spectroradiometric measurements of the FM 100 test and the development of the 3D virtual scene. Finally, in Sections IV and V, the experimental results are analyzed and discussed, and conclusions are drawn.

II. TESTS FOR COLOR DEFICIENCY

Color perception depends on the light falling on the three types of cones of the retina. When a person suffers from color vision deficiency (CVD), it can limit his or her daily life, academic life or even work life.

Color vision tests play an important role in detecting visual deficiencies that may be related to pathologies such as optical neuritis, pituitary adenoma, glaucoma, and diabetes. In order to diagnose these pathologies very sensitive tests are required [20] which, on the one hand, allow the detection of small deviations from normal color vision, and, on the other hand, allow discrimination between different degrees of alterations in color vision.

The methods used in these tests for the detection of visual impairment can be grouped into three types:

- Pseudo-isochromatic tests: This type of test is based on the use of films composed of small colored surfaces (background) from which some colored areas stand out, forming a figure that will only be visible to normal observers on some occasions, while on others, it will only be visible to abnormal or defective observers.

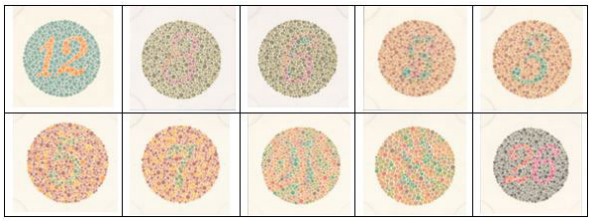

FIGURE 1. Different Ishihara test plates.

This method provides a quick result (Ishihara, HRR, SPP, Ulloa, etc.).

Among the pseudoisochromatic tests, the Ishihara test, the first version of which appeared in 1906 [21], is the most widespread and used for the study of chromatic defects. The main objective of this test is to detect red-green type deficiencies and in its current configuration, it consists of thirty-eight plates (Fig. 1), twenty-five with numbers for observers who can read and thirteen with sinuous lines for those who cannot. For this type of test, we simulated the visual aspect in virtual reality [22].

- Tests were carried out using special instruments such as an anomaloscope. This device is essentially a colorimeter that produces a metameric pair from a mixture of two pure spectral colors of variable proportions to equal a reference color on a bipartite field. This device can be adapted to each problem.
- Tests for sorting colored caps in the natural order, from blue to red and various shades in between. They allow the detection of color perception deficiencies (Farnsworth-Munsell test, FM 100 and its reduced versions D-15, B-20 and H-16, Roth 28-Hue test, Lanthony test, etc.).

  Ordering tests are currently one of the main tools for the diagnosis of congenital and acquired anomalies. They provide sufficient information while maintaining relative simplicity in the task to be performed by the subject compared to methods using an anomaloscope.

  Among the sorting tests, the most sensitive one is the 100-tone FM 100, although it actually consists of 93 (85 unfixed and 8 fixed) caps. This test is based on the notation system developed by Munsell [23]. It consists of a series of colored caps with constant saturation and clarity but different tones (Fig. 5). In this work, we develop a virtual scene with the FM 100 test applying color management techniques.

A. FM 100 TEST SCORING METHOD

The goal of this test is to place the color palettes in the correct order based on the color hue. Scores for the test are based on two factors:

- Frequency of the color caps are misplaced.
- The severity or distance of the misplacement.

The scoring tool provided with the test calculates the total error score (TES) and graphically represents the errors made by the observers (Figs. 2-4). A solid black line represents the observer's response to the test. The further it moves away from the center circle, the larger the errors will be. The test results can be classified according to the following ranges:

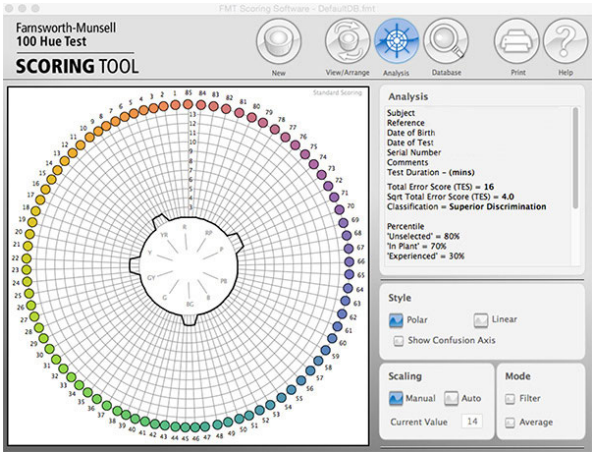

FIGURE 2. Superior (good) software score.

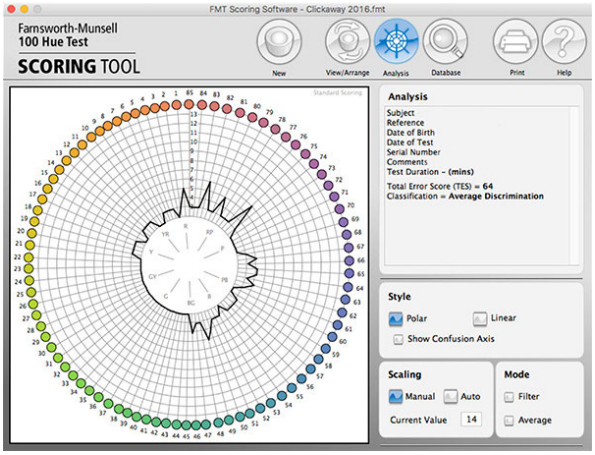

FIGURE 3. Average (normal) software score.

1) SUPERIOR (GOOD) SCORE

Approximately 16% of the population makes 0 to 4 transpositions on the first test or has total error scores of zero to 16. This is a superior range of competence for color discrimination.

2) AVERAGE (NORMAL) SCORE

Approximately 68% of the population scores between 16 and 100 on the first tests. This is a normal range of competence for color discrimination.

3) LOW (WEAK) SCORE

Approximately 16% of the population has a total error score above 100. The first retest may show an improvement, but further retests do not significantly affect the score.

III. METHODOLOGY

The methodology applied in this work can be divided into six stages. The first stage describes the method applied for the chromatic characterization of the virtual reality device and the results obtained. The second stage shows how color

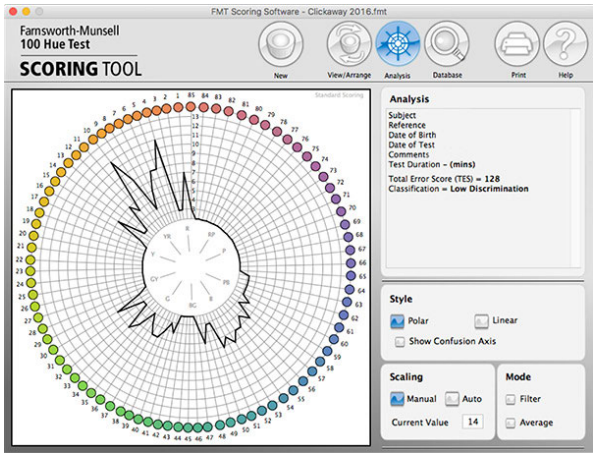

FIGURE 4. Low (weak) software score.

FIGURE 5. Original Farnsworth-Munsell 100 Hue test samples divided into four rows.

management has been carried out within the VR software platform. In the third stage, the results of the spectroradiometric measurements performed on the FM 100 test are shown. Finally, each of the following are described: the virtual scene design, the graphics settings employed, the population sample used and the procedure followed to perform the test.

A. CHROMATIC CHARACTERIZATION OF HEAD-MOUNTED DISPLAY

The first step to use a virtual reality system in tasks related to color vision research is the chromatic characterization of head-mounted displays (HMDs). Each device of this type has its own specific characteristics in terms of the chromaticity of its primary colors and the white point, as well as for the relationship between the digital values of the analog-to-digital converter (DAC) and the associated tristimulus values. However, the main commercial devices currently on the market use two LCD or OLED screens (one for each eye) and Fresnel-Aspherical hybrid lenses to adapt the observer's accommodation distance to infinity, even when the screens are at a short distance from the user's eyes. With these lenses, the field of view (FOV) covered is close to 110° per eye. The authors of this paper have used the same methodology with different HMDs in other works [22], [24] and have developed a simple color characterization model for VR devices. This model is based on a typical linear transformation between the RGB' values and the XYZ tristimulus values using a 3×3 matrix. RGB' values are obtained after a gamma correction

TABLE 1. Chromaticity coordinates of each primary channel and white point and gamma value of each channel.

Channel	Chromaticity		Luminance	Gamma	
	x	y	Y (Relative)	Value	R2
White	0.299 ± 0.002	0.315 ± 0.002	100.0		
Red	0.667 ± 0.004	0.332 ± 0.003	30.3 ± 1.1	2.34	0.999
Green	0.217 ± 0.007	0.710 ± 0.002	75.4 ± 2.4	2.30	0.999
Blue	0.139 ± 0.002	0.051 ± 0.002	7.8 ± 0.5	2.26	0.998
Black	0.335 ± 0.01	0.361 ± 0.004	0.4 ± 0.2		

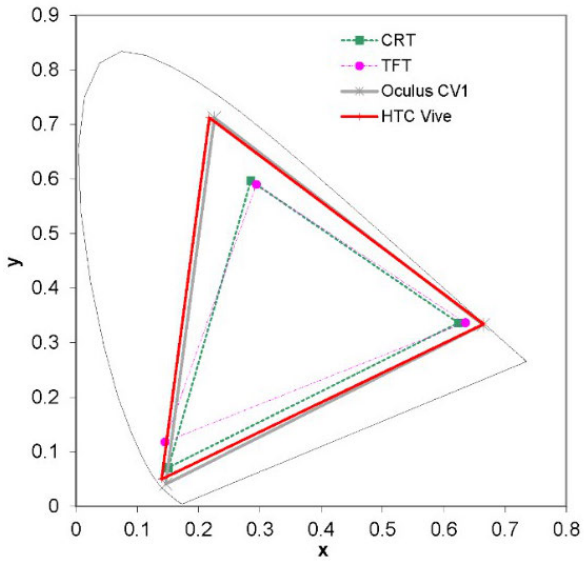

FIGURE 6. Color gamut of different displays represented in the CIE 1931 chromaticity diagram. The evolution of the color gamut with different display technologies can be seen.

of the original RGB values that guarantee the linearity of the system.

For the specific HMD model used in this work (HTC Vive), the chromaticity values of primary colors and the white point and the gamma value of each chromatic channel are shown in Table 1.

The color gamut associated with both HMD display types is similar to that of other displays with OLED technology, as shown in Fig. 6.

The measurements were performed in steps of 5 RGB values from 0 to 255 per channel. Then, we measured 50 random values to check the final error. Finally, we performed some systematic measurements. In total we have made 234 measurements. In the supplementary material, we have provided the RGB and XYZ values of these measurements. We obtained an average color error of 1.5 units in terms of CIEDE2000 with a standard deviation of 0.6.

B. COLORIMETRIC CALCULATIONS MODULE FOR VR

One of the main problems regarding color management in virtual reality devices is the high refresh frequency of images, between 90 and 120 Hz, due to the low latency in the interaction of the user with the environment. This high frequency reduces the time available for colorimetric calculations. For this reason, we have chosen a display characterization model

that does not require complex calculations but only seeks to relate, as simply and accurately as possible, the values of the DAC with chromatic values of the stimulus in any reference color space. In this case, the most appropriate color space will be the tristimulus space associated with the CIE 1931 standard observer; the chromatic characterization approach is a classical matrix model connecting RGB and XYZ spaces, including a previous linearizing gamma correction of RGB values. This simplified color characterization model is widely used in color management software. In this case, the most appropriate color space will be the tristimulus space associated with the CIE 1931 standard observer; the chromatic characterization approach is a classical matrix model connecting RGB and XYZ spaces, as shown in Eqn. 2, including a previous linearizing gamma correction from Eqn. 1.

$$\begin{aligned} R' &= R^{\gamma_1} \\ G' &= G^{\gamma_2} \\ B' &= B^{\gamma_3} \end{aligned} \tag{1}$$

$$\begin{pmatrix} X \\ Y \\ Z \end{pmatrix} = \begin{pmatrix} X_{R'max} & X_{G'max} & X_{B'max} \\ Y_{R'max} & Y_{G'max} & Y_{B'max} \\ Z_{R'max} & Z_{G'max} & Z_{B'max} \end{pmatrix} * \begin{pmatrix} R' \\ G' \\ B' \end{pmatrix} \tag{2}$$

C. FM 100 TEST: SPECTRORADIOMETRIC MEASUREMENTS

In 1943, Deanne Farnsworth proposed the 'Farnsworth-Munsell 100 - Hue' test starting from 100 Munsell samples on matte paper, all of which had the same values of chroma and value (5/5) but had different tones (hues) varying in step constants from the perceptive point of view [23]. Subsequently, the test samples were reduced to 85, although the name of the test was maintained at FM 100. The FM 100 test is a sorting test with which two objectives can be achieved: distinguishing among people with normal color vision and those who have a high and low color discrimination ability and identifying different types of defective color vision. The FM 100 test has also been the subject of numerous specific scientific investigations over the past 50 years [25]–[30] and is a valid and well-known reference for any color vision laboratory.

To implement the virtual version of this test in a virtual reality environment, we performed 3 independent spectroradiometric measurements for each of the 85 samples in a completely new FM 100 test. Specifically, the spectral reflectance of each sample and the CIE 1931 XYZ tristimulus values of each sample were measured. A Konica-Minolta CS-2000 spectroradiometer was employed. The spectroradiometer was inclined 45° to the horizontal, and a Spectralon diffuse reflectance pattern (LabSphere, USA) was used as a reference to measure spectral reflectance. All measurements were made using a D65 simulator as the light source, with which the LED viewing light booth was equipped (Just Normlicht, Germany). Fig. 7 shows the CIE 1931 chromaticity coordinates of each of the 85 samples of the FM 100 test under the CIE D65 theoretical illuminator and under simulator D65 of

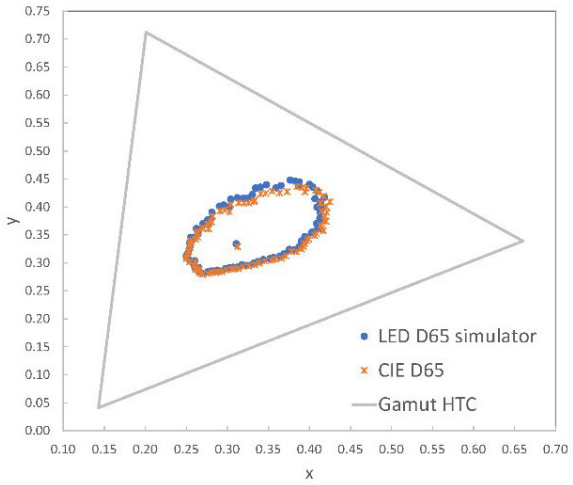

FIGURE 7. Chromaticity of 85 FM 100 samples illuminated with CIE D65 illuminant (orange star) or LED D65 simulator (blue circle).

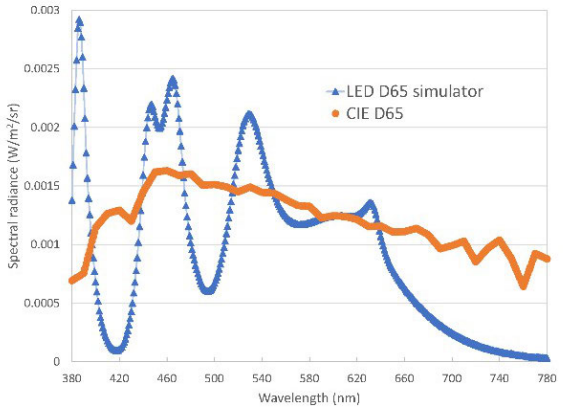

FIGURE 8. Spectral power distribution of the light sources employed in this work adjusted to a luminance value of 100 Cd/m2: CIE D65 (orange circles) and LED light booth D65 simulator (blue triangles).

the light booth. Both power spectral distributions are shown in Fig. 8.

D. VIRTUAL SCENE

A virtual scene was created using the Unity Game Engine software platform in the software version 2019.1.5, which allows 3D scenes to be generated and displayed on virtual reality devices through their corresponding rendering. The scene simulates the Just NormLicht LED, available in our laboratory equipment (Fig. 9). This light booth is equipped with 12 LED spotlights and has been simulated both in physical and lighting geometry.

We simulated each of the 85 samples of the FM 100 test within this light booth. Each sample consists of a support part made of black Bakelite and another flat part, where the chromatic sample is located. The color of each sample was defined as a texture associated with a virtual material created in Unity, which allowed us to assign an RGB color to each sample.

To calculate the RGB color of each of the samples, a script that computes the tristimulus values of the FM 100 test

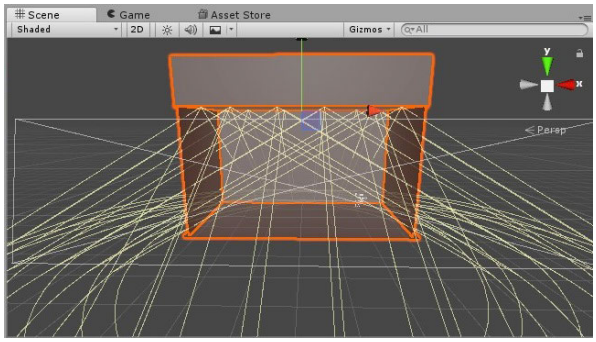

FIGURE 9. Virtual light booth designed in this work.

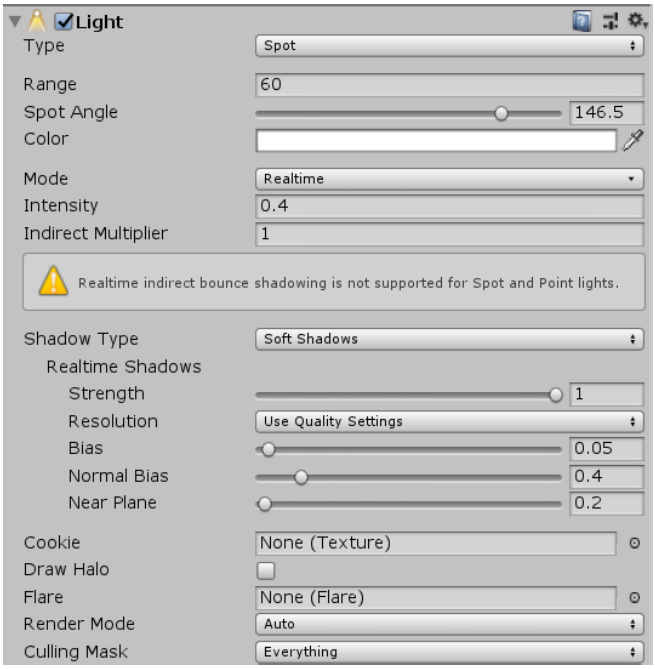

FIGURE 10. Spotlight settings.

samples under the SPD of the source used in the light booth was made. Subsequently, the corresponding RGB values were obtained through our colorimetric calculation module for VR.

We also measured every detail of the actual light booth. Details such as the angle of incidence of the lights or the separation between spotlights have been applied in the virtual scene. Next, in Fig. 10, an image of the lighting options is used to simulate the light booth.

Although the original recommendation was to use the C illuminant to perform the test, the CIE currently recommends using the D65 illuminant. However, it is not possible to use the D65 illuminant because of its theoretical nature. Many different D65 illuminant simulators exist on the market. A script has been introduced in the developed software that allows us to perform calculations on the RGB values for any light source so that it is possible to study the behavior of this test under different D65 simulators [31].

E. GRAPHIC SETTINGS

As we have described in the introduction section, the main objective of this work is to study the validity of commercial

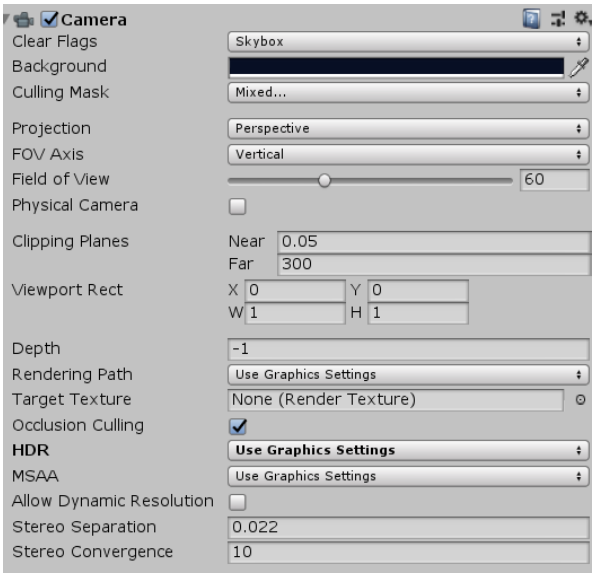

FIGURE 11. VR camera settings used.

virtual reality systems to be used in professional tasks in color vision and lighting laboratories. From this perspective, our priority has been to carry out a visual impairment test with the greatest fidelity to reality, using hyperspectral textures as a new method for this purpose but without excessively penalizing the rendering and response time that virtual reality requires. For this reason, the standard render pipeline with deferred rendering has been used in our VR scenario. A previous work demonstrated the effectiveness of this configuration [12]. Light treatment is based on real-time lighting without baked global illumination light maps. Because of the simplicity of our scenario and the fact that there is no metallic material or transparency, we employ only the diffuse component of light reflected at the material surface (albedo color in Unity Terms). We did not include reflection probes or activate the HDR mode.

For the VR camera settings, we used a skybox with a black background. We have also performed the recommended VR default settings of field of view and stereo separation and convergence. The values used for the VR camera settings are shown in Fig. 11.

F. OBSERVERS AND PROCEDURE

The population sample was composed of 20 observers (14 men and 6 women) aged between 20 and 56 years old. Three of them demonstrated color vision deficiencies by means of other color blindness validation tests, such as an Ishihara test. Those observers who need glasses in their daily life used the glasses for both the physical and virtual tests. Each observer answered the test five times randomly in different sessions. The test requires two parts: one corresponding to the physical test and another corresponding to the virtual version. All sessions were carried out on different days and by varying the order randomly.

The methodology employed with the physical test (Fig. 12 above) follows the recommendations of the original author of

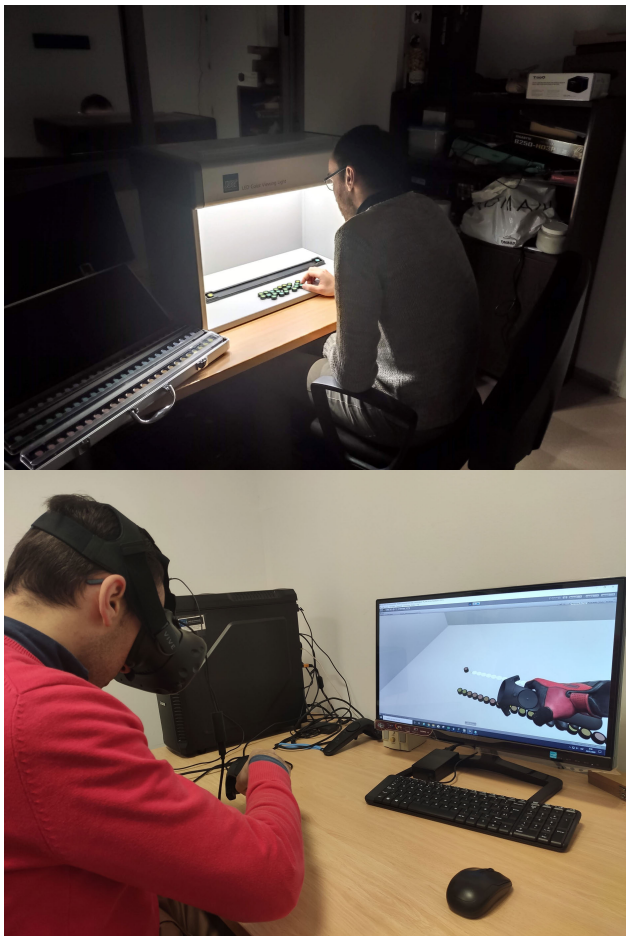

FIGURE 12. (Top) A user's procedure when taking the physical test. (Bottom) A user's procedure when taking the virtual test.

the FM 100 test [23]. The methodology applied to the virtual test follows this sequence: first, all color samples correctly ordered are shown to the observer (Fig. 14 above). Subsequently, the test starts only showing the samples belonging to a single row. This row is chosen randomly, leaving the first and last caps at a fixed position in the same way that the physical test is applied (Fig. 14 bottom). The observer must place all the samples in the order he/she considers correct with a remote control for the VR device (Fig. 12 bottom). There is an equivalent remote control to the real one in the virtual scene, and the observers can see this remote control controlled by a virtual hand. Observers can modify the position assigned to each sample at all the times they consider necessary. After finishing each row, the next row is shown, and at the end of the test, the score obtained and the time spent are reported.

IV. RESULTS

The results of this work can be divided into two parts. The first part is related to the fidelity of the color reproduction of the virtual scene in relation to the original real scene. The second part deals with the comparison of the results obtained by means of both tests (physical and virtual tests). The results are described next.

TABLE 2. Color difference values.

Row- Tablet	ΔE^*
1- 1	1.76
1- 10	2.42
1- 20	1.73
2- 23	0.99
2- 32	1.38
2- 41	1.44
3- 46	1.18
3- 55	1.43
3- 62	1.36
4- 64	1.36
4- 75	1.60
4- 83	1.42
Mean Error (Standar Desviation)	1.5 (0.4)

A. MEASURED COLOR DIFFERENCE BETWEEN THE PHYSICAL AND VIRTUAL TESTS

The International Commission on Illumination (CIE) defines the metric distance ΔE^*ab (also called ΔE^*) as a basic color difference formula associated with the CIELAB color space standardized in 1976 [32].

There are known perceptual nonuniformities in the CIELAB color space; during recent decades, several new color difference formulas have been proposed and employed to correct these nonuniformities (as recommended by the CIE in 1994 and 2000 [33]). These nonuniformities are important because the human eye is more sensitive to certain colors than to others. A good metric should take this into account to associate the notion of a ''just noticeable difference'' (JND) to a unity of its metric in the whole color space. Otherwise, a certain ΔE^* may be insignificant between two colors in one part of the color space while being significant in some other part. With the concept of JND in mind, CIEDE2000 color difference values between 1 and 2 units are considered close to imperceptible for the human visual system. Values between 2 and 3 are considered an accurate representation of the color. Above these values, the result is considered to be inaccurate.

To obtain the average color difference between the real and virtual scenes of this work, we measured 12 FM 100 test caps (3 from each row, at both ends and at the middle) of the physical test, and measured the equivalent caps at the virtual scene for the virtual test. Table 2 shows the color difference between each pair of caps (virtual and real). The results showed an average color difference of CIEDE2000 = 1.5 and a standard deviation of 0.4. This value matches the chromatic characterization mean error limit and reflects the accurate behavior of our system in a faithful color reproduction of a real scene in a virtual scene.

In addition, in Fig. 13, we see the values of chromaticity CIE 1931 (x, y) in each of the 12 physical and virtual tables. The results of both measurements denote a clear matching between the two systems.

Finally, in Fig. 14, we see the appearance of the virtual test, while if we look at Fig. 15, we see the appearance of the physical test. Although measuring the general appearance

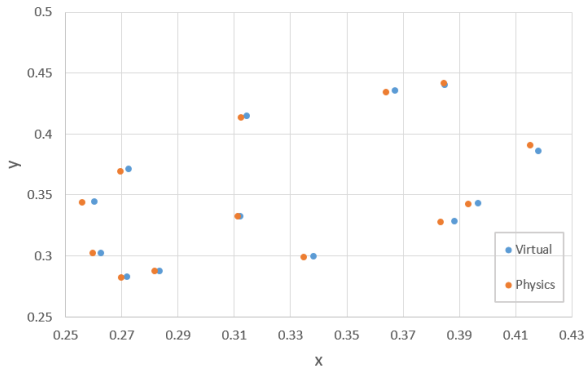

FIGURE 13. Chromaticity measurements (x,y) for the 12 FM 100 samples.

FIGURE 14. (Top) Initial aspect of the virtual reality application in which the 93 test caps are shown. (Bottom) Screen capture during the development of one of the tests in which the virtual interface is used to order the samples.

is not the main objective of this work, and we have only measured color values, we see that the appearance has many similarities.

B. SCORES OBTAINED BY THE OBSERVERS

As described in section II, the FM 100 test is a sorting test where a score is obtained according to the errors made in the sorting of color samples with equal saturation and clarity and different hues. With this score, it is possible to quantify how accurate the color discrimination ability of the person taking the test is.

Although it is possible to carry out a comparative study capsule by capsule, an accurate indicator of the correct functioning of the virtual test versus the physical test is the comparison of the errors obtained by the same observers in both tests. Since each of the tests was carried out 5 times, this comparison should be made with the average of the scores obtained in the 5 sessions.

Table 3 shows the results obtained by the 17 observers previously classified as normal observers and the three observers classified as defective. A first analysis of this data shows a high correlation between both scores: those corresponding to

FIGURE 15. (Top) Initial aspect of the real scene application in which the 93 test caps are shown. (Bottom) Screen capture during the development of one of the tests in which the virtual interface is used to order the samples.

TABLE 3. Results obtained by the 17 observers previously classified as normal observers and the three observers classified as defective.

Observer	Age	Sex	Physical Test	Virtual Test
Normal 1	55	W	35.2	68
Normal 2	54	W	26.4	47.2
Normal 3	56	W	19.2	34.4
Normal 4	56	M	29.6	43.2
Normal 5	26	M	4	19.2
Normal 6	21	M	13	25.6
Normal 7	29	M	5.6	21.6
Normal 8	31	W	13.6	29.6
Normal 9	26	M	4	16
Normal 10	24	M	40	80
Normal 11	45	M	14	23.2
Normal 12	26	W	7.2	51.2
Normal 13	27	W	1.6	28.5
Normal 14	56	M	26	32
Normal 15	56	M	22	46
Normal 16	26	M	8	24
Normal 17	25	M	16	52
Defective 1	59	M	189	191
Defective 2	19	M	133.6	155
Defective3	25	M	212	268
Mean (defective excluded)			16.8	37.7
Standard deviation (defective Excluded)			11.6	17.8
Upper limit for normals			51.5	91.3
Pearson Coef.			0.98	

the physical test and those corresponding to the virtual test (Pearson = 0.98, Confidence level = 99%, $p < 0.001$).

Moreover, the relationship between both scores is highly linear ($R^2 = 0.96$, Confidence Level = 99%, p-value < 0.001) with a slope value very close to 1, and only an independent term of 19 points is noteworthy, which indicates that the virtual test, on average, obtained an error that was 19 points higher. Statistical data related with this linear model and its confidence interval are shown in Table 4. We can point out that the errors in the virtual reality tests are higher than those in the physical tests due to a higher complexity caused by the use of a technological device such as HMD. An influencing

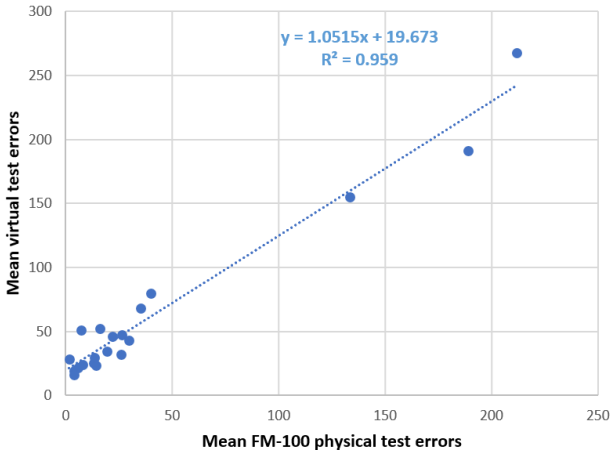

FIGURE 16. The correlations between the errors of the physical and virtual test.

TABLE 4. Statistical data obtained from the linear regression applied between physical and virtual test results.

Linear model	Coefficients	Error	t	Sigma	Confidence Interval 99%	
					Lower	Upper
Constant	19.673	3.720	5.288	0.000	8.964	30.382
Slope	1.052	0.051	20.522	0.000	0.904	1.199

factor is the quality of the image, which is still not perfect due to several known effects, such as the screen door effect or the blurring effect. Regarding the differences in scale between normal and defective observers, we think that the lower quality of the virtual image compared to real scenes is the cause of the 19 points of difference, on average, at the independent term of the linear equation. This difference in score appears as a 4-fold difference at lower scores (better color observers) because it is relatively easy to change the order of four caps (16 points) instead of two caps (4 points) in the more difficult VR scenario. However, this factor is not related to the diagnostic criterion because this criterion depends, in our opinion, on the closeness to the slop factor of the linear equation to 1.

Figure 16 shows the graphical representation of the results obtained and the expression of the linear relationship model between both sets of results. This figure clearly shows the difference between the observers classified as defective and normal. If we look at purely statistical criteria, a non-normal observer is one that is outside the normal probability distribution, which is usually defined as an observer who obtains a result that is more than 3 standard deviations away from the mean value of the population when calculating that mean value. This is what is known as the 99.9% confidence level. If we perform these calculations for the results obtained with normal observers, we can see how this upper limit would be marked by a score of 52 points for the physical test and 92 for the virtual test. In both cases, observers previously classified as defective are those who are outside these limits and would again be classified as defective.

No statistically significant differences were obtained after analyzing the data obtained according to the age and sex of the participants.

V. CONCLUSION

Virtual reality devices have been in constant evolution in recent years, allowing more diverse use. The general objective of this work was to contribute to the use of commercial virtual reality systems in professional tasks. Specifically, we have implemented a virtual version of a known arrangement test for color vision assessment, the FM 100 test, as an example of the use of this technology in research and diagnosis tasks at lighting and vision research labs. Our main objective was that the functionality of both tests (virtual and physical) would have the same behavior. The results obtained show that the functionality of both tests, the virtual and physical tests, are very similar. Furthermore, the diagnosis of both methods is equivalent. The scores obtained by real observers in both tests are slightly different in scale but have a clear linear relation. The small difference in scale does not affect the classification made of defective or normal observers and could be related to the greater difficulty in using an HMD as a display. The main limitation of this work lies in the dependence of a previous chromatic characterization of the virtual reality system (hardware and software). This limitation is identical for other types of electronic media used in research tasks (CRT, TFT, OLED). However, it is an advantage to use this technological support to perform color vision tests because there is no deterioration of the samples since the observers do not manipulate the samples. Another advantage is that we can control the illumination both in intensity and spatial distribution.

In view of the results, we conclude that this technology based on HMDs and virtual reality contents is valid for this research task. A future line of work could be to extend this type of generic tests based on virtual reality to other more specific types of tests such as visual evaluations carried out to obtain automobile driver or airline pilot licenses. This future work should be also oriented to deepen the improvement of the visual appearance of virtual 3D scenes. Despite the high quality of virtual reality systems, there is still room for progress both in the development of display devices and the improvement of the management of real-time rendering software. These improvements could expand the potential use of this virtual reality-based technology.

ACKNOWLEDGMENT

The authors would like to thank the Centro Universitario de Mérida, University of Extremadura for the cession of its areas and materials used during this work.

REFERENCES

[1] P. Cavanagh, D. Maurer, T. Lewis, D. MacLoad, and G. Mather, "Computer-generated screening test for color blindness," *Color Res.*, vol. 11, pp. 63–66, Oct. 1986.

[2] A. Hoffmann and M. Menozzi, "Applying the ishihara test to a PC-based screening system," *Displays*, vol. 20, no. 1, pp. 39–47, Feb. 1999.

[3] O. K. Ozgur, T. S. Emborgo, M. B. Vieyra, R. F. Huselid, and R. Banik, "Validity and acceptance of color vision testing on smartphones," *J. Neuro-Ophthalmol.*, vol. 38, no. 1, pp. 13–16, 2018.

[4] P. J. Pardo, A. L. Pérez, and M. I. Suero, "Validity of TFT-LCD displays for colour vision deficiency research and diagnosis," *Displays*, vol. 25, no. 4, pp. 159–163, Nov. 2004.

[5] E. A. Cooper, H. Jiang, V. Vildavski, J. E. Farrell, and A. M. Norcia, "Assessment of oled displays for vision research," *J. Vis.*, vol. 13, no. 12, p. 16, 2013.
[6] R. S. Berns, R. J. Motta, and M. E. Gorzynski, "CRT colorimetry. Part I: Theory and practice," *Color Res. Appl.*, vol. 18, no. 5, pp. 299–314, Oct. 1993.
[7] J. A. Díaz, J. R. Jiménez, E. Hita, and L. J. del Barco, "Optimizing the constant-channel chromaticity and color gamut of CRT color displays by control of brightness and contrast levels," *Appl. Opt.*, vol. 35, no. 10, pp. 1711–1718, 1996.
[8] K. Kam, Y. Tiantong, K. Behrman, Y. Caroline, and I. Kymissis, "57-3: Characterizing image retention for HDR OLED displays," in *SID Symp. Dig. Tech. Papers*, 2020, vol. 51, no. 1, pp. 850–853.
[9] D. Tian, L. Xu, and M. Luo, "The characterization of HDR OLED display," *Electron. Imag.*, vol. 2019, pp. 326-1–326-6, 2019.
[10] A. Almustanyir, J. Hovis, and M. G. Glaholt, "Predicting the Farnsworth–Munsell D15 and Holmes–Wright lantern outcomes with computer-based color vision tests," *J. Opt. Soc. Amer. A, Opt. Image Sci.*, vol. 37, no. 4, p. A1, Apr. 2020. [Online]. Available: http://josaa.osa.org/abstract.cfm?URI=josaa-37-4-A1
[11] J. S. Werner, B. Marsh-Armstrong, and K. Knoblauch, "Adaptive changes in color vision from long-term filter usage in anomalous but not normal trichromacy," *Current Biol.*, vol. 30, no. 15, pp. 3011–3015, 2020. [Online]. Available: https://www.sciencedirect.com/science/article/pii/S0960982220307417
[12] P. J. Pardo, M. I. Suero, and Á. L. Pérez, "Correlation between perception of color, shadows, and surface textures and the realism of a scene in virtual reality," *J. Opt. Soc. Amer. A, Opt. Image Sci.*, vol. 35, no. 4, p. B130, 2018.
[13] M. A. Cohen, T. L. Botch, and C. E. Robertson, "The limits of color awareness during active, real-world vision," *Proc. Nat. Acad. Sci. USA*, vol. 117, no. 24, pp. 13821–13827, Jun. 2020. [Online]. Available: https://www.pnas.org/content/117/24/13821
[14] D. Kamińska, T. Sapiński, M. Kucharczyk-Pośpiech, and M. Wilczyński, "Ishihara color test using a mobile virtual reality headset for immobilised patients," *Roczniki Kolegium Analiz Ekonomicznych/Szkoła Główna Handlowa*, pp. 297–304, 2017.
[15] K. Szczurowski and M. Smith, "Emulating perceptual experience of color vision deficiency with virtual reality," *Stud. Health Technol. Informat.*, vol. 256, pp. 378–389, Jan. 2018.
[16] J. Schanda, *Colorimetry: Understanding the CIE System*. Hoboken, NJ, USA: Wiley, 2007.
[17] W. G. Backhaus, R. Kliegl, and J. S. Werner, *Color Vision: Perspectives From Different Disciplines*. Berlin, Germany: Walter de Gruyter, 2011.
[18] J. J. Koenderink, "Virtual psychophysics," *Perception*, vol. 28, no. 6, pp. 669–674, Jun. 1999.
[19] D. A. Gusev, D. M. Whittinghill, and J. Yong, "A simulator to study the effects of color and color blindness on motion sickness in virtual reality using head-mounted displays," in *Mobile and Wireless Technologies* (Lecture Notes in Electrical Engineering), vol. 391. Singapore: Springer, 2016, pp. 197–204. [Online]. Available: https://link.springer.com/chapter/10.1007/978-981-10-1409-3_22, doi: 10.1007/978-981-10-1409-3_22.
[20] A. F. Zarazaga, J. G. Vásquez, and V. P. Royo, "Review of the main colour vision clinical assessment tests," *Arch. Sociedad*, vol. 94, no. 1, pp. 25–32, Jan. 2019.
[21] S. J. Dain, "Clinical colour vision tests," *Clin. Exp. Optometry*, vol. 87, nos. 4–5, pp. 276–293, Jul. 2004.
[22] F. Díaz-Barrancas, H. Cwierz, P. J. Pardo, Á. L. Pérez, and M. I. Suero, "Spectral color management in virtual reality scenes," *Sensors*, vol. 20, no. 19, p. 5658, Oct. 2020.
[23] D. Farnsworth, "The Farnsworth-Munsell 100-Hue and dichotomous tests for color vision," *J. Opt. Soc. Amer. A, Opt. Image Sci.*, vol. 33, no. 10, pp. 568–578, Oct. 1943. [Online]. Available: http://www.osapublishing.org/abstract.cfm?URI=josa-33-10-568
[24] F. Diaz-Barrancas, H. C. Cwierz, P. J. Pardo, A. L. Perez, and M. I. Suero, "Visual fidelity improvement in virtual reality through spectral textures applied to lighting simulations," *Electron. Imag.*, vol. 2020, no. 15, pp. 1–259, 2020.
[25] P. R. Kinnear, "Proposals for scoring and assessing the 100-HUE test," *Vis. Res.*, vol. 10, no. 5, pp. 423–433, May 1970.
[26] K. Knoblauch, F. Saunders, M. Kusuda, R. Hynes, M. Podgor, K. E. Higgins, and M. F. De Monasterio, "Age and illuminance effects in the Farnsworth-Munsell 100-Hue test," *Appl. Opt.*, vol. 26, no. 8, pp. 1441–1448, 1987.
[27] M. E. Breton, D. E. Fletcher, and T. Krupin, "Influence of serial practice on Farnsworth-Munsell 100-Hue scores: The learning effect," *Appl. Opt.*, vol. 27, no. 6, pp. 1038–1044, 1988.
[28] S. Ghose, D. Shrey, P. Venkatesh, T. Parmar, and S. Sharma, "A simple modification of the Farnsworth-Munsell 100-Hue test for much faster assessment of color vision," *Indian J. Ophthalmol.*, vol. 62, no. 6, p. 721, 2014.
[29] M. García-Romera, M. Grosman, M. Sánchez-Marañn, L. Gómez-Robledo, and M. Melgosa, "On the uniformity of the 'Farnsworth-Munsell 100-Hue' test," *Optica Pura Aplicada*, vol. 44, pp. 139–148, Jan. 2011.
[30] K. G. Foote, M. Neitz, and J. Neitz, "Comparison of the Richmond HRR 4th edition and Farnsworth–Munsell 100 Hue Test for quantitative assessment of tritan color deficiencies," *J. Opt. Soc. Amer. A, Opt. Image Sci.*, vol. 31, no. 4, p. A186, 2014.
[31] H. C. Cwierz, F. Diaz-Barrancas, P. J. Pardo, A. L. Perez, and M. I. Suero, "Application of spectral computing technics for color vision testing using virtual reality devices," *Electron. Imag.*, vol. 2020, no. 15, pp. 1–260, 2020.
[32] *Colorimetry*, vol. 1, CIE5, Vienna, Austria, 2018. [Online]. Available: https://cie.co.at/publications/colorimetry-4th-edition
[33] M. R. Luo, G. Cui, and B. Rigg, "The development of the CIE 2000 colour-difference formula: CIEDE2000," *Color Res. Appl.*, vol. 26, no. 5, pp. 340–350, 2001.

HALINA CWIERZ received the B.S. degree in computer engineering and the M.S. degree in computer technologies research from the University of Extremadura (UEx), Mérida, Spain, in 1987 and 2016, respectively. She is currently pursuing the Ph.D. degree in the application of virtual reality devices to the screening of color vision deficiencies.

She is currently an Associate Professor at UEx. She has been involved in several projects related to the application of augmented reality to education. Her research interests include color vision and augmented and virtual reality devices.

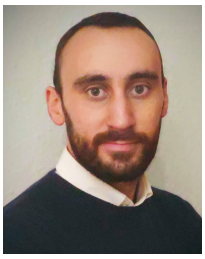

FRANCISCO DÍAZ-BARRANCAS received the B.S. degree in computer engineering and the M.S. degree in computer technologies research from the University of Extremadura (UEx), Mérida, Spain, in 2017 and 2018, respectively. He is currently pursuing the Ph.D. degree in the visual appearance in virtual reality devices.

He is currently a Research Assistant at UEx. He has been involved in several projects related to the application of hyperspectral and virtual reality techniques to measure the color performance of LED light sources.

JULIA GIL LLINÁS is currently an Associate Professor at the University Centre of Mérida, University of Extremadura, Spain. Her current research interests include active and collaborative learning strategies as well as learner-centered instructional and learning strategies in the context of higher education in science.

PEDRO J. PARDO received the B.S. degree in physical sciences and the M.Sc. and Ph.D. degrees in physics from the University of Extremadura (UEx), Mérida, Spain, in 1998, 2000, and 2004, respectively.

He is currently an Associate Professor at UEx. He has been involved in several projects related to the detection and influence of visual anomalies in students. His research interests include color vision, optical instrumentation, neural networks, computer networks, and physics education.

Capítulo 7

Article published in Coloration Technology

(Este artículo se encuentra bajo licencia copyright para la cual se han obtenido los permisos por parte de la editorial para reproducir dicho trabajo al ser el autor principal. El derecho de uso en el contenido de la tesis se encuentra en el Anexo III)

society of dyers and colourists

Coloration Technology

Promoting Understanding and Creativity in the Science and Technology of Coloured Materials

Volume 137 | No. 1 | 2021 | February | Pages 1–90

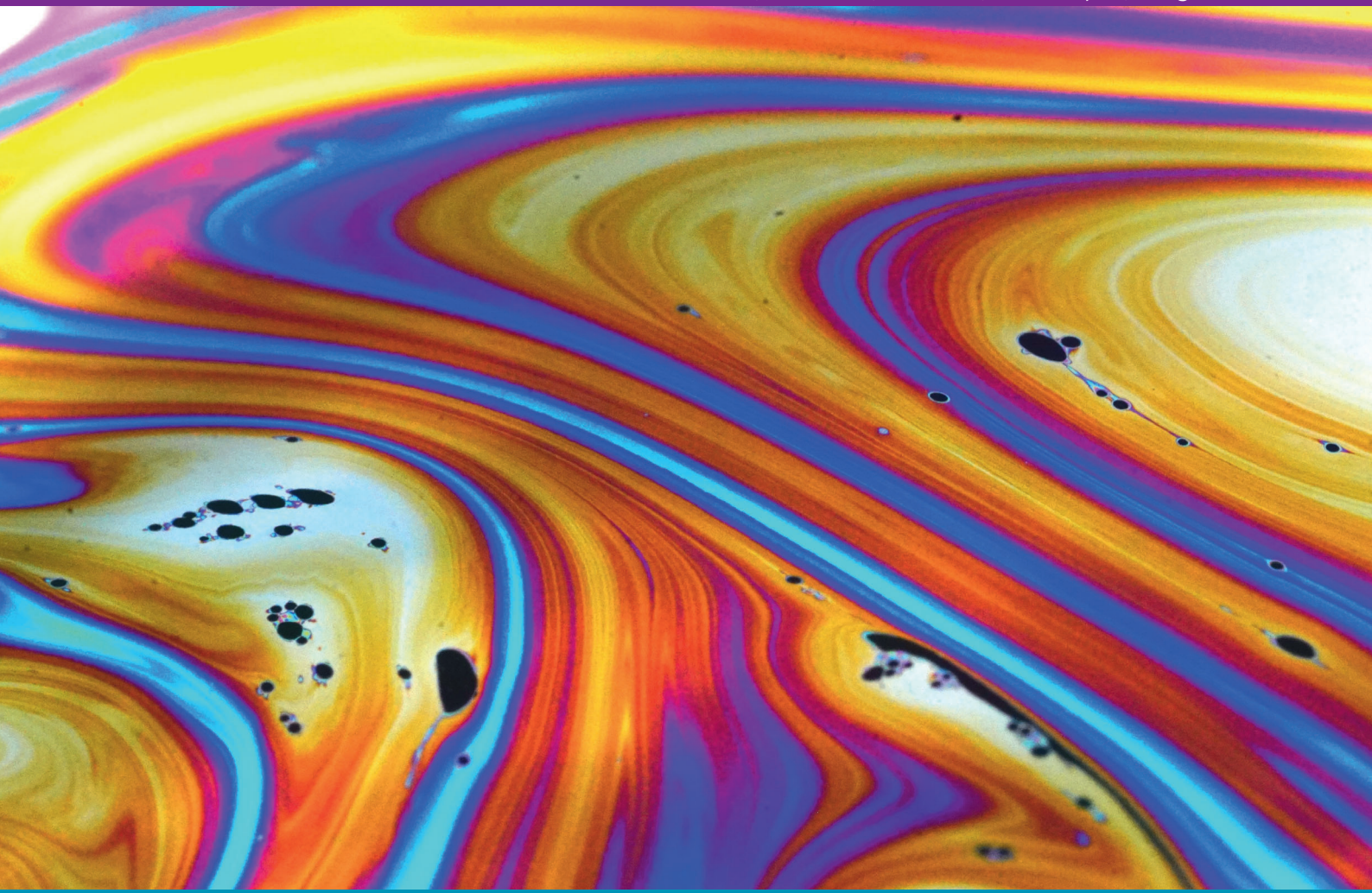

Challenges and Open Problems in Colorimetry Special Issue
Guest editors: Stephen Westland, Alessandro Rizzi

ISSN 1472-3581

WILEY

www.sdc.org.uk

wileyonlinelibrary.com/journal/colorationtechnology

Received: 28 March 2020 | Revised: 4 October 2020 | Accepted: 18 November 2020

DOI: 10.1111/cote.12513

ORIGINAL ARTICLE

Coloration Technology

Colour appearance in immersive three-dimensional virtual environments

Francisco Díaz-Barrancas[1] | **Halina Carmen Cwierz**[1] | **Pedro J. Pardo**[1] | **Angel L. Perez**[2] | **María Isabel Suero**[2]

[1]Department of Computer and Network Systems Engineering, Centro Universitario de Mérida, University of Extremadura, Mérida, Spain

[2]Department of Physics, Facultad de Ciencias, University of Extremadura, Badajoz, Spain

Correspondence
Francisco Díaz-Barrancas, Department of Computer and Network Systems Engineering, University of Extremadura, Centro Universitario de Mérida, C/Santa Teresa de Jornet 38, Mérida E06800, Spain.
Email: frdiaz@unex.es

Funding information
Regional Government of the Junta de Extremadura, Grant/Award Number: GR18131 and IB16004; European Regional Development Fund

Abstract

Technology is constantly evolving and, consequently, all the technological advances taking place are regularly integrated into the daily life of society. During recent years, there has been a trend towards virtual resources such as teleworking, telemedicine and e-commerce. In many countries, this virtualisation process has been accelerated by the changing circumstances caused by the COVID-19 pandemic. In any case, there is a growing demand for virtual systems, and virtual reality is a suitable field for the application of a multitude of solutions. However, advances in virtual reality occur without any regard to colour science, and there are several challenges to be overcome to improve the visual appearance and fidelity of colour reproduction in all types of related devices. This paper discusses three open issues related to the visual appearance and visual fidelity of virtual reality systems. We believe it is necessary to direct future research efforts in each of these directions to secure improvements in the visual fidelity of virtual reality systems.

1 | INTRODUCTION

The ultimate purpose of virtual reality (VR) is for users to experience a situation of total immersion that makes it difficult for them to distinguish between a virtual world and the real world.[1] Starting with the sense of sight, this feeling of immersion is achieved if the visual appearance of the objects appearing in a virtual scene is the same as the visual appearance of the corresponding real objects. Visual appearance is defined as the perception of objects in which the spectral and geometrical aspects of the objects are integrated with the lighting and the observation environment. The International Commission on Illumination (CIE) Technical Committee 1-65 agreed to define appearance as the visual sensation through which an object is perceived with attributes of size, shape, colour, texture, brightness, transparency and opacity. Subsequently, as a result of this work, in 2006 the CIE published Technical Report 175:2006:*A framework for the measurement of visual appearance*, which indicates how to measure visual appearance (as defined above).[2] The final aim was to correlate human perception with physical properties; therefore, because the visual aspect is one of the most important parts in perception, the first step was to characterise all materials from an optical viewpoint. As a starting point for measuring visual appearance, four optical properties (colour, gloss, translucency and texture) and two physical properties (size and shape) were defined and measured.

The measurement of physical properties, such as the shape and size of three-dimensional (3D) objects, is performed by 3D scanners and using photogrammetric techniques. The difficulty arises when these physical properties have to be linked to optical properties such as the colour at a particular point of 3D space. Classic colorimetry allows us to specify the colour of a simple visual stimulus using only three mathematical values. This represents a huge dimensional reduction from the infinite dimensions of the power spectral distribution of a physical stimulus. This transformation is based on the tri-variance of the human visual system. The validity

of these tri-stimulus values is determined by the conditions under which they are obtained (level of luminance, size of the stimulus, surrounding field, degree of adaptation) and by the validity of certain mathematical properties necessary for a Euclidean vector space (eg, additivity, linearity).[3] Although colorimetry can be a good starting point for studying the visual appearance of objects and their correlation with optical measurements, this approach is insufficient; this is why, for several years now, visual appearance in general, and the appearance of colour in particular, have been studied from a more global perspective, using colour appearance models that contemplate all the variables that influence it, including adaptation phenomena, the visual environment and spatial properties.

The expansion and popularisation of 3D digital environments like virtual reality systems (VRSs) have brought new challenges in terms of visual appearance and visual fidelity. Problems such as calculating the colour appearance of a virtual 3D object shown to wearers of VR glasses when changing the illuminant and/or the surrounding objects are open issues for colour researchers. In this paper we discuss three examples of unresolved problems related to VR and the colour appearance of 3D virtual scenes.

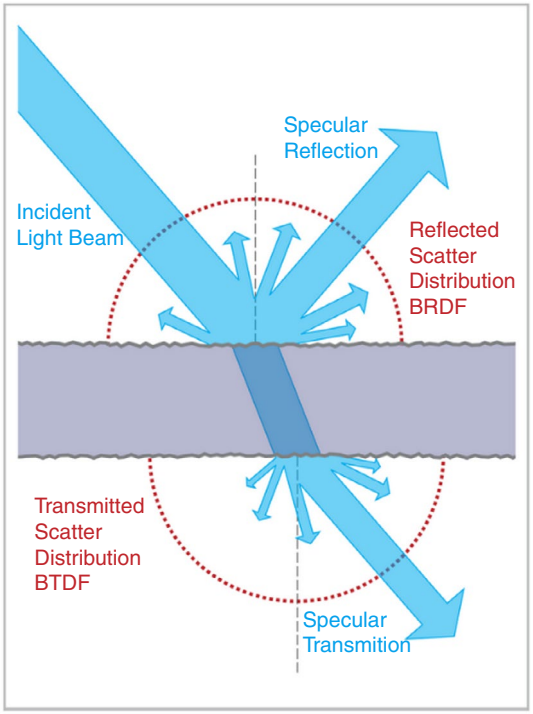

FIGURE 1 Graphical representation of BSDF = BRDF + BTDF,[5] where BSDF is the bidirectional scattering distribution function, BRDF is the bidirectional reflectance distribution function, and BTDF is the bidirectional transmittance distribution function

2 | MEASUREMENT OF OPTICAL PROPERTIES RELATED TO COLOUR APPEARANCE

As discussed in the Introduction, the road travelled to measure the physical properties of a 3D object such as its size and shape is a very long one; currently, devices such as 3D scanners enable a fairly detailed measurement of these properties. A typical result of one of these measurements is a dots cloud, with the spatial coordinates (X, Y, Z) of each point defining the surface of the 3D object. If the scanner is of high resolution then the number of dots defining a particular 3D object could be tens of thousands or even millions. If the 3D scanner is a colour scanner then a standard red green blue (sRGB) colour value is associated with each dot in the cloud. This RGB value is obtained using RGB charge-coupled device sensors that process the images using multiview photogrammetric algorithms. The colour coordinates obtained by a 3D colour scanner are device-dependent because they rely on the light source used by the 3D scanner. Colour researchers have been making device-independent colour measurements for a long time using spectroradiometers or spectrophotometers, but the measurement consists of one point each time. Commercial two-dimensional (2D) colorimeters have recently been launched, but for each type the measurement is always in one, fixed direction. However, there are modern materials with complex surface structures (eg, gonio-apparent) that produce very different colour perceptions at different angles of incidence and observation.[4] This means that it is no longer sufficient to specify only one colour measurement for a given geometry. The reflectance or transmittance of a 3D object must be measured at various angles of incidence and observation to properly describe its visual appearance.

The solution to the problems outlined above can be found by measuring the bidirectional scattering distribution function (BSDF) using a goniospectrophotometer. The BSDF is defined as the ratio of the radiance of an object in each direction of space in relation to the irradiance it receives. It indicates, therefore, how an object spatially distributes the light it reflects or transmits; thus it is the basic characteristic with which to determine the visual appearance of an object's colour, gloss, texture and translucency (Figure 1).

The two-way function of diffusion distribution (ie, BSDF) expresses how a given object diffuses radiant energy in each direction of space, that is, it indicates the amount of radiance per unit irradiance that is reflected in each direction as a function of the direction of incidence. Its definition is:

$$\mathrm{BSDF}\left(\theta_i, \phi_i; \theta_s, \phi_s\right) = \frac{dL\left(\theta_i, \phi_i; \theta_s, \phi_s\right)}{dE\left(\theta_i, \phi_i\right)}, \qquad (1)$$

where dL is the radiance differential element and dE is the irradiance differential element.

BSDF is the sum of two terms: one relating to transmittance (bidirectional transmittance distribution function [BTDF]) and the other taking into account the properties of reflectance (bidirectional reflectance distribution function [BRDF]). In the case of opaque objects, BSDF is reduced to BRDF. From the BRDF it is possible to calculate the reflectance and the factor of reflectance for any geometry at one point, that is, with any solid angle of observation ω_s when the object is irradiated from any solid angle ω_i.

$$R\left(\omega_i;\omega_s\right)=\left(\frac{\pi}{\Omega_i.\Omega_s}\right).\int_{\omega_i}\int_{\omega_s}\mathrm{BRDF}\left(\theta_i,\phi_i;\theta_s,\phi_s\right).d\Omega_s.d\Omega_i \tag{2}$$

However, within the framework of 3D computer graphics, use of the BRDF does not resolve the problem because it does not capture the spatial structure of textured materials. For this reason, the BRDF concept has been extended to a more generic definition of bidirectional texture function (BTF), which aims to capture all the variations of textured materials, including non-local effects in rough material structures such as occlusions, masking, subsurface spreading and inter-reflections.[6,7]

A monospectral BTF is a six-dimensional function BTF (x, y, θ_i, φ_i, θ_v, φ_v) that represents the appearance of a material sample at a surface point with coordinates (x, y) for the variable illumination I (θ_i, φ_i) and the point of view V (θ_v, φ_v), and where θ and φ are the elevation and azimuth angles, respectively. The spectral version of the BTF can introduce the photorealistic visual appearance of materials into 3D computer graphics. The open issue lies in how to measure the BTF function of a real 3D object at all its points and manage the huge set of data generated in real time for use as part of a VRS.

3 | REAL-TIME 3D RENDERING IMAGES FOR VR

When ray tracing is used to render a 3D scene, a process is carried out based on the geometrical definition of 3D objects, their position, the position of the camera and the position of the light sources. One of the most extended models of 3D rendering is the physically based rendering model (PBR) that applies a BRDF as a physical law governing the interaction between light and matter.[8] The result of applying this rendering model can be a photorealistic reproduction of real scenes, like the one shown in Figure 2.

BRDF introduces a large amount of data to 3D rendering, improving the final result but providing the scene with a great complexity of calculation.

This type of 3D rendering method theoretically enables the possibility of defining the spectral power distributions of light sources. In the same way, basic colorimetric calculations can be performed and applied to the image in terms of CIE 1931 XYZ tri-stimulus values. However, this type of 3D rendering needs a long processing time (typically hours) to produce one image. The problem arises when we need to apply these physical law-based rendering techniques in VR environments where active human interaction with the environment is required, adapting the image shown to the position of the observer in a very short time. The VR device must be able to detect the movements of the head and generate different views of the same scene with sufficient frequency (90-120 Hz) and very little delay to obtain a good experience of virtual immersion. This concept is known as low latency. The VRS must be able to change the image generated according to the movements performed by the observer's head as much as continuously possible for a better immersive experience. This reduces the computation time per frame to *ca.* 10 ms or less. With these restrictions, it is not possible to apply a classical 3D physical rendering method and it is necessary to apply more restrictions.

FIGURE 2 Example of a photorealistic reproduction of a real scene produced with POV-Ray 3.6[9]

Currently, new graphics processing units (GPUs) with high computing capabilities are employed by 3D game engine software platforms to reflect, to a greater or lesser extent, the real world through physical laws. Some graphics engines apply a reduced BRDF model based on four main components (diffuse, specular, normal, smoothness). These components are applied through bitmaps as 2D texture files associated with each 3D object. The diffuse component corresponds to material colour with perfect Lambertian behaviour following the Disney model[10]; the specular component includes the Smith joint GGX visibility term[11] as well as Schlick Fresnel approximation[12,13]; and both the normal and smoothness components correspond to surface texture. It is therefore possible to obtain rendered scenes with a high

degree of visual appearance fidelity when treating the light–matter interaction in this way.

However, colour management has been left out of this type of technique, since colour is processed from the beginning to the end in RGB values (eight-bit digital values per channel). The only colour correction that has been carried out to date has been the calibration of the display setting up a standard configuration that allows a similar appearance on all displays (typically sRGB). Considering this, it is possible to apply colour management techniques using scripts that let us modify the colour of the virtual light sources inside a VR scene in real time. Starting from the spectral power distribution of a real light source it is possible to calculate the RGB values of the virtual light sources inside the scene to simulate any other light source. This method fails when the light source to simulate has a spectral distribution that is very different to the reference illuminant D65. Figure 3 (left) shows the results of simulating the appearance of the ColorChecker illuminated with a light-emitting diode (LED) source composed of only two spectral peaks (spectral blue and spectral yellow), chosen in such a way that the chromaticity *xy* of this source over a diffuse reflectance target coincides exactly with the chromaticity of the D65 illuminant. The appearance of the ColorChecker is very close to the appearance when it is illuminated with a D65 simulator. However, Figure 3 (right) shows a real picture of the ColorChecker obtained in a six-peak LED light booth tuned to match the two peaks of spectral light source theoretically defined before. Although the colour match is not complete in neutral patches because the real light booth does not have a yellow spectral peak and we have employed a green-yellow peak instead, the absence of red colours in the image can clearly be appreciated. This represents its real behaviour because this spectral light source can only render colours whose chromaticity lies on a straight line between the chromaticity of both spectral peaks (blue and yellow).

Therefore, the next step in the challenge to obtain VR scenes with a higher degree of visual fidelity is to apply spectral calculation to the entire scene in real time. As we have shown above, this is not currently feasible because we have not characterised any 3D object with the spectral BTF function, due to the large number of frames per second required to obtain a good feeling of immersion, despite the great computing power of GPUs these days. The open issue consists of finding a compromise solution between visual fidelity and feasibility with a data reduction based on perceptive criteria.

4 | COLOUR APPEARANCE MODELS APPLIED TO RENDERED SCENES

At the beginning of this paper we established that a good feeling of immersion in a VRS is achieved if the visual appearance of the objects appearing in the scene is the same as the visual appearance of the real object, which we call visual fidelity. To obtain that visual fidelity in the reproduction of the real world inside the virtual world, a good physical characterisation of real objects through spectral BTF measurements is needed, and a suitable supply of the capabilities for spectral processing of 3D objects by VR software is required. These two steps would be sufficient if human perception was perfectly linear, but the reality is that seeing sight is not linear in many cases. In other colour-imaging fields different to 3D computer graphics, the solution to these non-linearities was to define then apply colour appearance models. These mathematical models were mainly developed for non-complex scenes like CIECAM02 or CAM16[14,15] or were created considering only 2D images, although they covered spatial phenomena like image Color Appearance Model (iCAM).[16,17] From the point of view of basic research, it remains to be seen whether VR systems are capable of integrating a colour appearance model that improves the colour appearance of rendered scenes in 3D.

All these types of appearance models include a colour adaptation stage to respond to changes in lighting. They also consider, in a different way, the effect of the environment and a non-linear compression stage. In the case of iCAM, it also analyses the details of the scene using a contrast sensitivity function and performs a contrast enhancement at certain points coinciding with the edges of the objects. The key issue is to know if the stereoscopic 3D scenes generated for VRSs can make use of these improvements provided by colour appearance models. On one hand it is necessary to check compatibility with PBR rendering. On the other hand, we must

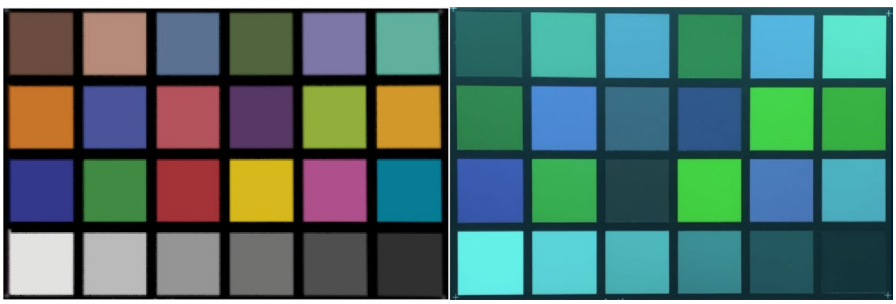

FIGURE 3 (Left) ColorChecker simulation using a two spectral peaks light source in a virtual reality system and (right) a real picture of the ColorChecker using a two spectral peaks light source

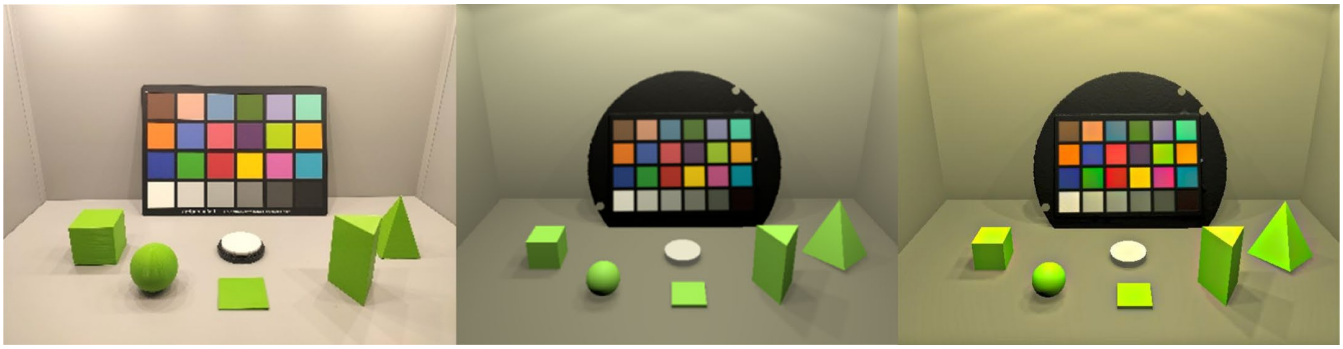

FIGURE 4 (Left) Real picture of a real scene inside a light booth, (centre) screen capture of the simulation of a real scene in a virtual reality system (VRS) without any post-processing, and (right) screen capture of the simulation of a real scene in a VRS processed with an iCAM06 appearance model

study whether the spatial effects collected by appearance models such as iCAM have already been generated by our own visual systems when using a stereoscopic image system, or conversely, if they improve the appearance of the image.[18]

As an example, Figure 4 (left) shows a real picture of a compound scene of a ColorChecker chart, a white diffuse reference and several geometrical pieces printed with a 3D printer from the same material, all inside a light booth. A simulation of the same scene using a 3D game engine typically used in VRSs without any post-processing can be seen in the centre of Figure 4, and on the right the same image processed with an iCAM06 colour appearance model.

The images in Figure 4 are only shown for the purposes of explanation because the open issue consists of assessing the visual fidelity between the real and virtual scenes with and without CAM models using real observers under real conditions, and not by using 2D images. Under such conditions, stereoscopic vision and perception of depth can have a major influence. Future visual fidelity research should focus on topics like chromatic adaptation, hue appearance in complex scenes, the contrast enhancement of 3D objects and other spatial effects.

5 | CONCLUSIONS

There are several challenges that colour scientists must surmount in the near future. Because of the evolution of technology, as we head towards a more interconnected society with greater possibilities of virtualisation, it is essential to start improving colour rendering and visual appearance in VR environments. Currently, because the COVID-19 pandemic has forced large numbers of employees to telework from home, it is important to discover if improvements in visual appearance and fidelity are possible. In this paper we have discussed three open issues related to capturing the real world through physical measurements, introducing spectral computation in lighting and objects as well as assessing the efficiency of appearance models applied to VRSs.

ACKNOWLEDGEMENTS

This work was supported by grants GR18131 and IB16004 of the Regional Government of the Junta de Extremadura and was partially financed by the European Regional Development Fund.

ORCID

Francisco Díaz-Barrancas https://orcid.org/0000-0002-4930-4780

REFERENCES

1. Pardo P, Suero M, Pérez Á. Correlation between perception of color, shadows, and surface textures and the realism of a scene in virtual reality. *J Opt Soc Am A*. 2018;35(4):130-135.
2. CIE 175:2006. *A Framework for the Measurement of Visual Appearance*. Vienna: Central Bureau of CIE; 2006.
3. Wyszecki G, Stiles W. *Color Science*. New York: Wiley; 1982:985.
4. Ferrero A, Rabal A, Campos J, Pons A, Hernanz M. Variables separation of the spectral BRDF for better understanding color variation in special effect pigment coatings. *J Opt Soc Am A*. 2012;29(6):842-847.
5. Wikimedia. BSDF. https://upload.wikimedia.org/wikipedia/en/d/d8/BSDF05_800.png. Accessed October 4, 2020
6. Filip J, Vávra R, Krupička M. Rapid material appearance acquisition using consumer hardware. *Sensors*. 2014;14(10):19785-19805.
7. Wu J, Chen H, Liu X, Cao L, Peng X, Jin G. Unsupervised texture reconstruction method using bidirectional similarity function for 3-D measurements. *Opt Commun*. 2019;439:85-93.
8. Pharr M, Jakob W, Humphreys G. *Physically Based Rendering: From Theory to Implementation*. Burlington, MA: Morgan Kaufmann; 2016. 1266.
9. Oyonale-3D art and graphic experiments. POV-Ray. http://www.oyonale.com/modeles.php?lang=en&page=40. Accessed October 4, 2020
10. Burley B, Animation Studios W. Physically based shading at disney. In *Proceedings, ACM SIGGRAPH*. Los Ángeles, CA, USA; 2012;1-7.
11. Walter B, Marschner S, Li H, Torrance K. Microfacet Models for Refraction through Rough Surfaces. In *Proceedings, Eurographics Symposium on Rendering*. Grenoble, France; 2007;195-206.
12. Heitz E. Understanding the masking-shadowing function in microfacet-based BRDFs. *JCGT*. 2014;3(2):48-107.

13. Schlick C. An inexpensive BRDF model for physically-based rendering. In *Proceedings, Computer Graphics Forum*. 1994;13(3):233-246.
14. CIE 159:2004. A Colour Appearance Model for Colour Management Systems. CIECAM02. Vienna: Central Bureau of CIE; 2004.
15. Li C, Li Z, Wang Z, et al. Comprehensive color solutions: CAM16, CAT16, and CAM16-UCS. *Color Res Appl*. 2017;42(6):703-718.
16. Fairchild M, Johnson G. iCAM framework for image appearance, differences, and quality. *J Electron Imaging*. 2004;13(1):126-138.
17. Kuang J, Johnson G, Fairchild M. iCAM06: A refined image appearance model for HDR image rendering. *JVCIR*. 2007;18(5):406-414.
18. McCann J, Parraman C, Rizzi A. Reflectance, illumination, and appearance in color constancy. *Front Psychol*. 2014;5:5.

How to cite this article: Díaz-Barrancas F, Cwierz HC, Pardo PJ, Perez AL, Suero MI. Colour appearance in immersive three-dimensional virtual environments. *Coloration Technol*. 2020;00:1–6. https://doi.org/10.1111/cote.12513

Capítulo 8

Resultados y análisis de datos

En este capítulo vamos a presentar la implementación de dos modelos de visualización de escenarios virtuales bajo 4 fuentes luminosas cada uno, en los cuales hemos desarrollado una cabina de iluminación que cuenta en su interior con varias figuras geométricas, un ColorChecker y una muestra de un blanco absoluto basado en un patrón de reflectancia espectral Spectralon. El hecho de utilizar figuras geométricas como objetos, es el de conseguir objetos estables en el tiempo, que no varíen su color o su forma durante las distintas sesiones de evaluación subjetivas, para que los observadores puedan realizar estas pruebas bajo las mismas condiciones en diferentes días. En uno de los modelos de visualización no hemos utilizado ninguna técnica de mejora computacional, es decir, hemos implementado la escena de realidad virtual tal y como lo haría cualquier desarrollador ahora mismo, con las técnicas que existen actualmente y con los gráficos configurados a la más alta definición (Fig. 8.1). Las texturas de este primer escenario se consiguieron mediante la captura de objetos reales utilizando un escáner de mano, definidas directamente con valores RGB de 8 bits por canal. Sin embargo, para el segundo modelo hemos utilizado todas las mejoras gráficas desarrolladas durante esta tesis doctoral: hemos incorporado un sistema de caracterización cromática del HMD y hemos introducido texturas hiperespectrales definidas en el dominio de las longitudes de onda visibles y, a partir de ahí, definiendo sus valores triestímulo XYZ y posteriormente convertidos a RGB en función de la fuente luminosa utilizada (Fig. 8.2). De esta forma lo que queremos demostrar es que todas las técnicas desarrolladas durante la tesis no solo mejoran las medidas de color, sino que también mejoran la sensación de realismo del usuario en cuanto a color se refiere. En una búsqueda por conseguir el tan ansiado hiperrealismo, se analizarán los datos obtenidos de la medición de las coordenadas de cromaticidad obtenidos a través del visor de realidad virtual, así como las valoraciones realizadas por la población de usuarios.

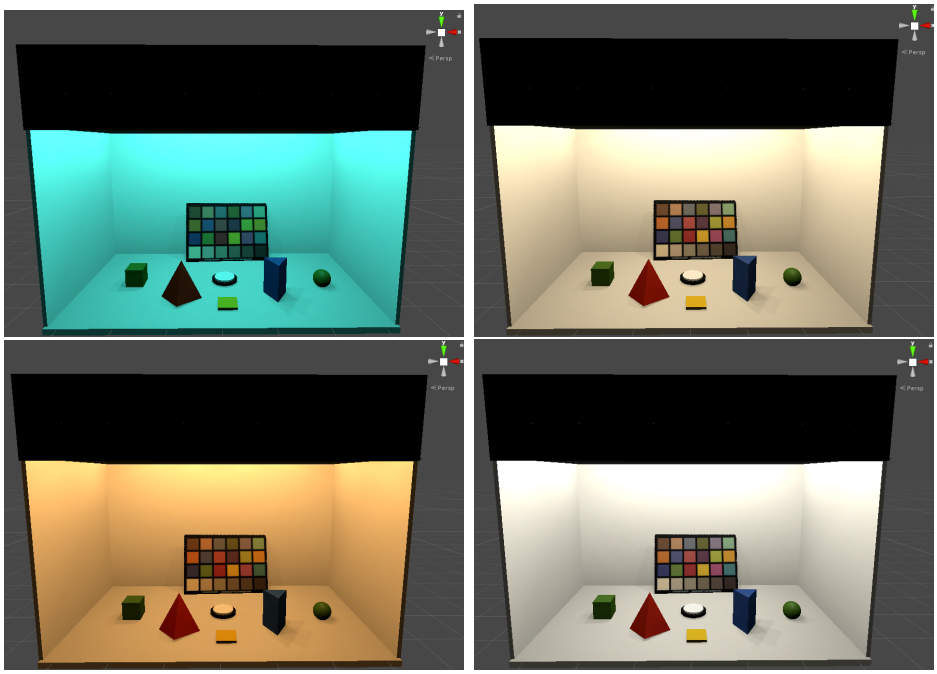

Figura 8.1: Diferentes fuentes luminosas representadas sin mejoras gráficas en un escenario de realidad virtual. 2Peaks (**Arriba izquierda**), D50 (**Arriba derecha**), A (**Abajo izquierda**) y D65 (**Abajo derecha**).

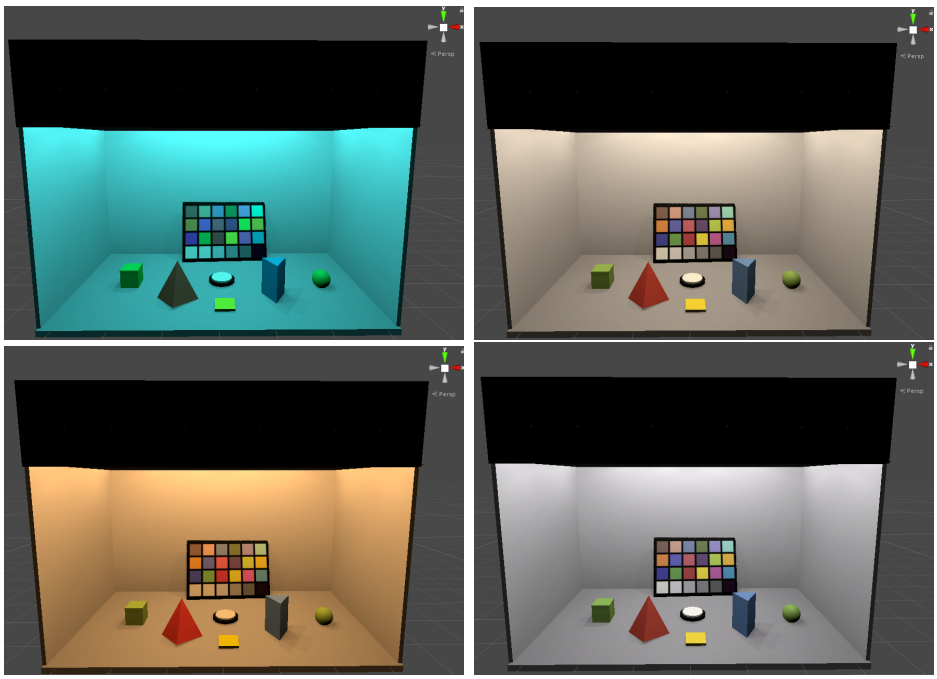

Figura 8.2: Diferentes fuentes luminosas representadas con mejoras gráficas en un escenario de realidad virtual. 2Peaks (**Arriba izquierda**), D50 (**Arriba derecha**), A (**Abajo izquierda**) y D65 (**Abajo derecha**).

8.1. Diferencia de color entre el escenario real, el escenario sin texturas hiperespectrales y con texturas hiperespectrales

En esta sección vamos a realizar mediciones con nuestro espectroradiómetro (Konica Minolta CS200) sobre las muestras de todos los colores de las figuras geométricas representadas en el escenario. De tal forma que, utilizando la fórmula de diferencia de color CIEDE2000, podemos observar cómo el error medio disminuye para todas las fuentes luminosas utilizadas tomando como referencia los valores de cromaticidad medidos sobre los objetos reales en la cabina de iluminación real (Tabla 8.1).

Colores	**ΔE^*_{00} sin mejora gráfica**				**ΔE^*_{00} con mejora gráfica**			
	2 Peaks	**D50**	**A**	**D65**	**2Peaks**	**D50**	**A**	**D65**
Rojo	8.24	0.80	4.14	0.91	2.18	0.70	3.75	0.41
Azul	11.66	7.41	3.24	8.02	5.31	3.65	2.08	2.93
Verde	8.60	6.53	3.51	6.02	1.83	1.48	1.66	1.55
Amarillo	2.48	5.38	3.27	5.39	4.27	3.65	2.47	0.66
Media	**3.83**	**5.03**	**3.54**	**2.99**	**1.66**	**2.04**	**2.49**	**1.14**

Tabla 8.1: Tabla comparativa de diferencias de color CIEDE2000 de muestras sin mejora gráfica y con mejora gráfica

Tras representar los resultados medidos en la Tabla 8.1 se puede observar cómo la mejora producida en los entornos virtuales es sustancial para la representación con las mejoras gráficas aplicadas durante esta tesis doctoral. Además, podemos observar que en los colores azules o verdes es donde se consigue mejor rendimiento. Por últimos podemos afirmar que la fuente luminosa que más se acerca a la representación de la realidad es la D65 con una ΔE^*_{00} media de 1.14. Estos resultados demuestran que la primera parte de nuestro objetivo, que es la de mejorar la representación del color real de los objetos en los dispositivos de realidad virtual, se ha logrado de una forma notoria. Para corroborar estos datos hemos decidido realizar otra prueba más, esta vez con observadores reales, los cuales valorarán cada escenario comparando el escenario real con el escenario virtual sin mejoras y con mejoras. En la siguiente sección podemos ver la metodología seguida y los resultados obtenidos.

8.2. Validación con usuarios de ambos escenarios

Con el objeto de realizar una validación con observadores reales hicimos diferentes preguntas a un grupo de usuarios acerca de la similitud entre los colores visualizados en el visor de realidad virtual sin las mejoras gráficas y con las mejoras gráficas. Los observadores podían otorgar una puntuación entre 0 a 5 puntos, siendo 0 nada similar la similitud

en apariencia de ambas escenas y 5 muy similar o igual en apariencia de ambas escenas. Para ello, entrevistamos a 5 usuarios y cada uno de ellos realizó la prueba 3 veces. De esta forma cada uno contestó a las 7 preguntas clave acerca de la apariencia (Iluminación, colores rojos, colores azules, colores verdes, colores amarillos, colores blancos y realismo general), más otras 2 de chequeo, sobre la geometría y el sombreado, las cuales no cambiaban entre escenarios y las utilizamos como elemento de chequeo. De manera general, el objetivo de esta prueba es comprobar si existen diferencias perceptivas estadísticamente significativas entre aplicar las técnicas de gestión de color y de texturas hiperespectrales o no en la escena de realidad virtual desarrollada en esta tesis.

Como hipótesis de partida, hipótesis nula H_0, se va a considerar que no existen estas diferencias estadísticamente significativas en cuanto a la percepción del color comparando ambas técnicas de procesado. Como hipótesis alternativa H_1, consideraremos que sí existen estas diferencias. Para determinar la validez de las hipótesis se hará uso de técnicas estadísticas basadas en el análisis de la varianza aplicadas sobre las valoraciones promedio hechas por los observadores.

Previamente a realizar la comparación del escenario sin mejora respecto el escenario con mejoras, es necesario realizar alguna comprobación inicial, como es la comprobación de que el conjunto de datos sigue una distribución normal, para lo que se ha realizado la prueba de normalidad Lilliefors [36]. Esta prueba se utiliza para probar la hipótesis nula de que los datos provienen de una población con distribución normal. El resultado de esta prueba indicó que nuestro conjunto de datos no seguían una distribución normal, por lo que en lugar de hacer un análisis de la varianza de tipo paramétrico, se les aplicó el test de Wilcoxon, que no presenta ese requisito de normalidad al ser una prueba no paramétrica. A continuación, estableceremos explícitamente el criterio para aceptar o no la hipótesis nula antes enunciada basada en la prueba de Wilcoxon. Este criterio nos servirá además para todos los siguientes subapartados en el que comprobaremos uno a uno si existe significatividad estadística en la diferencia de valor promedio de la valoración subjetiva aportada por los observadores. Para ello, hemos establecido un nivel de confianza de 95 %, lo que nos deja un nivel de significación α de 0.05

Si el p-valor de la Prueba de Wilcoxon es menor que el nivel de significación α=0.05, esto nos indicará que la diferencia entre las medianas de ambos conjuntos de datos es significativamente diferente y, por lo tanto, se debe rechazar la hipótesis nula H_0 y aceptar la hipótesis alternativa H_1. Por el contrario, si el p-valor es mayor que el nivel de significación α=0.05, debemos aceptar la hipótesis nula que nos indica que ambos conjuntos de datos son iguales estadísticamente.

En una primera comparación general, vamos a comparar a rasgos generales el escenario virtual sin mejora tomando como referencia el escenario virtual con mejoras, estando formado el conjunto de datos por cada una de las valoraciones hechas por los observadores sobre un objeto y fuente luminosa. El resultado puede verse en el gráfico de cajas (Fig. 8.3). Además, en la tabla 8.2 pueden observarse los resultados de la prueba estadística.

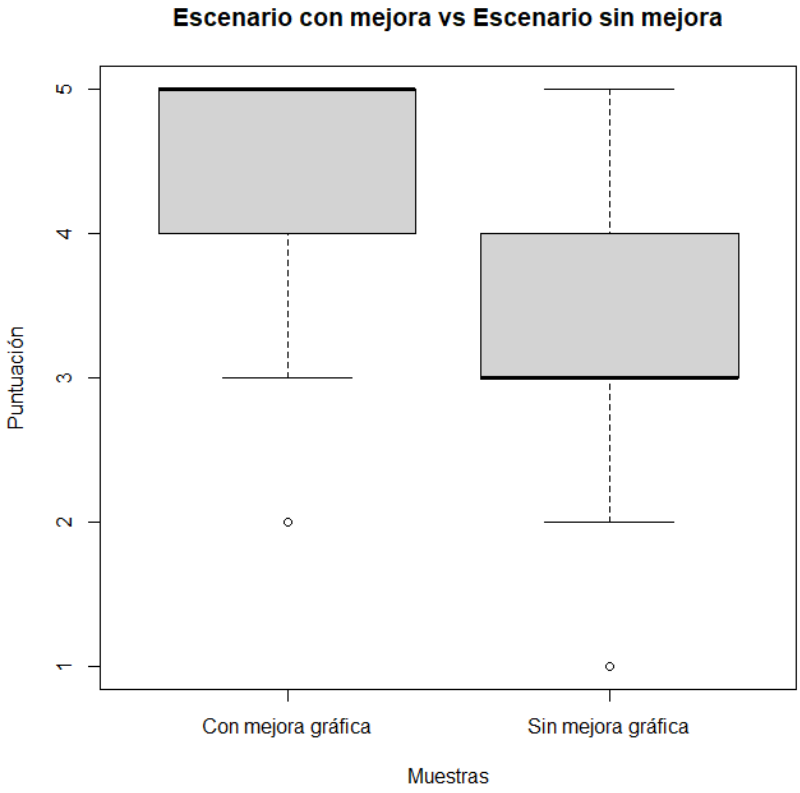

Figura 8.3: Diagrama de cajas del escenario virtual sin mejora tomando como referencia el escenario virtual con mejoras, estando formado el conjunto de datos por cada una de las valoraciones hechas por los observadores sobre un objeto y fuente luminosa.

Muestra	Media	Desviación típica	N	W	p-value
Sin mejora gráfica	3.13	0.90	540	245902	2.2^{-16}
Con mejora gráfica	4.41	0.72	540		

Tabla 8.2: Tabla de resumen estadístico para el escenario general entre ambas muestras

Como hemos observado anteriormente, las mejoras introducidas durante esta tesis doctoral han tenido gran relevancia en el comportamiento del sistema de realidad virtual. Los datos estadísticos nos muestran que el p-valor es inferior a 0.05, por lo tanto podemos rechazar la hipótesis nula y decir que existen diferencias significativas entre ambas muestras.

8.2.1. Iluminación

En la primera de las preguntas que hicimos a los usuarios sobre la iluminación entre los dos escenarios en comparación con la iluminación reproducida en la cabina real, se muestran diferencias significativas entre las muestras. Por lo tanto, podemos afirmar que una vez realizada la gestión de color sobre las fuentes luminosas, ésta mejora de manera clara. La figura 8.4 así como la tabla 8.3 lo demuestran.

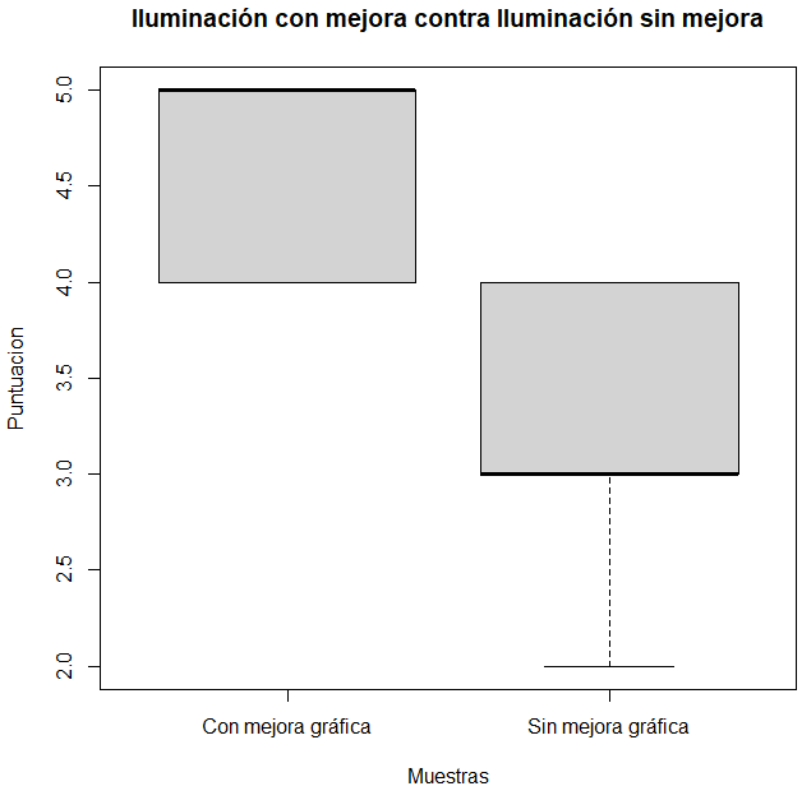

Figura 8.4: Diagrama de cajas comparando la iluminación con mejoras contra la iluminación sin mejoras

Muestra	Media	Desviación típica	N	W	p-value
Sin mejora gráfica	3.23	0.62	60	3400	2.2^{-16}
Con mejora gráfica	4.67	0.47	60		

Tabla 8.3: Tabla de resumen estadístico para la iluminación entre ambas muestras

8.2.2. Colores Rojos

La primera pregunta hacia los colores estaba referida a los colores rojizos que se encontraban en una de las figuras geométricas así como en algunas muestras del ColorChecker. El resultado en esta pregunta también resultó notorio, ya que aunque menos que en la anterior, también se producían diferencias significativas entre ambas muestras. La figura 8.5 y la tabla 8.4 así lo demuestran.

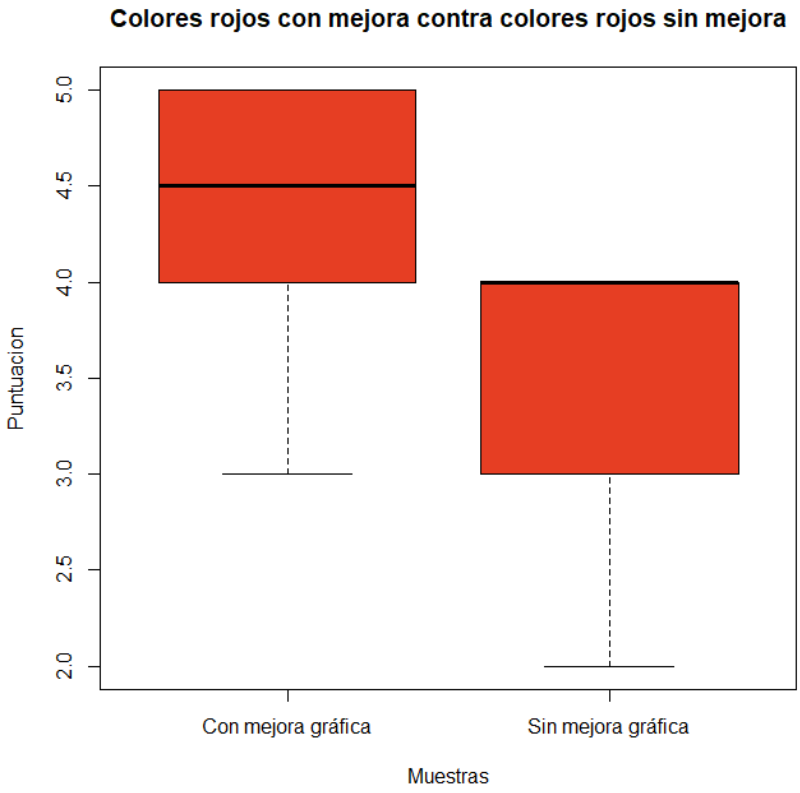

Figura 8.5: Diagrama de cajas comparando los colores rojos con mejoras contra los rojos sin mejoras

Muestra	Media	Desviación típica	N	W	p-value
Sin mejora gráfica	3.51	0.53	60	3061	6.20^{-13}
Con mejora gráfica	4.46	0.56	60		

Tabla 8.4: Tabla de resumen estadístico para los colores rojos entre ambas muestras

8.2.3. Colores Azules

En esta gama de colores, que se encuentra también en una figura geométrica así como en algunas muestras del ColorChecker, se produce la diferencia más significativa de todas las preguntas realizadas. Prueba de ello es que pasamos de una media de 2.53 sin mejora gráfica a 4.65 con mejora gráfica (Tabla 8.5). El diagrama de cajas presentado en la figura 8.6 nos permite visualizar de una forma muy gráfica la clara diferencia.

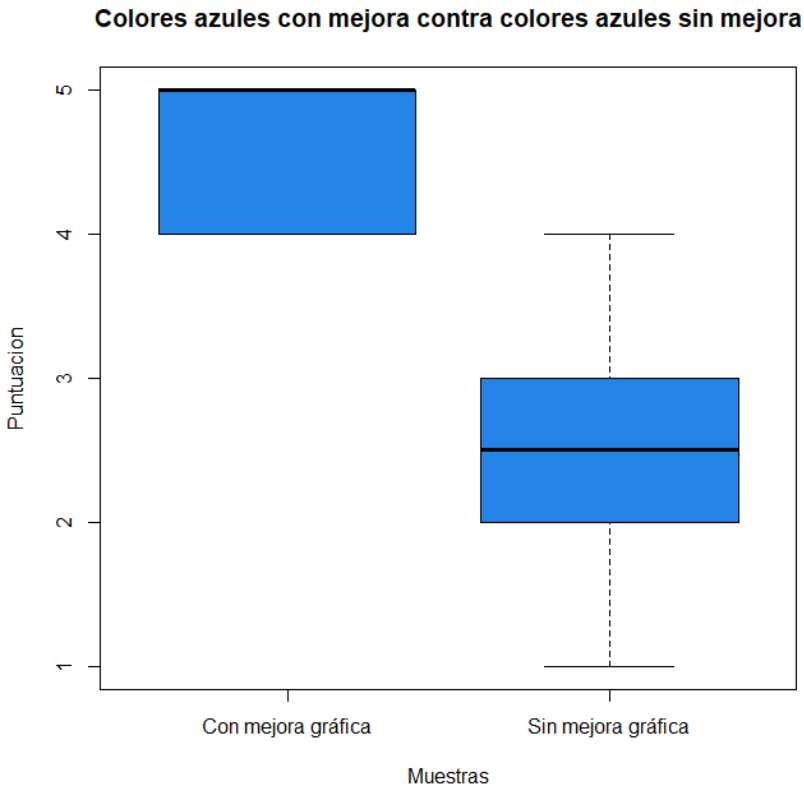

Figura 8.6: Diagrama de cajas comparando los colores azules con mejoras contra los azules sin mejoras

Muestra	Media	Desviación típica	N	W	p-value
Sin mejora gráfica	2.48	0.59	60	3591.5	2.2^{-16}
Con mejora gráfica	4.71	0.45	60		

Tabla 8.5: Tabla de resumen estadístico para los colores azules entre ambas muestras

8.2.4. Colores Verdes

Si nos centramos en analizar las muestras verdes del escenario, como son 2 de las figuras geométricas así como algunas muestras del ColorChecker, podemos comprobar que es la segunda de las preguntas que más significancia conlleva entre muestras. La tabla 8.6 y la figura 8.7 así lo argumentan.

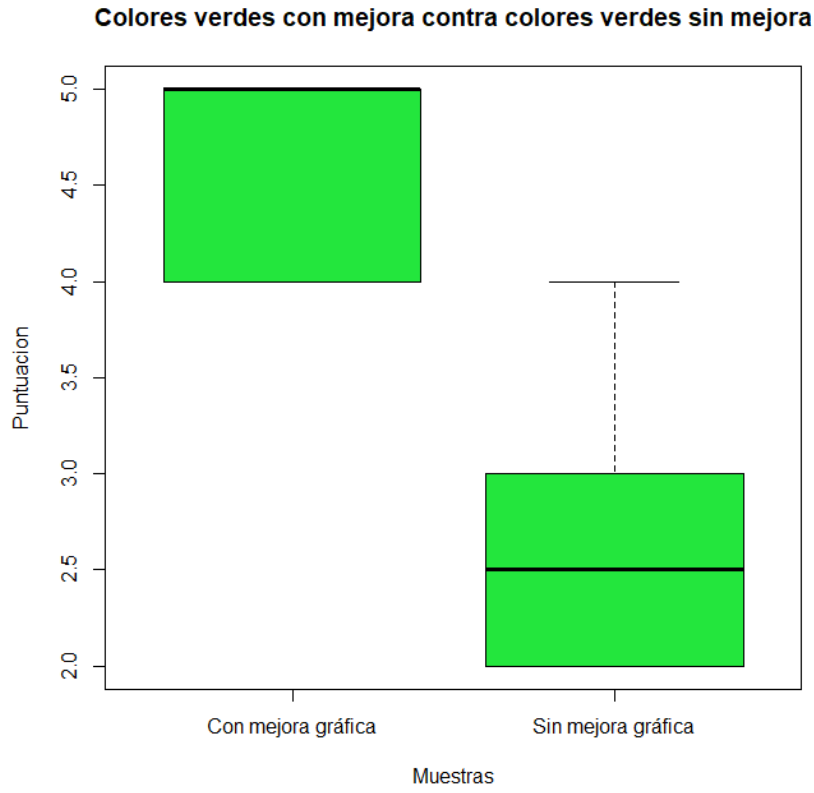

Figura 8.7: Diagrama de cajas comparando los colores verdes con mejoras contra los verdes sin mejoras

Muestra	Media	Desviación típica	N	W	p-value
Sin mejora gráfica	2.53	0.56	60	3579	2.2^{-16}
Con mejora gráfica	4.65	0.48	60		

Tabla 8.6: Tabla de resumen estadístico para los colores verdes entre ambas muestras

8.2.5. Colores Amarillos

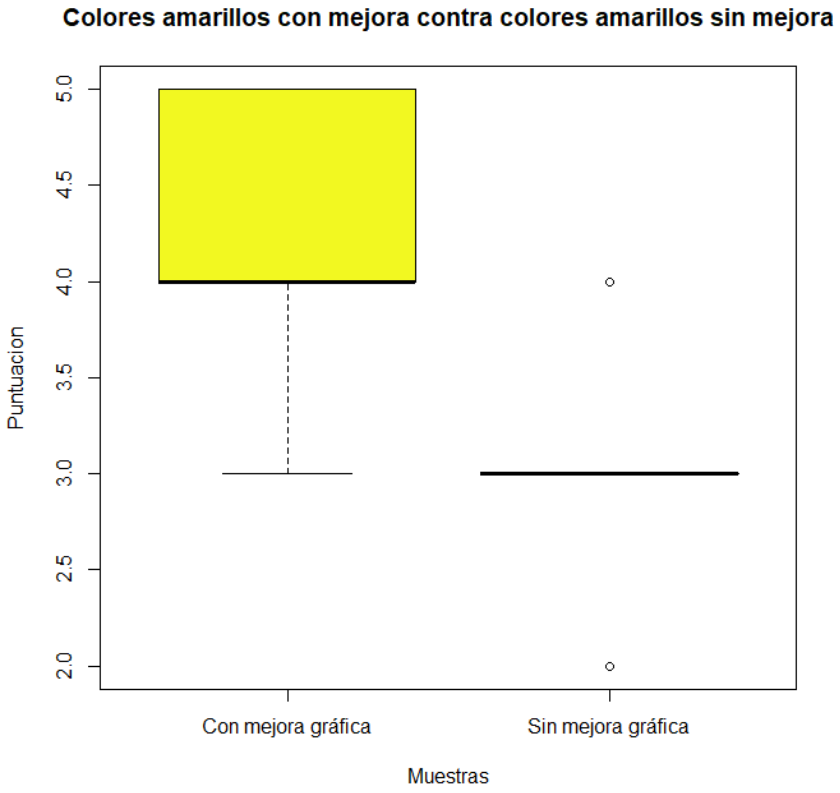

Figura 8.8: Diagrama de cajas comparando los colores amarillos con mejoras contra los amarillos sin mejoras

Muestra	Media	Desviación típica	N	W	p-value
Sin mejora gráfica	2.95	0.62	60	3393	2.2^{-16}
Con mejora gráfica	4.43	0.56	60		

Tabla 8.7: Tabla de resumen estadístico para los colores amarillos entre ambas muestras

8.2.6. Colores Blancos

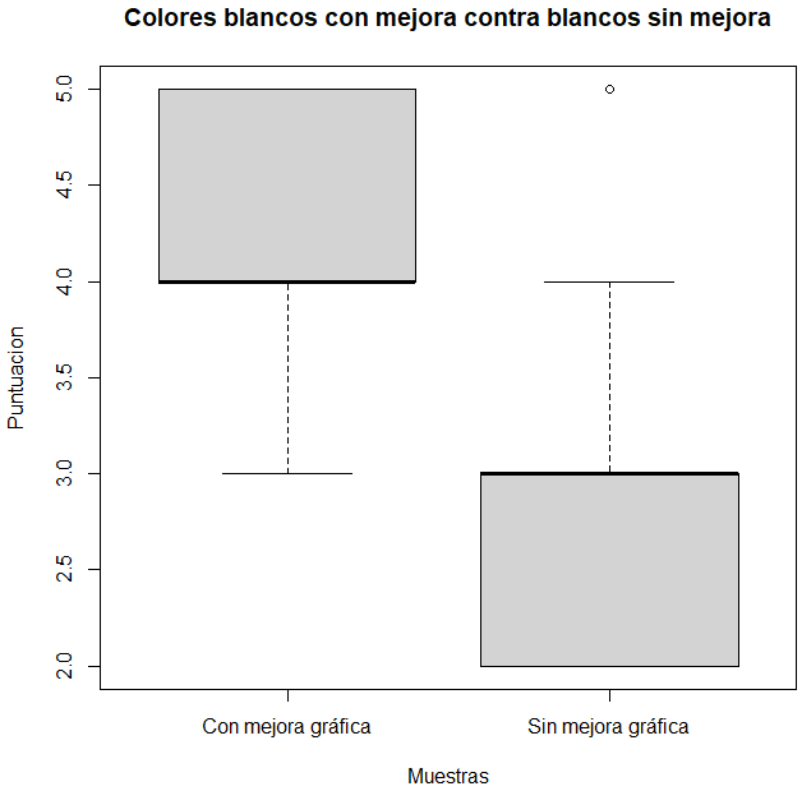

Figura 8.9: Diagrama de cajas comparando los colores blancos con mejoras contra los blancos sin mejoras

Muestra	Media	Desviación típica	N	W	p-value
Sin mejora gráfica	2.70	0.64	60	3460	2.2^{-16}
Con mejora gráfica	4.35	0.54	60		

Tabla 8.8: Tabla de resumen estadístico para los colores blancos entre ambas muestras

8.2.7. Realismo general del escenario

Con esta pregunta hacia el observador hemos querido recoger la puntuación que el observador consideraba oportuna para la sensación de realismo general del escenario. Se debía tener en cuenta la mezcla de todos los colores así como la iluminación, sombreados, geometrías... El hecho es que con la simple mejora gráfica en la parte de la colorimetría y la aplicación de texturas hiperespectrales, la puntuación obtenida entre ambas muestras refleja una gran diferencia significativa. Esto implica que el trabajo realizado durante dicha tesis doctoral permite al usuario tener una sensación de inmersión mucho más realista. La figura 8.10 y la tabla 8.9 muestran dichas diferencias.

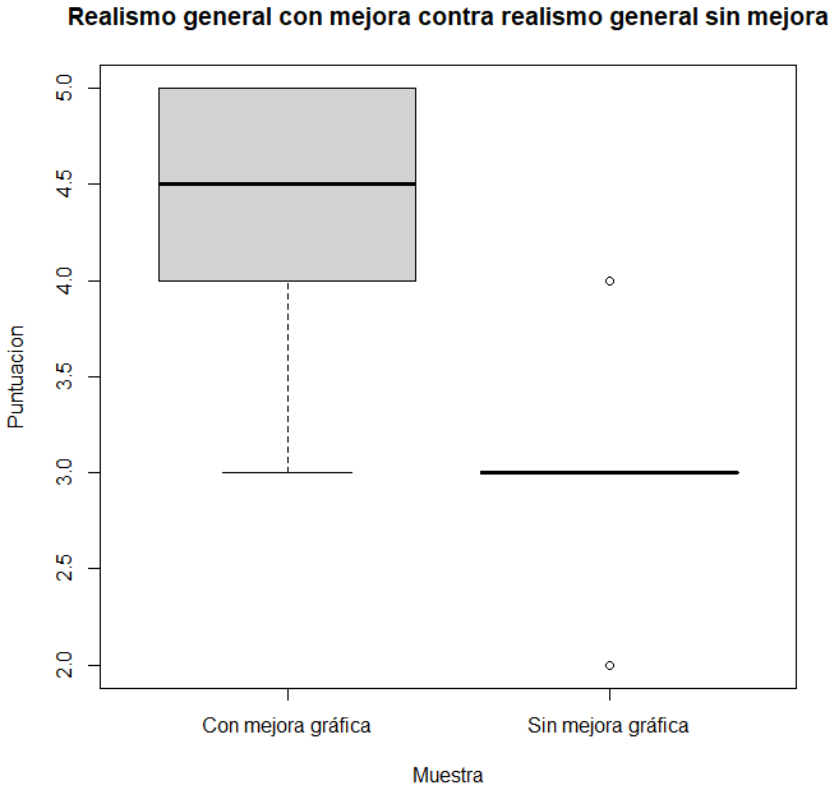

Figura 8.10: Diagrama de cajas comparando realismo general con mejoras contra realismo general sin mejoras

Muestra	Media	Desviación típica	N	W	p-value
Sin mejora gráfica	2.93	0.51	60	3485	2.2^{-16}
Con mejora gráfica	4.48	0.53	60		

Tabla 8.9: Tabla de resumen estadístico para la sensación de realismo general entre ambas muestras

Capítulo 9

Conclusiones

A la vista de los resultados obtenidos, podemos extraer varias conclusiones relacionadas con la introducción de la información hiperespectral en un sistema de realidad virtual. La primera conclusión que podemos sacar del trabajo realizado durante esta tesis doctoral es que es posible introducir un sistema gestor de color en un escenario de realidad virtual a pesar de la elevada tasa de refresco de la imagen y de la baja latencia necesaria. Además, se ha conseguido realizar la calibración correspondiente al visor de realidad virtual para asegurar una alta fidelidad en la reproducción de los colores. Esto nos ha permitido conocer las capacidades y limitaciones que los visores de realidad virtual tienen hoy en día en cuanto a reproducción del color. La segunda conclusión es que se ha conseguido mejorar los valores colorimétricos de los objetos virtuales en relación con los objetos reales mostrados en una cabina de luz real cuando se cambian las condiciones de iluminación. Para corroborar que los resultados obtenidos son mejores a los obtenidos mediante una textura RGB obtenida por otros medios, como por ejemplo un escáner de mano o una cámara digital, hemos realizado mediciones colorimétricas y hemos comprobado mediante la fórmula de diferencia de color CIEDE2000 que para todas las fuentes luminosas el error cometido era inferior en los escenarios que utilizaban texturas hiperespectrales. Fruto del trabajo llevado a cabo para representar valores de color en objetos 3D, nos vimos obligados a realizar una reconstrucción de objetos 3D mediante escáner para obtener su geometría y mejorar la representación de los valores colorimétricos con la aplicación de texturas hiperespectrales y su gestión. Esto nos permitió crear escenarios hiperrealistas en entornos virtuales. Por último, una vez comprobada la operatividad de las mejoras gráficas creadas, desarrollamos un escenario con todas las mejoras frente a un escenario sin las mejoras implementadas. Con una población de 5 observadores realizamos 15 pruebas de las cuales se obtuvieron los datos que indican que éstos perciben una diferencia significativa no solo en el escenario en general sino en cada una de las preguntas que se establecieron para comprobar el funcionamiento del sistema (iluminación, colores rojos, colores azules, colores verdes, colores amarillos, colores blancos y realismo general).

9.1. Líneas futuras

Durante el desarrollo de esta tesis doctoral se han utilizado técnicas de colorimetría clásica aplicadas a un novedoso sistema tecnológico como es la realidad virtual. Todas estas técnicas, como el uso de texturas hiperespectrales o el intercambio de un espacio de color a otro para garantizar la fidelidad cromática, han dado unos resultados excepcionales desde el punto de vista de la medición física del color. Sin embargo, el sistema visual humano funciona de una manera compleja, por ello es necesario seguir avanzando en dichos trabajos desde el punto de vista de la percepción y del entorno. El último de los trabajos presentados en esta tesis explica que podemos mejorar la fidelidad en la reproducción cromática de los visores, pero otra cosa a tener en cuenta es la apariencia percibida por el usuario. Son numerosos los aspectos que hacen que el sistema visual humano pueda verse condicionado, por ejemplo dependiendo de los objetos que haya a su alrededor o del color del fondo. Uno de esos aspectos a tener en cuenta es la adaptación cromática y la *color constancy* en la cual continuaremos trabajando después de la presentación de esta tesis doctoral.

Referencias

[1] T. Kiryu and R. H. So, "Sensation of presence and cybersickness in applications of virtual reality for advanced rehabilitation," *Journal of neuroengineering and rehabilitation*, vol. 4, no. 1, pp. 1–5, 2007.

[2] M. Mon-Williams, J. Wann, and S. Rushton, "Design factors in stereoscopic virtual-reality displays," *Journal of the Society for information Display*, vol. 3, no. 4, pp. 207–210, 1995.

[3] B. Julesz, "Stereoscopic vision," *Vision Research*, vol. 26, no. 9, pp. 1601–1612, 1986.

[4] J. T. Thorn, E. Migliorini, and D. Ghezzi, "Virtual reality simulation of epiretinal stimulation highlights the relevance of the visual angle in prosthetic vision," *Journal of Neural Engineering*, vol. 17, no. 5, p. 056019, 2020.

[5] R. Albert, A. Patney, D. Luebke, and J. Kim, "Latency requirements for foveated rendering in virtual reality," *ACM Transactions on Applied Perception (TAP)*, vol. 14, no. 4, pp. 1–13, 2017.

[6] J. Melzer and C. Spitzer, "Head-mounted displays," *Digital Avionics Handbook*, pp. 256–279, 2017.

[7] T. Akenine-Moller, E. Haines, and N. Hoffman, *Real-time rendering*. AK Peters/crc Press, 2019.

[8] J. Shin, G. An, J.-S. Park, S. J. Baek, and K. Lee, "Application of precise indoor position tracking to immersive virtual reality with translational movement support," *Multimedia tools and applications*, vol. 75, no. 20, pp. 12 331–12 350, 2016.

[9] P. Lincoln, A. Blate, M. Singh, T. Whitted, A. State, A. Lastra, and H. Fuchs, "From motion to photons in 80 microseconds: Towards minimal latency for virtual and augmented reality," *IEEE transactions on visualization and computer graphics*, vol. 22, no. 4, pp. 1367–1376, 2016.

[10] M. Di Luca, "New method to measure end-to-end delay of virtual reality," *Presence: Teleoperators and Virtual Environments*, vol. 19, no. 6, pp. 569–584, 2010.

[11] M. S. Elbamby, C. Perfecto, M. Bennis, and K. Doppler, "Toward low-latency and ultra-reliable virtual reality," *IEEE Network*, vol. 32, no. 2, pp. 78–84, 2018.

[12] L. Rodriguez-Gil, P. Orduna, J. Garcia-Zubia, I. Angulo, and D. Lopez-de Ipina, "Graphic technologies for virtual, remote and hybrid laboratories: Weblab-fpga hybrid lab," in *2014 11th International Conference on Remote Engineering and Virtual Instrumentation (REV)*. IEEE, 2014, pp. 163–166.

[13] J. Schmittler, S. Woop, D. Wagner, W. J. Paul, and P. Slusallek, "Realtime ray tracing of dynamic scenes on an fpga chip," in *Proceedings of the ACM SIGGRAPH/EUROGRAPHICS conference on Graphics hardware*, 2004, pp. 95–106.

[14] P. Zimmons and A. Panter, "The influence of rendering quality on presence and task performance in a virtual environment," in *IEEE Virtual Reality, 2003. Proceedings.* IEEE, 2003, pp. 293–294.

[15] A. Lauritzen, "Deferred rendering for current and future rendering pipelines," *SIGGRAPH Course: Beyond Programmable Shading*, pp. 1–34, 2010.

[16] A. S. Pacheu, "Advances on computational imaging, material appearance, and virtual reality," Ph.D. dissertation, Universidad de Zaragoza, 2019.

[17] C. R. Ingling Jr and B. H.-P. Tsou, "Orthogonal combination of the three visual channels," *Vision research*, vol. 17, no. 9, pp. 1075–1082, 1977.

[18] S. L. Guth, R. W. Massof, and T. Benzschawel, "Vector model for normal and dichromatic color vision," *JOSA*, vol. 70, no. 2, pp. 197–212, 1980.

[19] R. M. Boynton, "A system of photometry and colorimetry based on cone excitations," *Color Research & Application*, vol. 11, no. 4, pp. 244–252, 1986.

[20] R. L. De Valois and K. K. De Valois, "A multi-stage color model," *Vision research*, vol. 33, no. 8, pp. 1053–1065, 1993.

[21] S. Tominaga, "Color notation conversion by neural networks," *Color Research & Application*, vol. 18, no. 4, pp. 253–259, 1993.

[22] L. Ningfang and G. Zhiyun, "A comparative study of a crt colorimetric prediction model by neural networks and the models by conventional method," *Color Research & Application: Endorsed by Inter-Society Color Council, The Colour Group (Great Britain), Canadian Society for Color, Color Science Association of Japan, Dutch Society for the Study of Color, The Swedish Colour Centre Foundation, Colour Society of Australia, Centre Français de la Couleur*, vol. 24, no. 1, pp. 45–51, 1999.

[23] D. H. Alman and L. Ningfang, "Overtraining in back-propagation neural networks: A crt color calibration example," *Color Research & Application: Endorsed by Inter-Society Color Council, The Colour Group (Great Britain), Canadian Society for Color, Color Science Association of Japan, Dutch Society for the Study of Color, The Swedish Colour Centre Foundation, Colour Society of Australia, Centre Français de la Couleur*, vol. 27, no. 2, pp. 122–125, 2002.

[24] F. Díaz-Barrancas, H. Cwierz, P. J. Pardo, Á. L. Pérez, and M. I. Suero, "Spectral color management in virtual reality scenes," *Sensors*, vol. 20, no. 19, p. 5658, 2020.

[25] F. Díaz-Barrancas, H. Cwierz, and P. J. Pardo, "Real-time application of computer graphics improvement techniques using hyperspectral textures in a virtual reality system," *Electronics*, vol. 10, no. 22, p. 2852, 2021.

[26] H. Cwierz, F. Díaz-Barrancas, J. G. Llinás, and P. J. Pardo, "On the validity of virtual reality applications for professional use: A case study on color vision research and diagnosis," *IEEE Access*, vol. 9, pp. 138 215–138 224, 2021.

[27] F. Díaz-Barrancas, H. C. Cwierz, P. J. Pardo, A. L. Perez, and M. I. Suero, "Colour appearance in immersive three-dimensional virtual environments," *Coloration Technology*, vol. 137, no. 1, pp. 38–43, 2021.

[28] R. G. Kuehni, "Color space and its divisions," *Color Research & Application: Endorsed by Inter-Society Color Council, The Colour Group (Great Britain), Canadian Society for Color, Color Science Association of Japan, Dutch Society for the Study of Color, The Swedish Colour Centre Foundation, Colour Society of Australia, Centre Français de la Couleur*, vol. 26, no. 3, pp. 209–222, 2001.

[29] M. Shaw and M. Fairchild, "Evaluating the 1931 cie color-matching functions," *Color Research & Application: Endorsed by Inter-Society Color Council, The Colour Group (Great Britain), Canadian Society for Color, Color Science Association of Japan, Dutch Society for the Study of Color, The Swedish Colour Centre Foundation, Colour Society of Australia, Centre Français de la Couleur*, vol. 27, no. 5, pp. 316–329, 2002.

[30] T. Ejaz, T. Horiuchi, G. Ohashi, and Y. Shimodaira, "Development of a camera system for the acquisition of high-fidelity colors," *IEICE transactions on electronics*, vol. 89, no. 10, pp. 1441–1447, 2006.

[31] M. Melgosa, G. Cui, C. Oleari, P. J. Pardo, M. Huang, C. Li, and M. R. Luo, "Revisiting the weighting function for lightness in the ciede 2000 colour-difference formula," *Coloration Technology*, vol. 133, no. 4, pp. 273–282, 2017.

[32] P. Bodrogi, B. Sinka, A. Borbely, N. Geiger, and J. Schanda, "On the use of the srgb colour space: the 'gamma'problem," *Displays*, vol. 23, no. 4, pp. 165–170, 2002.

[33] F. Díaz Barrancas, "Estudio de la fidelidad de la reproducción cromática en dispositivos de realidad virtual," Master's thesis, 2018.

[34] H. C. Cwierz, F. Diaz-Barrancas, P. J. Pardo, A. L. Perez, and M. I. Suero, "Cómo realizar una correcta gestión del color en sistemas de realidad virtual," in *XII Congreso Nacional del Color*. Comité del color, 2019.

[35] B. Kitchenham, "Procedures for performing systematic reviews," *Keele, UK, Keele University*, vol. 33, no. 2004, pp. 1–26, 2004.

[36] H. W. Lilliefors, "On the kolmogorov-smirnov test for the exponential distribution with mean unknown," *Journal of the American Statistical Association*, vol. 64, no. 325, pp. 387–389, 1969.

Apéndice A

Anexo I

A.1. Contribuciones realizadas: Revistas y congresos

A continuación, se muestra una relación de las publicaciones realizadas durante el desarrollo de esta investigación.

A.1.1. Revistas

- Francisco Díaz-Barrancas, Halina Cwierz, Pedro José Pardo, Ángel Luis Pérez and María Isabel Suero. Spectral Color Management in Virtual Reality Scenes. Sensors 2020, 20(19), pp. 5658. JCR: Q1, IF: 3.275.
- Francisco Díaz-Barrancas, Halina Cwierz, Pedro José Pardo, Ángel Luis Pérez and María Isabel Suero. Colour appearance in immersive three-dimensional virtual environments. Coloration Technology 2021, 137(1), pp. 38-43. JCR: Q2, IF: 1.5.
- Halina Cwierz, Francisco Díaz-Barrancas, Julia Gil LLinás and Pedro J. Pardo. On the validity of virtual reality applications for professional use: A case study on color vision research and diagnosis. IEEE Access 2021, vol. 9, pp. 138215-138224, 2021. JCR: Q2, IF: 3.367.
- Francisco Díaz-Barrancas, Halina Cwierz and Pedro José Pardo. Real-Time Application of Computer Graphics Improvement Techniques Using Hyperspectral Textures in a Virtual Reality System. Electronics 2021, 10(22), pp. 2852. JCR: Q3, IF: 2.397.

A.1.2. Conferencias

- Francisco Díaz-Barrancas, Pedro José Pardo, Ángel Luis Pérez and María Isabel Suero. Is it possible to apply colour management technics in Virtual Reality devices?

Proceedings of the 14th Conferenza del Colore 2018. ISBN: 978-88-99513-09-2

- Halina Cwierz, Francisco Díaz-Barrancas, Pedro José Pardo, Ángel Luis Pérez and María Isabel Suero. Colour Management in Virtual Reality applied to Lighting Simulations. Proceedings of the International Colour Association (AIC) Conference 2018. ISBN: 978-0-6484724-0-7

- Francisco Díaz-Barrancas, Halina Cwierz, Pedro José Pardo, Ángel Luis Pérez and María Isabel Suero. Improvement of realism sensation in virtual reality scenes applying spectral and colour management techniques. The 25th Symposium of the International Colour Vision Society 2019. ISBN: 978-9934-556-46-3

- Pedro José Pardo, Halina Cwierz, Francisco Díaz-Barrancas, Ángel Luis Pérez and María Isabel Suero. Validity of virtual-reality-based systems applied to lighting and colour rendering research.The 25th Symposium of the International Colour Vision Society 2019. ISBN: 978-9934-556-46-3

- Francisco Díaz-Barrancas, Halina Cwierz, Pedro José Pardo, Ángel Luis Pérez and María Isabel Suero. Hyperspectral textures for a better colour reproduction in virtual reality. Proceedings of the 15th Conferenza del Colore 2019. ISBN: 978-88-99513-11-5

- Francisco Díaz-Barrancas, Halina Cwierz, Pedro José Pardo, Ángel Luis Pérez and María Isabel Suero. Aplicación de texturas hiperespectrales a objetos 3D en escenas de Realidad Virtual. XII Congreso Nacional del Color 2019. ISBN: 978-84-09-15750-1

- Francisco Díaz-Barrancas, Halina Cwierz, Pedro José Pardo, Ángel Luis Pérez and María Isabel Suero. Reconstrucción de objetos 3D mediante técnicas SFM y obtención de texturas hiperespectrales. XII Congreso Nacional del Color 2019. ISBN: 978-84-09-15750-1

- Halina Cwierz, Francisco Díaz-Barrancas, Pedro José Pardo, Ángel Luis Pérez and María Isabel Suero. Herramienta para la valoración de la capacidad de discriminación del color de observadores normales y defectivos mediante un test de ordenación de color, reproducido en un entorno de realidad virtual. XII Congreso Nacional del Color 2019. ISBN: 978-84-09-15750-1

- Halina Cwierz, Francisco Díaz-Barrancas, Pedro José Pardo, Ángel Luis Pérez and María Isabel Suero. Cómo realizar una correcta gestión del color en sistemas de realidad virtual. XII Congreso Nacional del Color 2019. ISBN: 978-84-09-15750-1

- Francisco Díaz-Barrancas, Halina Cwierz, Pedro José Pardo, Ángel Luis Pérez and María Isabel Suero. A virtual scene with conservation objects with different illuminants and colour management. A Conservation Carol 2019.

- Francisco Díaz-Barrancas, Halina Cwierz, Pedro José Pardo, Ángel Luis Pérez and María Isabel Suero. Visual fidelity improvement in virtual reality through spectral

textures applied to lighting simulations. Electronic Imaging 2020. ISSN: ISSN 2470-1173

- Halina Cwierz, Francisco Díaz-Barrancas, Pedro José Pardo, Ángel Luis Pérez and María Isabel Suero. Application of spectral computing technics for color vision testing using virtual reality devices. Electronic Imaging 2020. ISSN 2470-1173.
- Pedro J. Pardo, Francisco Díaz-Barrancas, Halina Cwierz. Color Constancy in virtual reality scenes. A first step toward a color appearance model in virtual reality. AIC 14th Congress Milano 2021. ISBN: 978-0-6484724-3-8.
- Francisco Díaz-Barrancas, Halina Cwierz, Pedro J. Pardo. A study of physical and perceived linearity in a virtual reality environment. AIC 14th Congress Milano 2021. ISBN: 978-0-6484724-3-8.

A.2. Participación en proyectos de investigación

A continuación, se muestra una relación de los proyectos de investigación en los que se ha participado durante el desarrollo de la Tesis.

- Aplicación de técnicas hiperespectrales y de realidad virtual a la medida del rendimiento de color de fuentes luminosas LED (IB16004).
  - Investigador principal: Pedro José Pardo Fernández
  - Entidad financiadora: Consejeria de economía, competitividad e innovación
  - Nº de investigadores: 6
  - Duración: 03/06/2017 - 08/11/2020
  - Cuantía: 115.261,30€
- Ayudas a grupos: Grupo Orión (GR18131)
  - Investigador principal: María Isabel Suero López
  - Entidad financiadora: Consejeria de economía, ciencia y agenda digital
  - Nº de investigadores: 10
  - Duración: 29/05/2018 - 04/11/2021
  - Cuantía: 26.360,25€
- Puesta a punto de un sistema de captura y generación de modelos 3D con técnicas hiperespectrales
  - Investigador principal: Ángel Manuel Felicísimo Pérez
  - Entidad financiadora: Consejeria de educación y empleo

  - Nº de investigadores: 2
  - Duración: 01/10/2020 - 31/03/2022
  - Cuantía: 40.677,14€

- Desarrollo e integración de mejoras en sistemas realidad extendida aplicadas a las prácticas clínicas (IB20094)
  - Investigador principal: Pedro José Pardo Fernández
  - Entidad financiadora: Consejeria de economía, ciencia y agenda digital
  - Nº de investigadores: 9
  - Duración: 17/06/2021 - 16/06/2024
  - Cuantía: 127.292,00€

Apéndice B

Anexo II

B.1. Informe de consentimiento

En las siguientes páginas se presenta un modelo del informe de consentimiento que ha sido utilizado para la recopilación de datos por parte de observadores que han participado para proporcionar los resultados de dicha tesis doctoral.

Centro Universitario de Mérida
Universidad de Extremadura
2018-2021

Consentimiento Informado

Estimado Participante:

El Centro Universitario de Mérida (Universidad de Extremadura) se encuentra realizando una investigación titulada "***APLICACIÓN DE TÉCNICAS HIPERESPECTRALES PARA UNA MEJORA DE LA APARIENCIA VISUAL Y DE LA SENSACIÓN DE REALISMO EN DISPOSITIVOS DE REALIDAD VIRTUAL***", desarrollada por Francisco Díaz Barrancas, en el marco del programa de doctorado "Tecnologías informáticas" de la Universidad de Extremadura.
El presente documento tiene como finalidad hacerle conocer los detalles del estudio y solicitarle su consentimiento informado para participar en él.

1. Objetivo de la investigación
El objetivo de esta investigación es el de conocer si se han producido mejoras gráficas en el ámbito del color en entornos de realidad virtual mediante el uso de diferentes técnicas espectrales.

2. Breve descripción del proyecto
La Realidad Virtual es una de las numerosas tecnologías que se encuentran en continuo crecimiento en estos nuevos tiempos. Sin embargo, cuando hablamos de computación gráfica en el mundo virtual, la tecnología actual no permite que nuestro sistema visual humano responda de la misma manera que lo hace ante el mundo real. En este contexto, hemos introducido técnicas de gestión del color y de computación gráfica, introduciendo texturas hiperespectrales para obtener un mejor resultado de visualización del mundo virtual.

3. Metodología
El presente proyecto consta de 5 pruebas iguales que se realizarán en distintos días. Cada prueba consiste en realizar un test de daltonismo (Farnsworth Munsell 100 Hue) de la forma tradicional (ordenación de unas cápsulas por tonalidades de forma manual) y el mismo test en realidad virtual, para lo cual se deberá colocar unas gafas de realidad virtual y usar un mando para realizar el test. Deberá disponer de aproximadamente 40 minutos para cada una de las pruebas.

4. Su participación en el estudio
Su participación en este estudio es de carácter libre y voluntario, pudiendo solicitar ser excluido de esta investigación y que sus intervenciones no sean consideradas en esta investigación sin justificación previa ni perjuicio para usted.
Si usted participa en esta investigación lo hace bajo su expreso consentimiento informado que firma y autoriza.

5. Confidencialidad
La confidencialidad de su identidad será resguardada por las siguientes medidas:

1. Las encuestas serán anónimas y solo el investigador responsable tendrá acceso a los datos proporcionados en ellas.
2. Las entrevistas recibirán un código por cada participante, que solo conocerá el investigador responsable de este estudio y serán realizadas en un ambiente propicio que estimule la comunicación y el anonimato elegido por el participante.

En el análisis general de los datos se utilizará una estructura de códigos para identificar la información que surja, su pertenencia al instrumento y el momento en que se realizó. Dadas las características del estudio los datos serán usados solamente en instancias académicas de investigación y aquellas propias de la divulgación investigativa.
En la presentación de resultados se utilizarán nombres ficticios y se reservará todo posible indicio que permita una identificación posible como lugares, instituciones, guardias, etc.
Asimismo, el Investigador Responsable asume un compromiso de confidencialidad para resguardar identidad de todos los involucrados en este estudio.

6. Beneficios
Este estudio no tiene beneficios directos para usted. En este sentido, producto de su participación no se generan incentivos económicos ni de ningún tipo. Cabe destacar también que su participación en este estudio tampoco tiene asociado ningún tipo de costo para usted.
En tal sentido creemos que la investigación produce más bien beneficios indirectos en sus participantes puesto que podrán comprobar el estado actual de su visión del color.

7. Riesgos o molestias asociadas a la participación
Si se generara alguna controversia o molestia durante su participación en el estudio y/o entrevistas, el Investigador Responsable procurará brindar la asistencia requerida al participante y si es necesario cancelar la participación.

8. Almacenamiento y resguardo de la información
Toda la información que se recabe de esta investigación estará siempre resguardada y al cuidado del Investigador Responsable.
Las entrevistas y encuestas, además de las transcripciones asociadas, serán solo realizadas por el Investigador Responsable. Todo material electrónico será debidamente almacenado y respaldado en los equipos computacionales con contraseña del investigador.
Tanto este consentimiento, como los documentos impresos que se generen y sean necesarios utilizar se almacenarán por cinco años a contar del término del estudio, una vez finalizado el plazo se procederá a su eliminación de forma reservada.

9. Acceso a los resultados de la investigación
Los participantes podrán consultar la información que ha generado en cualquier momento durante la ejecución del proyecto previa solicitud al investigador responsable del estudio, quien se compromete a brindar cooperación y proponer vías para tal acceso.
Asimismo, el Investigador Responsable se compromete con cada participante a enviar el informe de investigación que se genere al final del estudio a los correos electrónicos respectivos, así también copia de los artículos científicos que pudieran resultar del estudio.

10. Compromiso
Por su aceptación los participantes se comprometen a:

1. Proveer información real en cada instancia que me sea solicitada y responder de acuerdo con mis concepciones, conocimientos y experiencias así también a utilizar mi lenguaje habitual al escribir, responder o reflexionar.
2. Asistir a todas las pruebas.

11. Contacto
Si usted tiene preguntas acerca de sus derechos como participante de este estudio, reclamos o dudas acerca de esta investigación, por favor contáctese con el Investigador Responsable, Francisco Díaz Barrancas, correo electrónico frdiaz@unex.es, o con el director de la presente investigación, Dr. Pedro José Pardo Fernández, al correo electrónico pjpardo@unex.es

Declaro conocer los términos de este consentimiento informado, los objetivos de la investigación, las formas de participación, de los costos y riesgos implicados, y del acceso a la información y resguardo de información que sea producida en el estudio. Reconozco que la información que provea en el curso de esta investigación es estrictamente confidencial y anónima. Además, esta será usada solo con fines de difusión científica.

He sido informado(a) de que puedo hacer preguntas sobre el proyecto en cualquier momento y que puedo retirarme del mismo cuando así lo decida, sin tener que dar explicaciones ni sufrir consecuencia alguna por tal decisión.

Nombre completo del participante:…..……

Correo electrónico: ……

Firma

Se deja constancia en este instante que este documento (consentimiento informado) será firmado a dos copias, dejando una de ellas en manos del investigador responsable y la otra copia en manos del participante.

Apéndice C

Anexo III

C.1. Licencia de copyright

Para todos los artículos publicados en revistas con Creative Commons Attribution CC BY 4.0, los derechos de autor pertenecen a los autores. Los artículos tienen una licencia de acceso abierto Creative Commons Attribution CC BY 4.0, lo que significa que cualquier persona puede descargar y leer el documento de forma gratuita. Además, el artículo puede ser reutilizado y citado siempre que se cite la versión original publicada. Estas condiciones permiten el máximo uso y exposición del trabajo, al mismo tiempo que aseguran que los autores reciban el crédito adecuado.

JOHN WILEY AND SONS LICENSE
TERMS AND CONDITIONS

Jan 12, 2022

This Agreement between Mr. Francisco Barrancas ("You") and John Wiley and Sons ("John Wiley and Sons") consists of your license details and the terms and conditions provided by John Wiley and Sons and Copyright Clearance Center.

License Number	5196451494952
License date	Nov 26, 2021
Licensed Content Publisher	John Wiley and Sons
Licensed Content Publication	Coloration Technology
Licensed Content Title	Colour appearance in immersive three-dimensional virtual environments
Licensed Content Author	Francisco Díaz-Barrancas, Halina Carmen Cwierz, Pedro J. Pardo, et al
Licensed Content Date	Dec 14, 2020
Licensed Content Volume	137
Licensed Content Issue	1

Licensed Content Pages	6
Type of use	Dissertation/Thesis
Requestor type	Author of this Wiley article
Format	Print and electronic
Portion	Full article
Will you be translating?	No
Title	APLICACIÓN DE TÉCNICAS HIPERESPECTRALES PARA UNA MEJORA DE LA APARIENCIA VISUAL Y DE LA SENSACIÓN DE REALISMO EN DISPOSITIVOS DE REALIDAD VIRTUAL
Institution name	University of Extremadura
Expected presentation date	Jan 2022
Order reference number	123456789
Requestor Location	Mr. Francisco Barrancas Santa Teresa Jornet Street, 38 Merida, Badajoz 06800 Spain Attn: Mr. Francisco Barrancas
Publisher Tax ID	EU826007151
Total	0.00 EUR

Terms and Conditions

TERMS AND CONDITIONS

This copyrighted material is owned by or exclusively licensed to John Wiley & Sons, Inc. or one of its group companies (each a"Wiley Company") or handled on behalf of a society with which a Wiley Company has exclusive publishing rights in relation to a particular work (collectively "WILEY"). By clicking "accept" in connection with completing this licensing transaction, you agree that the following terms and conditions apply to this transaction (along with the billing and payment terms and conditions established by the Copyright Clearance Center Inc., ("CCC's Billing and Payment terms and conditions"), at the time that you opened your RightsLink account (these are available at any time at http://myaccount.copyright.com).

Terms and Conditions

- The materials you have requested permission to reproduce or reuse (the "Wiley Materials") are protected by copyright.

- You are hereby granted a personal, non-exclusive, non-sub licensable (on a stand-alone basis), non-transferable, worldwide, limited license to reproduce the Wiley Materials for the purpose specified in the licensing process. This license, **and any CONTENT (PDF or image file) purchased as part of your order,** is for a one-time use only and limited to any maximum distribution number specified in the license. The first instance of republication or reuse granted by this license must be completed within two years of the date of the grant of this license (although copies prepared before the end date may be distributed thereafter). The Wiley Materials shall not be used in any other manner or for any other purpose, beyond what is granted in the license. Permission is granted subject to an appropriate acknowledgement given to the author, title of the material/book/journal and the publisher. You shall also duplicate the copyright notice that appears in the Wiley publication in your use of the Wiley Material. Permission is also granted on the understanding that nowhere in the text is a previously published source acknowledged for all or part of this Wiley Material. Any third party content is expressly excluded from this permission.

- With respect to the Wiley Materials, all rights are reserved. Except as expressly granted by the terms of the license, no part of the Wiley Materials may be copied, modified, adapted (except for minor reformatting required by the new Publication), translated, reproduced, transferred or distributed, in any form or by any means, and no derivative works may be made based on the Wiley Materials without the prior permission of the respective copyright owner.**For STM Signatory Publishers clearing permission under the terms of the STM Permissions Guidelines only, the terms of the license are extended to include subsequent editions and for editions in other languages, provided such editions are for the work as a whole in situ and does not involve the separate exploitation of the permitted figures or extracts,** You may not alter, remove or suppress in any manner any copyright, trademark or other notices displayed by the Wiley Materials. You may not license, rent, sell, loan, lease, pledge, offer as security, transfer or assign the Wiley Materials on a stand-alone basis, or any of the rights granted to you hereunder to any other person.

- The Wiley Materials and all of the intellectual property rights therein shall at all times remain the exclusive property of John Wiley & Sons Inc, the Wiley Companies, or their respective licensors, and your interest therein is only that of having possession of and the right to reproduce the Wiley Materials pursuant to Section 2 herein during the continuance of this Agreement. You agree that you own no right, title or interest in or to the Wiley Materials or any of the intellectual property rights therein. You shall have no rights hereunder other than the license as provided for above in Section 2. No right,

license or interest to any trademark, trade name, service mark or other branding ("Marks") of WILEY or its licensors is granted hereunder, and you agree that you shall not assert any such right, license or interest with respect thereto

- NEITHER WILEY NOR ITS LICENSORS MAKES ANY WARRANTY OR REPRESENTATION OF ANY KIND TO YOU OR ANY THIRD PARTY, EXPRESS, IMPLIED OR STATUTORY, WITH RESPECT TO THE MATERIALS OR THE ACCURACY OF ANY INFORMATION CONTAINED IN THE MATERIALS, INCLUDING, WITHOUT LIMITATION, ANY IMPLIED WARRANTY OF MERCHANTABILITY, ACCURACY, SATISFACTORY QUALITY, FITNESS FOR A PARTICULAR PURPOSE, USABILITY, INTEGRATION OR NON-INFRINGEMENT AND ALL SUCH WARRANTIES ARE HEREBY EXCLUDED BY WILEY AND ITS LICENSORS AND WAIVED BY YOU.

- WILEY shall have the right to terminate this Agreement immediately upon breach of this Agreement by you.

- You shall indemnify, defend and hold harmless WILEY, its Licensors and their respective directors, officers, agents and employees, from and against any actual or threatened claims, demands, causes of action or proceedings arising from any breach of this Agreement by you.

- IN NO EVENT SHALL WILEY OR ITS LICENSORS BE LIABLE TO YOU OR ANY OTHER PARTY OR ANY OTHER PERSON OR ENTITY FOR ANY SPECIAL, CONSEQUENTIAL, INCIDENTAL, INDIRECT, EXEMPLARY OR PUNITIVE DAMAGES, HOWEVER CAUSED, ARISING OUT OF OR IN CONNECTION WITH THE DOWNLOADING, PROVISIONING, VIEWING OR USE OF THE MATERIALS REGARDLESS OF THE FORM OF ACTION, WHETHER FOR BREACH OF CONTRACT, BREACH OF WARRANTY, TORT, NEGLIGENCE, INFRINGEMENT OR OTHERWISE (INCLUDING, WITHOUT LIMITATION, DAMAGES BASED ON LOSS OF PROFITS, DATA, FILES, USE, BUSINESS OPPORTUNITY OR CLAIMS OF THIRD PARTIES), AND WHETHER OR NOT THE PARTY HAS BEEN ADVISED OF THE POSSIBILITY OF SUCH DAMAGES. THIS LIMITATION SHALL APPLY NOTWITHSTANDING ANY FAILURE OF ESSENTIAL PURPOSE OF ANY LIMITED REMEDY PROVIDED HEREIN.

- Should any provision of this Agreement be held by a court of competent jurisdiction to be illegal, invalid, or unenforceable, that provision shall be deemed amended to achieve as nearly as possible the same economic effect as the original provision, and the legality, validity and enforceability of the remaining provisions of this Agreement shall not be affected or impaired thereby.

- The failure of either party to enforce any term or condition of this Agreement shall not constitute a waiver of either party's right to enforce each and every term and condition of this Agreement. No breach under this agreement shall be deemed waived or excused by either party unless such waiver or consent is in writing signed by the party granting such waiver or consent. The waiver by or consent of a party to a breach of any provision of this Agreement shall not operate or be construed as a waiver of or consent to any other or subsequent breach by such other party.

- This Agreement may not be assigned (including by operation of law or otherwise) by you without WILEY's prior written consent.

- Any fee required for this permission shall be non-refundable after thirty (30) days from receipt by the CCC.

- These terms and conditions together with CCC's Billing and Payment terms and conditions (which are incorporated herein) form the entire agreement between you and WILEY concerning this licensing transaction and (in the absence of fraud) supersedes all prior agreements and representations of the parties, oral or written. This Agreement may not be amended except in writing signed by both parties. This Agreement shall be binding upon and inure to the benefit of the parties' successors, legal representatives, and authorized assigns.

- In the event of any conflict between your obligations established by these terms and conditions and those established by CCC's Billing and Payment terms and conditions, these terms and conditions shall prevail.

- WILEY expressly reserves all rights not specifically granted in the combination of (i) the license details provided by you and accepted in the course of this licensing transaction, (ii) these terms and conditions and (iii) CCC's Billing and Payment terms and conditions.

- This Agreement will be void if the Type of Use, Format, Circulation, or Requestor Type was misrepresented during the licensing process.

- This Agreement shall be governed by and construed in accordance with the laws of the State of New York, USA, without regards to such state's conflict of law rules. Any legal action, suit or proceeding arising out of or relating to these Terms and Conditions or the breach thereof shall be instituted in a court of competent jurisdiction in New York County in the State of New York in the United States of America and each party hereby consents and submits to the personal jurisdiction of such court, waives any objection to venue in such court and consents to service of process by registered or certified mail, return receipt requested, at the last known address of such party.

WILEY OPEN ACCESS TERMS AND CONDITIONS

Wiley Publishes Open Access Articles in fully Open Access Journals and in Subscription journals offering Online Open. Although most of the fully Open Access journals publish open access articles under the terms of the Creative Commons Attribution (CC BY) License only, the subscription journals and a few of the Open Access Journals offer a choice of Creative Commons Licenses. The license type is clearly identified on the article.

The Creative Commons Attribution License

The Creative Commons Attribution License (CC-BY) allows users to copy, distribute and transmit an article, adapt the article and make commercial use of the article. The CC-BY license permits commercial and non-

Creative Commons Attribution Non-Commercial License

The Creative Commons Attribution Non-Commercial (CC-BY-NC)License permits use, distribution and reproduction in any medium, provided the original work is properly cited and is not used for commercial purposes.(see below)

Creative Commons Attribution-Non-Commercial-NoDerivs License

The Creative Commons Attribution Non-Commercial-NoDerivs License (CC-BY-NC-ND) permits use, distribution and reproduction in any medium, provided the original work is properly cited, is not used for commercial purposes and no modifications or adaptations are made. (see below)

Use by commercial "for-profit" organizations